

PhD Thesis

Model-independent Determination of Proton Polarizabilities from Compton Scattering

Dissertation
zur Erlangung des Grades
"Doktor der Naturwissenschaften"

am Fachbereich Physik, Mathematik und Informatik
der Johannes Gutenberg Universität Mainz

vorgelegt von

NADIJA KRUPINA
geboren in Charkiw, USSR

2016

Summary (English)

The scalar and spin polarizabilities of the proton are fundamental quantities that characterize the ability of proton's constituents to rearrange themselves in external electromagnetic fields. Their PDG values combine the Dispersion relation (DR) and the chiral perturbation theory (ChPT) results, whereas individually these theoretical approaches yield different values. In particular, ChPT and fixed- t DR (combined with Compton scattering data) give at present different values of the magnetic polarizability. Here we offer two model-independent approaches to extract the polarizabilities which are based on the low-energy and multipole expansions of Compton scattering observables. These approaches are complementary to the existing theoretical methods, and as such they give additional insight into the problem. What is more important, they offer an additional route to calculate observables that potentially can resolve the controversy over the values of the polarizabilities.

In the first part of this dissertation we derive the low-energy expansions of the helicity amplitudes and observables for the beam and spin-1/2 target polarizations. Here we identify and study three independent spin asymmetries which can be used to measure the proton polarizabilities. In particular, we show that the leading-order non-Born contribution to the beam asymmetry is given by the magnetic polarizability alone. Hence, this observable is a good candidate for a precision measurement of the magnetic dipole polarizability. To support this statement, we present preliminary results of a pilot measurement of the beam asymmetry below the pion production threshold. These results are obtained by the A2 collaboration at the Mainz Microtron. We provide a similar analysis for the target asymmetries, which, as we argue, give an access to the proton spin polarizabilities.

In the second part of this dissertation we obtain the multipole expansions of the helicity amplitudes and observables below the pion production threshold. To this end, we develop a fitting procedure which yields the scalar and spin polarizabilities from unpolarized Compton scattering data. We make several fits either using the full database or excluding a few inconsistent data points. We find that in the former case the fitted scalar polarizabilities coincide with the values in the DR framework, whereas in the latter case they are similar to the values computed using the baryon ChPT approach. This observation allows us to suggest that the difference between the baryon ChPT and DR values of the scalar polarizabilities is due to inconsistencies in the database used in the DR analysis. To resolve this inconsistency we propose to measure the unpolarized Compton scattering cross section at energy $\nu \approx 110$ MeV and backward angles. As far as the spin polarizabilities are concerned, the values we extract are consistent among the different fits, and are as well consistent with the values obtained in the baryon ChPT and DR analyses.

The presented multipole analysis of Compton scattering is the first of its kind. We believe that in the near future it will give us a unique opportunity to obtain accurate values of the polarizabilities in a model-independent way. The achievement of this goal will be facilitated by improvements of the existing data that are to come in the following years at experimental facilities around the globe, in particular, at the Mainz Microtron, and at the high-intensity electron facility MESA which currently is under construction in Mainz.

Summary (German)

Die Skalar- und Spinpolarisierbarkeiten des Protons sind fundamentale Größen, welche die Fähigkeit der Protonkonstituenten charakterisieren, sich in externen elektromagnetischen Feldern auszurichten. Bis heute sind ihre genauen Werte weitgehend unbekannt, da die unterschiedlichen, theoretischen Ansätze verschiedene Resultate ergeben. Beispielsweise liefern die chirale Störungstheorie (ChPT) sowie fixed-t dispersion relation (DR) Frameworks offensichtlich unterschiedliche Werte der magnetischen Polarisierbarkeit. Diese Arbeit liefert zwei modellunabhängige Ansätze zur Extraktion der Polarisierbarkeiten, welche auf Niedrigenergie- und Multipolentwicklungen von Observablen der Compton-Streuung basieren. Diese Ansätze verhalten sich zu den bereits existierenden, theoretischen Methoden komplementär und liefern als solche eine zusätzliche Einsicht in das betrachtete Problem. Noch wichtiger ist, dass sie eine weitere Möglichkeit darstellen, Observablen zu berechnen, welche eventuell die Kontroverse zwischen den Werten der Polarisierbarkeiten auflösen könnten.

Im ersten Teil der Dissertation leiten wir die Niedrigenergie-Entwicklung der Helizitätsamplituden und der Observablen für die Strahl- und Targetpolarisation mit Spin-1/2 ab. Wir bestimmen und untersuchen drei unabhängige Spinasymmetrien, welche zur Messung der Polarisierbarkeiten des Protons verwendet werden können. Im Besonderen zeigen wir, dass der nicht-bornsche Beitrag führender Ordnung zur Strahlasymmetrie allein durch die magnetische Polarisierbarkeit gegeben ist. Somit stellt diese Observable ein guter Kandidat für eine präzise Messung der magnetischen Dipolpolarisierbarkeit dar. Um diese Aussage zu unterstützen, präsentieren wir vorläufige Resultate einer Pilotmessung der Strahlasymmetrie unterhalb der Pionproduktionsschwelle. Diese Resultate wurden von der A2 Kollaboration am Mainzer Mikrotron gewonnen. Wir liefern eine ähnliche Analyse für die Targetasymmetrien, welche, nach unserer Argumentation, einen Zugang zu den Spinpolarisierbarkeiten des Protons darstellen.

Im zweiten Teil dieser Dissertation erhalten wir die Multipolentwicklungen der Helizitätsamplituden und Observablen unterhalb der Pionproduktionsschwelle. Zu diesem Zweck entwickeln wir eine Fitprozedur, welche die Skalar- und Spinpolarisierbarkeiten aus Daten der unpolarisierten Compton-Streuung liefert. Wir führen zahlreiche Fitanpassungen durch, sowohl auf Basis aller vorhandenen Daten, als auch unter Ausschluss weniger, inkonsistenter Datenpunkte. Wir stellen fest, dass im ersteren Fall die gefitteten Skalarpolarisierbarkeiten mit den Werten, welche im DR Framework gewonnen wurden, übereinstimmen, während sie im letzteren Fall eine Ähnlichkeit zu den Werten aufweisen, welche unter Verwendung des Baryon ChPT Ansatzes berechnet wurden. Aufgrund dieser Beobachtung schlagen wir vor, dass die Unterschiede zwischen den Werten der Skalarpolarisierbarkeiten, welche unter Verwendung der Modelle des Baryon ChPT Ansatzes beziehungsweise des DR Frameworks gewonnen wurden, durch Inkonsistenzen innerhalb der Daten der DR- basierten Analyse bedingt sind. Um

diese Inkonsistenzen zu beseitigen, schlagen wir vor, den Wirkungsquerschnitt der unpolarisierten Compton-Streuung bei einer Energie von $\nu \approx 110$ MeV und unter Rückwärtswinkeln zu messen. Bezüglich der Spinpolarisierbarkeiten sind die von uns, unter Verwendung der aus unterschiedlichen Fitanpassungen extrahierten Werte, untereinander konsistent. Ebenso decken sie sich mit den Werten, welche in der Baryon ChPT sowie der DR-basierten Analyse gewonnen wurden.

Die von uns vorgestellte Multipolanalyse der Compton-Streuung ist die Erste ihrer Art. Es ist unsere Überzeugung, dass sie uns in naher Zukunft die einzigartige Möglichkeit eröffnen wird, präzise Werte der Polarisierbarkeiten auf modellunabhängigem Wege zu erhalten. Die Erreichbarkeit dieses Ziels wird durch die Verbesserung des existierenden Datenbestands durch experimentelle Einrichtungen auf der ganzen Welt innerhalb der kommenden Jahre erleichtert. Im Besonderen sind dies das Mainzer Mikrotron sowie die derzeit im Aufbau befindliche, neue Linearbeschleunigeranlage MESA, welche einen Elektronenstrahl mit sehr hoher Intensität bereitstellen wird.

Contents

Table of Contents	v
List of Publications	vii
1 Introduction and Thesis Outline	1
1.1 Introduction	1
1.2 Thesis Outline	7
1.3 List of Abbreviations	9
2 Methods	11
2.1 Introduction	11
2.2 Effective Lagrangian and Polarizabilities	12
2.2.1 Lagrangian for a Pointlike Proton	13
2.2.2 Contribution of Polarizabilities to Lagrangian	14
2.3 Multipole Expansion of Compton Amplitude	17
2.3.1 Derivation of $\hat{L}_{J\pi\zeta\zeta'}(\vec{k}', \vec{k})$	17
2.3.2 Derivation of the Helicity Amplitudes	23
2.3.3 Relation between the Polarizabilities and Multipoles	25
2.4 Summary	26
2.5 Supplementary Material	27
3 Low-energy Expansion of Observables	29
3.1 Introduction	29
3.2 CS Cross Section and Spin Asymmetries	29
3.3 Invariant Response Functions	32
3.4 Low-energy Expansion. Contribution of Scalar Polarizabilities	34
3.5 Low-energy Expansion of $d\sigma/d\Omega$	36
3.6 Low-energy Expansion of Σ_3	37
3.7 Measurement of Σ_3	39
3.8 Contribution of Spin Polarizabilities to R_i Functions and Σ_3	45
3.9 Low-energy Expansion of Σ_{2x} and Σ_{2z}	48
3.10 Summary	50
3.11 Supplementary Material	51
4 Multipole Expansion of Observables	57
4.1 Introduction	57
4.2 Description of the Method	58

4.2.1	Born Contribution to $f_{\rho'\rho}^{\ell\pm}$	58
4.2.2	Non-Born Contribution to $f_{\rho\rho'}^{\ell\pm}$	60
4.2.3	Observables in Terms of Multipoles	62
4.3	Fitting to Experimental Data	64
4.4	Results and Discussion	66
4.4.1	Unpolarized Cross Section	67
4.4.2	Multipoles	70
4.4.3	Polarizabilities	71
4.4.4	Asymmetries	73
4.5	Summary	77
4.6	Supplementary Material	79
5	Concluding Remarks	83
	Bibliography	87

List of Publications

This thesis is based on the following papers

- N. Krupina, V. Lensky and V. Pascalutsa
"Towards a model-independent extraction of proton polarizabilities by means of multipole analysis of Compton scattering data"
In preparation.
- V. Sokhoyan, E. J. Downie, E. Mornacchi, J. A. McGovern, N. Krupina et al.
"Determination of the scalar polarizabilities of the proton using beam asymmetry Σ_3 in Compton scattering"
arXiv:1611.03769 [nucl-ex].
- N. Krupina
"Proton polarizabilities from polarized Compton scattering. Low-energy expansion"
PoS Bormio2014 (2014) 027
- N. Krupina and V. Pascalutsa
"Separation of proton polarizabilities with the beam asymmetry of Compton scattering"
Phys. Rev. Lett. 110 (2013) no.26, 262001 doi:10.1103/PhysRevLett.110.262001 [arXiv:1304.7404 [nucl-th]].

Introduction and Thesis Outline

1.1 Introduction

In the 1910s Ernest Rutherford in his famous series of scattering experiments [Rutherford 1911] demonstrated that the positive charge of an atom and most of its mass is attributed to a tiny core, the atomic nucleus. Furthermore, he argued that these cores always contain the nucleus of the smallest atom — hydrogen. He assumed that this nucleus can be regarded as the simplest structureless building block of matter, and suggested to name it 'proton' after the Greek word for 'first'. During the next decades this new particle was under a thorough investigation, and in the mid-twentieth century, it became clear that the proton itself is a non-point particle. Since then the structure of the proton was among the hottest topics in both theoretical and experimental physics.

The bulk of our current understanding of the proton structure comes from the Standard Model of particle physics (see, e.g., Refs. [Schwartz 2014, Spiesberger 2000]), which unifies the theories of Electroweak, and strong (Quantum chromodynamics or in short QCD) interactions. The Electroweak theory provides a combined description of the electromagnetic (described by Quantum electrodynamics or QED) and weak forces. The former force acts between charged particles and is mediated by the photon. It is used, in particular, to describe the internal structure of the matter, e.g., bound states of an electron and a proton, i.e., the hydrogen atom. The weak interaction introduced to explain beta decay occurs between all particles in the Standard Model, and is mediated by the massive W^\pm and Z^0 bosons. Finally, QCD describes the strong interactions between quarks and gluons, which make up hadrons (strongly interacting particles, such as proton, neutron etc.). At the level of the Lagrangian, QCD is almost as simple as QED, the main difference is the non-abelian nature of the underlying interactions. However, despite of that the physics of the strong interactions is very complicated and rich. It exhibits a range of fascinating phenomena, e.g., color confinement (see, e.g., [Greensite 2011]), mass gap [Jaffe], chiral symmetry breaking [Cheng 1984, Wilczek 1999], quark-gluon plasma [Braun-Munzinger 2007, Arsene 2005, Adcox 2005, Back 2005, Adams 2005, Khachatryan 2015] etc.

The proton in the Standard Model [Gell-Mann 1964, Zweig 1964a, Zweig 1964b] is a system of three interacting valence quarks and an arbitrary number of quark-antiquark pairs and gluons. However, in spite of having this theoretical set-up, we still lack its complete description.

The reason is that one needs to perform calculations in QCD, which enjoys color confinement. The latter implies that at small energies (correspondingly large distances) the strong coupling constant α_s is large¹, making standard techniques from perturbation theory useless. Therefore, one needs to utilise other methods, for instance, one can employ the lattice QCD [Creutz 1985, Rothe 2005, Gattringer 2010, Wilson 1974], chiral effective field theory (also referred to as chiral perturbation theory (ChPT)) [Weinberg 1979, Gasser 1984, Gasser 1988] or Dispersion relation (DR) [Nussenzweig 1972, Hamilton 1975]. The results of these methods, however, are not always accurate and often give the largest uncertainties in calculations. For instance, the dominant part of the uncertainty in the calculations of the anomalous magnetic moment of the muon is due to hadronic effects, see Refs. [Miller 2007, Jegerlehner 2009, Miller 2012].

Besides the lattice QCD and other approaches listed above, one could use the low-energy or multipole expansions of observables to develop model-independent methods for interpreting experimental data. In this thesis we discuss this approach in detail, as we employ it to extract the polarizabilities of the proton.

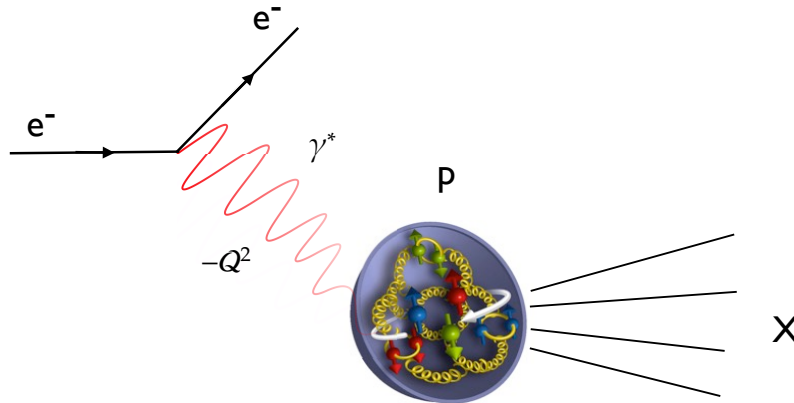


Figure 1.1: A schematic diagram of the electron-proton scattering. The particles interact via a virtual photon with virtuality $-Q^2$, see the text for details. In the case of the elastic scattering X denotes the outgoing proton, whereas in the inelastic case it stands for the produced new particles (hadrons).

Traditional experimental tools to study the proton structure are the elastic and inelastic electron-proton (e-p) scattering processes (see Fig. 1.1). The interaction in these processes is mediated by a virtual photon with virtuality $-Q^2$, and described by the four structure functions $f_1(\nu, Q^2)$, $f_2(\nu, Q^2)$, $g_1(\nu, Q^2)$ and $g_2(\nu, Q^2)$ with ν being the photon energy (see, e.g., Refs. [Drechsel 2003] and [Yndurain 2006]). In the elastic scattering one can measure the charge and density distributions inside the proton, as in this case the structure functions, and hence the measured cross sections, are parametrized by the electric $G_E(Q^2)$ and magnetic $G_M(Q^2)$ Sachs

¹Note that at high energies α_s is a small parameter (phenomenon known as asymptotic freedom). This feature of the QCD was first noted by David Politzer, Frank Wilczek and David Gross [Gross 1973, Politzer 1973]. For their discovery they were awarded the Nobel Prize in Physics in 2004.

form factors, which are the Fourier transforms of the charge and magnetization density distributions. In the inelastic case the structure functions, and hence observables, at high Q are related to the parton distribution functions (PDFs) [Peskin 1995, Collins 2012, Feltesse 2010], whereas at low Q they can be connected to the physical quantities called polarizabilities [Drechsel 2003]. For instance, the sum rule involving $f_1(\nu, Q^2)$, i.e., $\int d\nu f_1(\nu, Q^2)/\nu^3$, is related to the sum of the electric $\alpha_{E1}(Q^2)$ and magnetic $\beta_{M1}(Q^2)$ generalized dipole polarizabilities.

The polarizabilities of the proton are of main interest to us, and before we discuss them in more detail, let us recall their classical definitions. It is known that if one places a macroscopic system in the uniform electric field \vec{E} , negative and positive charges will move in opposite directions, creating an electric dipole moment. For an isotropic system in a weak field this dipole moment is given by $\alpha_{E1}\vec{E}$. If now one places the same system in the uniform magnetic field \vec{H} instead of \vec{E} , intrinsic dipole moments will align with \vec{H} , inducing the magnetic dipole moment $\beta_{M1}\vec{H}$. Thus, we see that the response of the system to weak external fields is fully characterized by the so-called electric and magnetic polarizabilities α_{E1} and β_{M1} . On the one hand, the knowledge of these quantities gives us a valuable theoretical insight into the internal structure of the system. On the other hand, α_{E1} and β_{M1} are of fundamental importance in applications as they quantify the stiffness of the system.

In the 1950s the classical polarizabilities inspired the introduction of a similar concept for protons [Klein 1955, Baldin 1960]. It turns out that the values of the proton polarizabilities are small when measured in natural units. Indeed, the polarizabilities have dimension $length^3$ and the proton polarizabilities are several orders of magnitude smaller² than the volume of the proton ($\alpha_{E1} \sim 10^{-3} \text{ fm}^3$ and $\beta_{M1} \sim 10^{-4} \text{ fm}^3$). Even though α_{E1} and β_{M1} are tiny in this sense, the knowledge of them is crucial for a precision determination of other quantities. For instance, they are the main source of the uncertainty in theoretical calculations of the muonic hydrogen Lamb shift, and, hence, in the extracted value of the proton charge radius (see, e.g., Ref. [Carlson 2015]). At the present time this uncertainty is a hot topic of debate in the physics community due to the so-called proton radius puzzle – the inconsistency in the measured values of the proton radius [Pohl 2010, Bernauer 2014].

It is not feasible to measure α_{E1} and β_{M1} by placing a proton in the static \vec{E} and \vec{H} . Indeed, small values of α_{E1} and β_{M1} imply that the proton is very stiff, and, to induce any measurable dipole moment, one needs very strong external fields, which are not available in laboratories. Nevertheless, the polarizabilities can be accessed experimentally in low-energy Compton scattering (CS) on protons if the photon energy ν in this process is not too small. Indeed, if the photon wavelength becomes smaller than the size of the proton, (starting from $\nu \approx 50 \text{ MeV}$), the internal structure of the proton is resolved and the effect of the polarizabilities can be measured. To extract the polarizabilities from the obtained data, one first isolates the contribution

²For atoms, for comparison, they are estimated to be of the order of \AA^3 (cf. Ref. [Holstein 2014]).

of the polarizabilities to observables by expanding the CS amplitude in powers of energy. Then one evaluates this contribution by analyzing the experimental data. Let us illustrate these steps by considering the unpolarized cross section, $d\sigma/d\Omega_{lab}$, see also Section 3.5. To write it in terms of the polarizabilities we expand the CS amplitude. The lowest-order energy-independent term in the obtained expansion is called the Thomson amplitude [Low 1954, Gell-Mann 1954a]. It assumes that the photon wavelength is much larger than the proton which is then treated simply as an unpolarizable point particle with mass M , and charge e . With higher powers of the photon energy come other contributions, e.g., with the first power³ comes the contribution of the anomalous magnetic moment, κ , then of α_{E1} and β_{M1} , then of the four spin polarizabilities, γ_{E1E1} , γ_{M1M1} , γ_{M1E2} , and γ_{E1M2} , etc. see Refs. [Griesshammer 2012, Holstein 2014] and also Eqs. (2.8) and (2.13). Having expanded the CS amplitude we write the leading-order non-Born (NB) contribution to the cross section. This contribution is determined by the polarizabilities or more precisely by the linear combination of α_{E1} and β_{M1}

$$\frac{d\sigma^{(NB)}}{d\Omega_{lab}} = -\frac{\alpha}{M} \left(\frac{\nu'}{\nu}\right)^2 \nu\nu' \left[\alpha_{E1} (1 + \cos^2 \theta_{lab}) + 2\beta_{M1} \cos \theta_{lab} \right] + O(\nu^3), \quad (1.1)$$

where $\alpha = e^2/(4\pi) \simeq 1/137$ is the fine-structure constant, ν and ν' are, respectively, the energies of the incoming and outgoing photons in the laboratory frame, and θ_{lab} is the scattering angle (see Supplementary Material 3.11). At very low energies ($\nu \leq 50$ MeV) the effect of the polarizabilities is suppressed by the factor $\nu\nu'$, and, therefore, it cannot be separated from the Born term in modern experiments. On the other hand, at higher energies, the contribution of α_{E1} and β_{M1} is large and a precision measurement of $d\sigma/d\Omega_{lab}$ at different angles should allow one to extract α_{E1} and β_{M1} , cf. Fig. 1.2. The ideal energy region to measure α_{E1} and β_{M1} is $\nu \approx 50 - 100$ MeV, as at higher energies the higher order (spin, quadrupole etc.) polarizabilities complicate the analysis.

These simple theoretical considerations motivated a number of experimental groups to measure the unpolarized cross section for low-energy CS (see table 4.1 for references) and to use the collected data to determine the polarizabilities. We present α_{E1} and β_{M1} found in this way together with the most recent theoretical results in Fig. 1.3. The theoretical calculations here are done within baryon chiral perturbation theory (BChPT), see Ref. [Lensky 2015], and heavy baryon chiral perturbation theory (HBChPT), see Ref. [McGovern 2013]. We also show the PDG values [Olive 2014], which combine the Dispersion relation (DR) [Olmos de Leon 2001] and the HBChPT results (see Table 1.1). Note that due to the differences between the BChPT and the DR approaches⁴, their outcomes are not guaranteed to coincide. The figure indeed shows

³Here the zeroth- and first-order terms in energy are often called the Born amplitude, and all the other terms, which are defined by the polarizabilities, the non-Born amplitude.

⁴For example, the DR approach requires the knowledge of the unpolarized Compton scattering data to fix $\alpha_{E1} - \beta_{M1}$, whereas BChPT and HBChPT predict α_{E1} and β_{M1} (up to $O(p^4)$) without it.

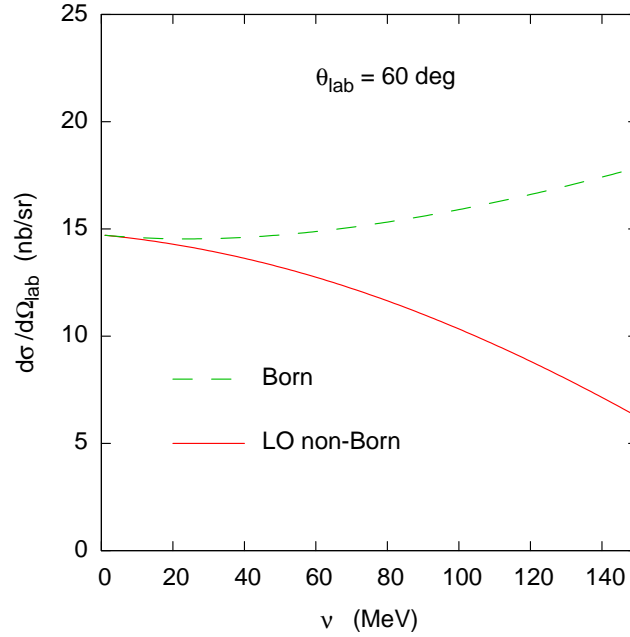


Figure 1.2: The unpolarized cross section as a function of the photon energy at $\theta_{lab} = 60$ degrees. The green dashed curve depicts the Born part of the cross section, and the red solid curve corresponds to the Born part together with the leading-order contribution of the polarizabilities (cf. Eq. (1.1)).

that some of these analyses are not in unison with the others. For instance, the value of the magnetic polarizability, obtained using the DR approach with the unpolarized CS data, is not consistent with the one calculated within the BChPT approach (see Table 1.1). The source of

Table 1.1: The values of α_{E1} and β_{M1} in units 10^{-4} fm^3 obtained from BChPT and DR as well as the values quoted in PDG.

	α_{E1}	β_{M1}
BChPT	11.2 ± 0.7	3.9 ± 0.7
DR fit	12.1	1.6
PDG (2014)	11.2 ± 0.4	2.5 ± 0.4

this discrepancy has not been yet understood, and further theoretical and experimental studies are required to resolve it.

In this dissertation we propose other means (cf. the LEX and MEX below) of determining the magnetic polarizability that can potentially resolve the discrepancy between BChPT and DR.

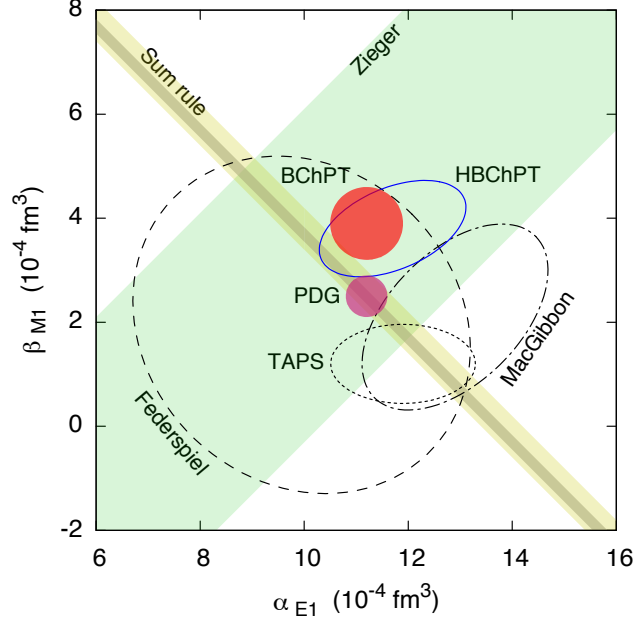


Figure 1.3: The values for the proton scalar polarizabilities. The magenta blob represents the PDG summary [Olive 2014]. The experimental data are from Federspiel et al. [Federspiel 1991], Zieger et al. [Zieger 1992], MacGibbon et al. [MacGibbon 1995], and TAPS [Olmos de Leon 2001]. The ‘Sum Rule’ shaded area corresponds to the Baldin sum rule evaluations of $\alpha_{E1} + \beta_{M1}$ in Ref. [Olmos de Leon 2001] (broader band) and in Ref. [Babusci 1998b] (narrow band). The red blob represents the BChPT prediction from Ref. [Lensky 2015], and the blue ellipse is due to the HBChPT fit from Ref. [McGovern 2013].

Another goal of this thesis is to establish the values of the spin polarizabilities γ_{E1E1} , γ_{M1M1} , γ_{E1M2} and γ_{M1E2} by analyzing higher-order corrections to Eq. (1.1). These polarizabilities define higher-order corrections to observables and are important at energies above $\nu \approx 100$ MeV. This investigation is timely and important in particular due to the recent experiments at MAMI, in which the effect of these quantities can be measured [Martel 2015].

To reach our goals we use two model-independent theoretical approaches based on the low-energy expansion (LEX) and the multipole expansion (MEX) of CS observables. Both approaches satisfy basic symmetries, such as invariance under parity, time-reversal, gauge and Lorentz transformations. However, the parameters in these theories are different. Within the LEX approach the CS amplitude $T_{H',H}$ (here H' and H are the total helicities of the final and initial states respectively) is expressed in terms of the mass, charge, anomalous magnetic moment, two scalar polarizabilities, and four spin polarizabilities. Within the MEX approach $T_{H',H}$ is expressed in terms of multipole amplitudes which depend on energy. An advantage of the MEX over the LEX is that it has larger energy-range of applicability, i.e., while the LEX approach is accurate only up to the photon energy $\nu \approx 100$ MeV, the MEX does not have such limitations. However, the number of parameters (multipoles) in the latter approach depends on the energy region, i.e., the

larger the energy, the larger the number of multipoles that should be taken into account. In this thesis we limit ourselves to the energies below the pion production threshold, i.e., $\nu < 150$ MeV. At these energies to a good approximation one can truncate the series of the MEX at angular momentum $J = 3/2$.

As these approaches are cornerstones of this thesis, let us discuss them in more detail. In the LEX we write the amplitude $T_{H',H}$ using the effective Lagrangian \mathcal{L} , that describes the Compton scattering on the proton at low energies. In doing so we introduce the main physical quantities of this work, i.e., the scalar and spin polarizabilities, in a Lorentz-invariant fashion. Having obtained the amplitude we construct various CS observables, and study their sensitivity to the polarizabilities. For instance, we show (cf. Ref. [Krupina 2013]) that the beam asymmetry depends only on the magnetic polarizability, see Eq. (3.24). This is a very important observation as it allows one to find β_{M1} by direct measurement.

In the MEX below the pion production threshold we parametrize the amplitude $T_{H',H}$ by ten parameters (multipoles). We divide these multipoles into the Born and non-Born parts. The Born part depends only on M , e and κ , and we calculate it exactly. The non-Born part contains the polarizabilities of interest. To isolate them we develop a fitting procedure that uses the existing unpolarized CS data as an input [Krupina 2016]. The main results here are the values of the polarizabilities listed in Table 4.5.

1.2 Thesis Outline

Chapter 2 presents the basic ingredients of the two frameworks that we use and introduces the main physical quantities of this thesis, i.e., the scalar and spin polarizabilities of the proton. We start by writing the effective Lagrangian that describes CS on the proton at low energies, thus, providing us with a starting point for the discussion of the LEX-based approach. We first discuss the terms of the Lagrangian that describe a pointlike proton and yield the Born part of the Feynman CS amplitude, and then the terms that define the scalar and spin polarizabilities. The latter are used in Chapter 3 to calculate the non-Born part of the amplitude. Subsequently, we present the derivation of the multipole expansion of the CS amplitudes. This expansion is utilized in Chapter 4 to obtain the multipole expansion of CS observables. At the end of Chapter 2 we relate the multipoles to the polarizabilities. The obtained relations are essential elements of the approach developed in Chapter 4 to calculate the polarizabilities.

Chapter 3 presents the low-energy expansions of the four Compton scattering observables, the unpolarized cross section, $d\sigma/d\Omega$, the beam asymmetry, Σ_3 , and the beam-target asymmetries, Σ_{2x} and Σ_{2z} , and analyzes the sensitivity of these observables to the scalar and spin polarizabilities. This analysis puts Σ_3 forward (cf. Ref. [Krupina 2013] and Ref. [Sokhoyan 2016]) as a

possible candidate for the precision determination of the magnetic polarizability, β_{M1} , as it is difficult to extract β_{M1} directly from the low-energy unpolarized cross section. It also suggests that Σ_{2x} and Σ_{2z} should be used to measure the spin polarizabilities, since $d\sigma/d\Omega$ and Σ_3 are mainly sensitive to the scalar polarizabilities.

Chapter 4 presents a MEX-based approach which yields values of the polarizabilities. Here we discuss the method and its main ingredient – the relation between the multipoles with $\ell = 1$ and the static polarizabilities (cf. Ref. [Krupina 2016]). Using this relation we find the polarizabilities by fitting them to the existing experimental data. We explain all the details of the employed fitting procedure, i.e., we show the used data, we discuss the constraints that had to be implemented to reduce the number of fitted parameters etc. The results obtained using the unpolarized CS data are presented in Table 4.5.

Chapter 5 concludes the thesis with the summary of the results presented in the previous chapters.

1.3 List of Abbreviations

BChPT	baryon chiral perturbation theory
CM	center-of-mass
CS	Compton scattering
DR	dispersion relation
HBChPT	heavy baryon chiral perturbation theory
LEX	low-energy expansion
MAMI	Mainz Microtron
MEX	multipole expansion
NB	non-Born
NLO	next-to-leading order
NNLO	next-to-next-to-leading order
PDG	Particle data group
QED	quantum electrodynamics
QCD	quantum chromodynamics

Methods

This chapter introduces the main physical quantities of this thesis, i.e., the scalar and spin polarizabilities, and theoretical frameworks that we will use to calculate them.

2.1 Introduction

In this thesis we present two model-independent approaches to analyze Compton scattering on the proton that utilise the LEX and the MEX of Compton observables. This chapter contains important definitions and derivations that we later use in Chapters 3 and 4 to develop these approaches.

The starting point for the LEX-based approach is the effective Lagrangian that describes the photon-proton interaction at low energies. It naturally satisfies all the basic symmetries, such as Lorentz and gauge invariance as well as discrete symmetries (parity, charge conjugation and time reversal invariance), and, hence, allows us to introduce the main physical quantities of this work, i.e., the scalar and spin polarizabilities, in a Lorentz-invariant fashion. An advantage of this method is that we can use the non-relativistic limit as a reference point. In particular, we use the fact that in this limit the terms that contain the scalar and spin polarizabilities must yield the well-known effective Hamiltonian

$$\begin{aligned}
 \mathcal{H}_{eff}^{(2)} &= -4\pi \left[\frac{1}{2} \alpha_{E1} \vec{E}^2 + \frac{1}{2} \beta_{M1} \vec{H}^2 \right], \\
 \mathcal{H}_{eff}^{(3)} &= -4\pi \left[\frac{1}{2} \gamma_{E1E1} \vec{\sigma} \cdot (\vec{E} \times \dot{\vec{E}}) + \frac{1}{2} \gamma_{M1M1} \vec{\sigma} \cdot (\vec{H} \times \dot{\vec{H}}) \right. \\
 &\quad \left. - \gamma_{M1E2} E_{ij} \sigma_i H_j + \gamma_{E1M2} H_{ij} \sigma_i E_j \right],
 \end{aligned} \tag{2.1}$$

where $\dot{\vec{E}} = \partial_t \vec{E}$, $\dot{\vec{H}} = \partial_t \vec{H}$, $E_{ij} = \frac{1}{2}(\nabla_i E_j + \nabla_j E_i)$, $H_{ij} = \frac{1}{2}(\nabla_i H_j + \nabla_j H_i)$. The superscripts (2), (3) denote the number of space-time derivatives of the electromagnetic field $A^\nu(x)$ (see the discussion below).

The starting point for the MEX-based approach is the scattering matrix $\hat{S}(\vec{k}', \vec{k})$ that contains all information about the scattering. In practical calculations one usually extracts this information in the form of the helicity amplitude, $T_{H', H} \equiv \langle \theta \varphi H' | \hat{S} | 00 H \rangle$, which describes the $2 \rightarrow 2$ process with given initial (H) and final (H') helicities. The angles ($\theta_0 = 0, \varphi_0 = 0$) here define

the direction of the relative momentum of the incoming particles with the helicities σ and λ , thus, $H \equiv \sigma - \lambda$. The variables $\theta, \varphi, \sigma', \lambda'$ and H' are used for the respective characteristics of the outgoing particles. In this thesis we analyze Compton scattering using the multipole expansion of these amplitudes. This expansion is known [Pfeil 1974], however, because we are not aware of a reference with its full derivation, we obtain it for convenience of the reader in this chapter.

The chapter is organized as follows. In Section 2.2 we introduce the effective Lagrangian. Here, we firstly list the terms of the Lagrangian that describe the pointlike proton and yield the Born part of the Feynman CS amplitude. Secondly, in Subsection 2.2.2 we write down the piece that contains the scalar polarizabilities, i.e., α_{E1} and β_{M1} . Thirdly, in the same subsection we present the term that defines the spin polarizabilities γ_{E1E1} , γ_{M1M1} , γ_{E1M2} and γ_{M1E2} . In addition to that, Subsection 2.2.2 contains also the original part of this chapter — the contributions of the scalar and spin polarizabilities to the invariant amplitudes $\mathcal{A}_1, \dots, \mathcal{A}_8$ from Ref. [Pascalutsa 2003]. In Section 2.3 we derive the multipole expansion of the CS amplitudes, and present the result in Eq. (2.52) in terms of the conventional multipole amplitudes (multipoles). In Subsection 2.3.3 we relate these multipoles to the polarizabilities. Later, in Chapter 4, we develop an approach that uses these relations to establish the polarizabilities. Finally, for the sake of completeness, we sketch in the Supplementary Material how to obtain the Feynman amplitude from the introduced Lagrangian.

2.2 Effective Lagrangian and Polarizabilities

In this section we present the effective Lagrangian \mathcal{L} that describes the electromagnetic structure of the proton at low energies. For convenience, we divide \mathcal{L} into the non-interacting, \mathcal{L}_0 , and interacting, $\mathcal{L}_1 + \mathcal{L}_{\text{pol}}$, parts, i.e.,

$$\mathcal{L} = \mathcal{L}_0 + \mathcal{L}_1 + \mathcal{L}_{\text{pol}}, \quad (2.2)$$

where \mathcal{L}_0 describes the propagation of free photon and proton. The first term in the interacting Lagrangian, i.e., \mathcal{L}_1 , is linear in the photon field $A^\nu(x)$ and describes the interaction of the photon with a pointlike proton. It includes only the well-known mass of the proton, M , its electric charge, e , and anomalous magnetic moment, κ . The second term of the interacting part, \mathcal{L}_{pol} , is quadratic in $A^\nu(x)$ and defines the polarizabilities. We organize \mathcal{L}_{pol} in classes according to the number of derivatives of the photon field¹ $A^\nu(x)$,

$$\mathcal{L}_{\text{pol}} = \mathcal{L}_2 + \mathcal{L}_3 + \dots \quad (2.3)$$

¹On the level of the CS amplitude this ordering corresponds to the small momentum expansion, because a derivative in coordinate space implies the photon momentum in momentum space.

Here the term with two derivatives of $A^\nu(x)$ (\mathcal{L}_2) contains the scalar polarizabilities α_{E1} and β_{M1} , whereas the term with three derivatives (\mathcal{L}_3) includes the spin polarizabilities² γ_{E1E1} , γ_{M1M1} , γ_{E1M2} and γ_{M1E2} . The terms with a higher number of derivatives ($\mathcal{L}_{i>3}$) contain the higher order polarizabilities [Holstein 2000]. For instance, the spin-independent fourth-order term (\mathcal{L}_4) in the Lagrangian contains the fourth-order scalar polarizabilities $\alpha_{E\nu}$, $\beta_{M\nu}$, α_{E2} and β_{M2} . However, as these higher order polarizabilities will not be discussed in the thesis, we do not introduce here the terms \mathcal{L}_i with $i > 3$.

2.2.1 Lagrangian for a Pointlike Proton

Here we present \mathcal{L}_0 and \mathcal{L}_1 terms of the Lagrangian given in Eq. (2.2). The former term here describes a free photon and a free proton, i.e.,

$$\mathcal{L}_0 = -\frac{1}{4}F^{\mu\nu}F_{\mu\nu} + \bar{N}(x)(i\gamma^\mu\partial_\mu - M)N(x), \quad (2.4)$$

where $F^{\mu\nu} = \partial^\mu A^\nu(x) - \partial^\nu A^\mu(x)$ is the electromagnetic field-strength tensor, $N(x)$ is the proton Dirac-spinor field, and γ^μ is the Dirac matrix. And the latter term includes the $NN\gamma$ interaction (see e.g. [Peskin 1995])

$$\mathcal{L}_1 = -e\bar{N}(x)\gamma^\mu A_\mu(x)N(x) - \frac{ie\kappa}{4M}\bar{N}(x)\gamma^{\mu\nu}N(x)F_{\mu\nu},$$

where $\gamma^{\mu\nu} \equiv \frac{1}{2}(\gamma^\mu\gamma^\nu - \gamma^\nu\gamma^\mu)$. This term assumes that a proton is a point³, and describes such a proton in an electromagnetic field.

Now, using this Lagrangian we calculate the Born contribution to the Feynman CS amplitude (see Fig. 3.1a and 3.1b). For this purpose we first find the Feynman rules for the $NN\gamma$ vertex and the proton propagator (see Supplementary Material 2.5), and then use them to write down the Feynman amplitude

$$i\mathcal{M}_B^{\mu\nu} = -i\Gamma^\mu(p', p+k)\frac{\not{p} + \not{k} + M}{s - M^2}\Gamma^\nu(p+k, p) - i\Gamma^\nu(p', p'-k)\frac{\not{p}' - \not{k} + M}{u - M^2}\Gamma^\mu(p'-k, p), \quad (2.5)$$

where $i\Gamma^\mu(p', p+k) = ie\gamma^\mu - \frac{ie}{2M}\kappa(\gamma^{\mu\rho}p'_\rho - \gamma^{\mu\delta}(p+k)_\delta)$ is the electromagnetic vertex, k is the four-momentum of the incoming photon, p (p') is the four-momentum of the incoming (outgoing) proton, and s, u are the Mandelstam variables (see Supplementary Material 3.11). Note that, in principle, the derived terms describe not only a proton but any pointlike charged spin-1/2

²The expressions for \mathcal{L}_2 , \mathcal{L}_3 are given in Eqs. (2.6) and (2.12). Note, however, that we could have written these terms in a different form. For instance, we could have included $\bar{N}\gamma_5 N \tilde{F}^{\mu\nu} F_{\mu\nu}$ (where $F^{\mu\nu} = \partial^\mu A^\nu(x) - \partial^\nu A^\mu(x)$ and $\tilde{F}_{\mu\nu} = \epsilon_{\mu\nu\rho\sigma}F^{\rho\sigma}/2$) in \mathcal{L}_2 , as it contains two derivatives. This term is, however, related to the spin polarizabilities due to an additional momentum in $\bar{N}\gamma_5 N$, and therefore we include it in \mathcal{L}_3 , see Eq. (2.12).

³A pointlike proton is fully characterized by its mass, electric charge and anomalous magnetic moment.

particle described by the spin-1/2 particle field $N(x)$.

2.2.2 Contribution of Polarizabilities to Lagrangian

Scalar polarizabilities We write down the term \mathcal{L}_2 from Eq. (2.3), introducing the scalar polarizabilities in a Lorentz-invariant fashion (cf. Ref. [Belousova 2000a]), as

$$\mathcal{L}^{(2)} = -\frac{2\pi}{M^2}(\partial_\alpha \bar{N})(\partial_\beta N)(\alpha_{E1} F^{\alpha\rho} F_\rho^\beta + \beta_{M1} \widetilde{F}^{\alpha\rho} \widetilde{F}_\rho^\beta), \quad (2.6)$$

where $\widetilde{F}_{\mu\nu} = \epsilon_{\mu\nu\rho\sigma} F^{\rho\sigma}/2$ with $\epsilon_{\mu\nu\rho\sigma}$ being the Levi-Civita symbol with $\epsilon_{0123} = 1$. Let us first verify that this term yields the well-known Hamiltonian in the static limit, i.e.,

$$\mathcal{H}_{eff}^{(2)} = -4\pi \left[\frac{1}{2} \alpha_{E1} \vec{E}^2 + \frac{1}{2} \beta_{M1} \vec{H}^2 \right], \quad (2.7)$$

where \vec{E} and \vec{H} are the electric and magnetic fields. In order to do this, we work in the proton rest frame where $\partial_i N = 0$, $\partial_0 N = -iMN$, $\partial_0 \bar{N} = iM\bar{N}$, and, hence,

$$\mathcal{H}_{eff}^{(2)} = -\mathcal{L}_2 = -2\pi \left\{ \beta_{M1} (\vec{H}^2 - \vec{E}^2) + (\alpha_{E1} + \beta_{M1}) \vec{E}^2 \right\} \bar{N}N,$$

note that to obtain this expression we have used the identities $\widetilde{F}^{\alpha\rho} \widetilde{F}_\rho^\beta = F^{\alpha\rho} F_\rho^\beta - \frac{1}{2} \delta^{\alpha\beta} F^2$ and $F^2 = -2(F^{0i})^2 + (F^{ij})^2 = -2\vec{E}^2 + 2\vec{H}^2$.

The Lagrangian in Eq. (2.6) yields the following Feynman amplitude (see graph 3.1c and Supplementary Material 2.5)

$$\begin{aligned} i \mathcal{M}_{NB(2)}^{\mu\nu} &= 4\pi i \left[\beta_{M1} (k \cdot k' g^{\mu\nu} - k^\mu k'^\nu) \right. \\ &\quad \left. - \frac{\alpha_{E1} + \beta_{M1}}{2M^2} (p'_\alpha p_\beta + p_\alpha p'_\beta) (k'^\alpha k^\beta g^{\mu\nu} - k'^\alpha k^\mu g^{\nu\beta} - k'^\nu k^\beta g^{\mu\alpha} + k \cdot k' g^{\mu\alpha} g^{\nu\beta}) \right], \end{aligned} \quad (2.8)$$

where $g_{\mu\nu} = \text{diag}(1, -1, -1, -1)$ is the Minkowski metric and k' is the four-momentum of the outgoing photon. The subscript *NB* indicates that it is the non-Born contribution to the amplitude, whereas (2) indicates that this term is obtained from \mathcal{L}_2 .

Finally we show that the helicity amplitude obtained from $\mathcal{M}_{NB(2)}^{\mu\nu}$ and the standard amplitude (cf. Ref. [Pascalutsa 2003]) differ in their higher-order (in energy) terms. To this end, we write the helicity amplitude

$$\begin{aligned} T_{H'H} &= \bar{u}_{\lambda'}(p') \mathcal{M}_{NB(2)}^{\mu\nu} \varepsilon'_{(\sigma')\mu} \varepsilon_{(\sigma)\nu} u_\lambda(p) \\ &= \bar{u}_{\lambda'}(p') \left(-\mathcal{A}_1^{(NB)}(s, t) \varepsilon'_{(\sigma')} \cdot \varepsilon_{(\sigma)} + \mathcal{A}_2^{(NB)}(s, t) k \cdot \varepsilon'_{(\sigma')} k' \cdot \varepsilon_{(\sigma)} \right) u_\lambda(p), \end{aligned} \quad (2.9)$$

where s, t are the Mandelstam variables (see Supplementary Material 3.11), and $\mathcal{E}_{(\sigma)}$ is the gauge-invariant polarization vector, i.e.,

$$\mathcal{E}_{(\sigma)\mu}(k) = \varepsilon_{(\sigma)\mu}(k) - \frac{(p+p') \cdot \varepsilon_{(\sigma)}}{(p+p') \cdot k} k_\mu. \quad (2.10)$$

The functions $\mathcal{A}_1^{(\text{NB})}$, $\mathcal{A}_2^{(\text{NB})}$ are

$$\mathcal{A}_1^{(\text{NB})}(s, t) = 2\pi(\alpha_{E1} + \beta_{M1})(v^2 + v'^2) + 4\pi M\beta_{M1}(v' - v), \quad (2.11a)$$

$$\mathcal{A}_2^{(\text{NB})}(s, t) = -4\pi\beta_{M1} - \frac{\pi t}{2M^2}(\alpha_{E1} + \beta_{M1}), \quad (2.11b)$$

where v and v' denote the energies of the incident and scattered photon in the laboratory frame respectively (see Supplementary Material 3.11). Note that these functions are Lorentz invariant as they are written in terms of the invariant variables v , v' and t . The function $\mathcal{A}_1^{(\text{NB})}$ in Eq. (2.11a) differs from the conventional definition (cf. Ref. [Lensky 2015]) by $-(\pi/M^2)(\alpha_{E1} + \beta_{M1})t(\omega_B^2 - \frac{1}{4}t)$ and $\mathcal{A}_2^{(\text{NB})}$ by $-\frac{\pi t}{2M^2}(\alpha_{E1} + \beta_{M1})$. However, we have checked that this difference does not affect our LEX results. In particular, it does not affect the contribution (from the terms up to and including $O(v^4)$) of the scalar polarizabilities to the beam asymmetry, see Chapter 3.

Spin polarizabilities Here we discuss the term \mathcal{L}_3 in Eq. (2.3), which describes the interaction between the induced electromagnetic moments and the spin of proton (cf. [Belousova 2000b]),

$$\begin{aligned} \mathcal{L}_3 &= \frac{\pi}{4M^2} \left(\bar{N} \left(\vec{\partial}_\alpha \vec{\partial}_\beta + \vec{\partial}_\beta \vec{\partial}_\alpha \right) \gamma^\mu \gamma^5 N \right) \\ &\times \left\{ -\frac{1}{2} \gamma_{E1E1} F^{\alpha\nu} \vec{\partial}_\beta \vec{F}_{\mu\nu} + \frac{1}{2} \gamma_{M1M1} \vec{F}^{\alpha\nu} \vec{\partial}_\beta F_{\mu\nu} \right. \\ &\left. - \gamma_{M1E2} \left(F^{\alpha\nu} \vec{\partial}_\mu \vec{F}_\nu^\beta - \vec{F}^{\alpha\nu} \vec{\partial}_\nu F_\mu^\beta \right) + \gamma_{E1M2} \left(\vec{F}^{\alpha\nu} \vec{\partial}_\mu F_\nu^\beta - F^{\alpha\nu} \vec{\partial}_\nu \vec{F}_\mu^\beta \right) \right\}, \end{aligned} \quad (2.12)$$

here $\vec{\partial}_\alpha = \vec{\partial}_\alpha - \vec{\partial}_\alpha$ and $\gamma^5 = i\gamma^0\gamma^1\gamma^2\gamma^3$ is the fifth Dirac matrix. Note that \mathcal{L}_3 introduces the spin polarizabilities in a Lorentz-invariant fashion. In the non-relativistic limit this Lagrangian yields the well-known Hamiltonian

$$\begin{aligned} \mathcal{H}_{eff}^{(3)} &= -4\pi \left[\frac{1}{2} \gamma_{E1E1} \vec{\sigma} \cdot (\vec{E} \times \dot{\vec{E}}) + \frac{1}{2} \gamma_{M1M1} \vec{\sigma} \cdot (\vec{H} \times \dot{\vec{H}}) \right. \\ &\left. - \gamma_{M1E2} E_{ij} \sigma_i H_j + \gamma_{E1M2} H_{ij} \sigma_i E_j \right], \end{aligned} \quad (2.13)$$

where $\dot{\vec{E}} = \partial_t \vec{E}$, $\dot{\vec{H}} = \partial_t \vec{H}$, $E_{ij} = \frac{1}{2}(\nabla_i E_j + \nabla_j E_i)$, $H_{ij} = \frac{1}{2}(\nabla_i H_j + \nabla_j H_i)$. The relativistic corrections to Eq. (2.13) can depend on the particular choice of \mathcal{L}_3 . However, since in this thesis we investigate the leading-order effect of the spin polarizabilities on the observables, we do not discuss possible choices of the leading-order spin-polarizabilities coupling other than included in Eq. (2.12).

The Lagrangian \mathcal{L}_3 yields the Feynman amplitude (see graph 3.1c and Supplementary Material 2.5),

$$\begin{aligned}
 \mathcal{M}_{\text{NB}(3)}^{\mu\nu} = & \frac{\pi}{4M^2} \left\{ \gamma_{E1E1} \left[-2\gamma^{\alpha\nu\mu} (k_\alpha + k'_\alpha) k \cdot P^2 - 2\gamma^{\alpha\beta\nu} k_\alpha k'_\beta P^\mu k \cdot P - 2\gamma^{\alpha\beta\mu} k_\alpha k'_\beta P^\nu k \cdot P \right] \right. \\
 & + \gamma_{E1M2} \left[-2\gamma^{\alpha\beta\nu} k_\alpha k'_\beta P^\mu k \cdot P - 2\gamma^{\alpha\beta\mu} k_\alpha k'_\beta P^\nu k \cdot P - 2\gamma^{\alpha\nu\mu} (k_\alpha + k'_\alpha) k \cdot P^2 \right. \\
 & + 4\gamma^{\alpha\beta\nu} P_\alpha k_\beta k^\mu k \cdot P - 4\gamma^{\alpha\beta\nu} P_\alpha k_\beta P^\mu k \cdot k' - 4\gamma^{\alpha\beta\mu} P_\alpha k'_\beta k'^\nu k \cdot P + 4\gamma^{\alpha\beta\mu} P_\alpha k'_\beta P^\nu k \cdot k' \left. \right] \\
 & + \gamma_{M1E2} \left[-2\gamma^{\alpha\beta\nu} k_\alpha k'_\beta P^\mu k \cdot P - 2\gamma^{\alpha\beta\mu} k_\alpha k'_\beta P^\nu k \cdot P - 2\gamma^{\alpha\nu\mu} (k_\alpha + k'_\alpha) k \cdot P^2 \right. \\
 & - 4\gamma^{\alpha\beta\rho} P_\alpha k_\beta k'_\rho (g^{\mu\nu} k \cdot P - k^\mu P^\nu - P^\mu k'^\nu) + 4\gamma^{\alpha\nu\mu} P_\alpha k \cdot k' k \cdot P - 4\gamma^{\alpha\beta\mu} P_\alpha k_\beta P^\nu k \cdot k' \\
 & + 4\gamma^{\alpha\beta\nu} P_\alpha k'_\beta P^\mu k \cdot k' \left. \right] \\
 & + \gamma_{M1M1} \left[-2\gamma^{\alpha\beta\nu} k_\alpha k'_\beta P^\mu k \cdot P - 2\gamma^{\alpha\beta\mu} k_\alpha k'_\beta P^\nu k \cdot P - 2\gamma^{\alpha\nu\mu} (k_\alpha + k'_\alpha) k \cdot P^2 \right. \\
 & + 4\gamma^{\alpha\beta\rho} P_\alpha k_\beta k'_\rho g^{\mu\nu} k \cdot P - 4\gamma^{\alpha\beta\mu} P_\alpha k_\beta k'^\nu k \cdot P + 4\gamma^{\alpha\beta\nu} P_\alpha k'_\beta k^\mu k \cdot P \\
 & \left. + 4\gamma^{\alpha\nu\mu} P_\alpha k \cdot k' k \cdot P \right\}, \tag{2.14}
 \end{aligned}$$

where $\gamma^{\mu\nu\rho} = \frac{1}{2}(\gamma^{\mu\nu}\gamma^\rho + \gamma^\rho\gamma^{\mu\nu})$, $P = p + p'$, and we have used the identity $k \cdot P = k' \cdot P$. As before, the subscript *NB* indicates that it is the non-Born contribution to the amplitude; (3) indicates that this term is obtained from \mathcal{L}_3 .

The presented expressions allow us to calculate the contribution of the spin polarizabilities to the invariant amplitudes, and, hence, to observables. For this we write the helicity amplitude⁴

$$\begin{aligned}
 T_{H'H} &= \bar{u}_\lambda(p') \mathcal{M}_{\text{NB}(3)}^{\mu\nu} \varepsilon'_{(\sigma')\mu} \varepsilon_{(\sigma)\nu} u_\lambda(p) \\
 &= \bar{u}_\lambda(p') \left\{ -\mathcal{A}_1^{\text{NB}(3)}(s, t) \varepsilon'_{(\sigma')} \cdot \varepsilon_{(\sigma)} + \mathcal{A}_2^{\text{NB}(3)}(s, t) k \cdot \varepsilon'_{(\sigma')} k' \cdot \varepsilon_{(\sigma)} \right. \\
 &- \mathcal{A}_3^{\text{NB}(3)}(s, t) (\varepsilon'_{(\sigma')} \cdot \gamma \cdot \varepsilon_{(\sigma)}) + \mathcal{A}_4^{\text{NB}(3)}(s, t) (k' \cdot \gamma \cdot k) \varepsilon'_{(\sigma')} \cdot \varepsilon_{(\sigma)} \\
 &+ \mathcal{A}_5^{\text{NB}(3)}(s, t) \left[(k' \cdot \gamma \cdot \varepsilon_{(\sigma)}) k \cdot \varepsilon'_{(\sigma')} - (k \cdot \gamma \cdot \varepsilon'_{(\sigma')}) k' \cdot \varepsilon_{(\sigma)} \right] \\
 &+ \mathcal{A}_6^{\text{NB}(3)}(s, t) \left[(k \cdot \gamma \cdot \varepsilon_{(\sigma)}) k \cdot \varepsilon'_{(\sigma')} - (k' \cdot \gamma \cdot \varepsilon'_{(\sigma')}) k' \cdot \varepsilon_{(\sigma)} \right] \\
 &\left. + \mathcal{A}_7^{\text{NB}(3)}(s, t) (k' \cdot \gamma \cdot k) k \cdot \varepsilon'_{(\sigma')} k' \cdot \varepsilon_{(\sigma)} - \mathcal{A}_8^{\text{NB}(3)}(s, t) i\gamma_5 \varepsilon^{\mu\nu\alpha\beta} \varepsilon'_{(\sigma')\mu} \varepsilon_{(\sigma)\nu} k'_\alpha k_\beta \right\} u_\lambda(p), \tag{2.15}
 \end{aligned}$$

where we use the notation $k' \cdot \gamma \cdot k \equiv k'_\mu \gamma^{\mu\nu} k_\nu$. The functions $\mathcal{A}_1^{\text{NB}(3)}, \dots, \mathcal{A}_8^{\text{NB}(3)}$ are

$$\begin{aligned}
 \mathcal{A}_1^{\text{NB}(3)}(s, t) &= -\frac{\pi}{2} t (v + v')^2 (\gamma_{M1E2} - \gamma_{M1M1}), \\
 \mathcal{A}_2^{\text{NB}(3)}(s, t) &= -\pi (v + v')^2 (\gamma_{E1M2} + \gamma_{M1M1}), \\
 \mathcal{A}_3^{\text{NB}(3)}(s, t) &= \frac{\pi}{2} (v + v') \left[(v + v')^2 \gamma_0 - 2t (\gamma_{M1E2} + \gamma_{M1M1}) \right], \\
 \mathcal{A}_4^{\text{NB}(3)}(s, t) &= -\frac{\pi}{2} (-4 + t) (v + v') (\gamma_{M1E2} - \gamma_{M1M1}), \tag{2.16}
 \end{aligned}$$

⁴Note that to write the amplitude in a covariant form we need to use the eight invariant amplitudes $\mathcal{A}_1 - \mathcal{A}_8$ from Ref. [Pascalutsa 2003]. However, one can show that this form can be reduced to the one with the six standard independent CS amplitudes (see, e.g., [McGovern 2001]).

$$\begin{aligned}
 \mathcal{A}_5^{\text{NB}(3)}(s, t) &= \frac{\pi}{4} (v + v') [t (\gamma_{E1M2} + \gamma_{M1E2}) + 8\gamma_{M1M1}], \\
 \mathcal{A}_6^{\text{NB}(3)}(s, t) &= -\frac{\pi}{4} (v + v') [(-8 + t)\gamma_{E1M2} + t\gamma_{M1E2}], \\
 \mathcal{A}_7^{\text{NB}(3)}(s, t) &= \pi (v + v') (\gamma_{E1M2} + \gamma_{M1M1}), \\
 \mathcal{A}_8^{\text{NB}(3)}(s, t) &= -\frac{\pi}{2} (v + v')^2 \gamma_0,
 \end{aligned}$$

where $\gamma_0 = -\gamma_{E1E1} - \gamma_{E1M2} - \gamma_{M1E2} - \gamma_{M1M1}$.

2.3 Multipole Expansion of Compton Amplitude

The scattering processes for particles with spin can be described by means of the scattering matrix \hat{S} , which connects the initial state i to the corresponding final state f . For systems invariant under rotations and reflections, this matrix conserves the total angular momentum J , its projection M , and the parity π , allowing one to write it as

$$\hat{S}(\vec{k}', \vec{k}) = \sum_{JM\pi\zeta\zeta'} |\psi_{JM\pi\zeta'}^{*f}(\vec{k}')\rangle S_J^{fi}(\omega) \langle \psi_{JM\pi\zeta}^i(\vec{k}) |, \quad (2.17)$$

here ζ and ζ' are additional quantum numbers needed to describe the system, $\langle \psi_{JM\pi\zeta}^{i(f)}(\vec{k}) |$ is the operator that yields the probability for the system to be in the state characterized by the set $\{J, M, \pi, \zeta\}$, $\psi_{JM\pi\zeta}^{i(f)}(\vec{k})$, and $S_J^{fi}(\omega)$ are the partial-wave amplitudes. To emphasize that the projection operators describe only the geometry of the process, the above expression is often rearranged as

$$\hat{S}(\vec{k}', \vec{k}) = \sum_{J\pi\zeta\zeta'} S_J^{fi}(\omega) \sum_M |\psi_{JM\pi\zeta'}^{*f}(\vec{k}')\rangle \langle \psi_{JM\pi\zeta}^i(\vec{k}) | = \sum_{J\pi\zeta\zeta'} S_J^{fi}(\omega) \hat{L}_{J\pi\zeta\zeta'}(\vec{k}', \vec{k}), \quad (2.18)$$

where $\hat{L}_{J\pi\zeta\zeta'}(\vec{k}', \vec{k})$ is the so-called angular operator, which for Compton scattering was first derived in Ref. [Ritus 1957].

In this thesis we analyze Compton scattering using the multipole expansion of the helicity amplitudes $T_{H',H}$. We derive this expansion in two steps. First, in Subsection 2.3.1 we obtain $\hat{L}_{J\pi\zeta\zeta'}$, see Eqs. (2.42) and (2.45). After that, in Subsection 2.3.2, we use this operator to write down the scattering matrix $\hat{S}(\vec{k}', \vec{k})$, and to compute the helicity amplitude $T_{H',H}$. The latter is written in terms of the conventional multipole amplitudes in Eq. (2.52).

2.3.1 Derivation of $\hat{L}_{J\pi\zeta\zeta'}(\vec{k}', \vec{k})$

To derive $\hat{L}_{J\pi\zeta\zeta'}(\vec{k}', \vec{k})$ we consider Compton scattering in the center-of-mass (CM) frame (see Section 3.11). We assume that the initial (final) photon propagates in the direction of the unit

vector \vec{k} (\vec{k}') with the total angular momentum j (j'), its projection m (m'), the orbital angular momentum l (l'), and spin 1.

First, we decompose the wave function of the system into the wave function of the photon $\vec{D}_{jm}(\vec{k})$ and the wave function of the proton $\mathcal{Q}_{1/2\lambda}$

$$\psi_{JM\pi\zeta}(\vec{k}) = \sum_{\lambda} C_{jM-\lambda,1/2\lambda}^{JM} \vec{D}_{jM-\lambda}(\vec{k}) \mathcal{Q}_{1/2\lambda}, \quad (2.19)$$

where $\lambda = \pm 1/2$ is the spin projection of the proton, $C_{jM-\lambda,1/2\lambda}^{JM}$ is the Clebsch-Gordan coefficient, and $\mathcal{Q}_{1/2\lambda}$ is the Pauli spinor. With $\vec{D}_{jM-\lambda}(\vec{k})$ we denote a linear combination of the three spherical harmonics with spin, i.e., $\vec{D}_{jM-\lambda}(\vec{k})$, with $l = j, j \pm 1$ (see Eq. (2.25) below). The decomposition in Eq. 2.19 allows us to rewrite the angular operator as

$$\hat{L} = \sum_{\lambda'\lambda} L^{\lambda'\lambda} \mathcal{Q}_{1/2\lambda'} \mathcal{Q}_{1/2\lambda}^{\dagger}, \quad (2.20)$$

where the indices J, M, π, ν are omitted for simplicity, and

$$L^{\lambda'\lambda} \equiv \sum_M C_{j'M-\lambda',1/2\lambda'}^{JM} C_{jM-\lambda,1/2\lambda}^{JM} \vec{D}_{j'M-\lambda'}(\vec{k}') \vec{D}_{jM-\lambda}^*(\vec{k}). \quad (2.21)$$

For convenience, from now on, we will use the notation $|\uparrow\rangle$ ($|\downarrow\rangle$) for the spin operator with a positive (negative) spin projection $|\mathcal{Q}_{1/21/2}\rangle$ ($|\mathcal{Q}_{1/2-1/2}\rangle$). Using this notation, we rewrite the angular operator from Eq. (2.20)

$$\hat{L} = L^{\uparrow\uparrow} |\uparrow\rangle\langle\uparrow| + L^{\uparrow\downarrow} |\uparrow\rangle\langle\downarrow| + L^{\downarrow\uparrow} |\downarrow\rangle\langle\uparrow| + L^{\downarrow\downarrow} |\downarrow\rangle\langle\downarrow|, \quad (2.22)$$

where $L^{\uparrow\uparrow} = L^{\frac{1}{2}\frac{1}{2}}$, $L^{\uparrow\downarrow} = L^{\frac{1}{2}-\frac{1}{2}}$ etc. The corresponding matrix form of this operator is

$$\hat{L} = L^{\uparrow\uparrow} \frac{1}{2}(1 + \sigma_z) + L^{\uparrow\downarrow} \frac{1}{2}(\sigma_x + i\sigma_y) + L^{\downarrow\uparrow} \frac{1}{2}(\sigma_x - i\sigma_y) + L^{\downarrow\downarrow} \frac{1}{2}(1 - \sigma_z), \quad (2.23)$$

where, to obtain the Pauli matrices σ_x, σ_y and σ_z , we use the vector representation of the proton wave functions, i.e.,

$$|\uparrow\rangle = \begin{pmatrix} 1 \\ 0 \end{pmatrix}, \quad |\downarrow\rangle = \begin{pmatrix} 0 \\ 1 \end{pmatrix}. \quad (2.24)$$

The photon wave function. We see that the operator \hat{L} requires the knowledge of $\vec{D}_{jm}(\vec{k})$, which following Ref. [Akhiezer 1965] we write as

$$\vec{D}_{jm}(\vec{k}) = \sum_{l=j-1}^{j+1} a_l \vec{D}_{jlm}(\vec{k}), \quad (2.25)$$

where the spherical harmonic with spin is

$$\vec{D}_{jlm}(\vec{k}) = \sum_{\sigma} C_{lh,1\sigma}^{jm} Y_{lh}(\vec{k}) \vec{\varepsilon}_{\sigma}. \quad (2.26)$$

Here $Y_{lh}(\vec{k})$ is the spherical harmonic function of degree l and order h , $h \leq |l|$ is the projection of orbital momentum, $\vec{\varepsilon}_{\sigma}$ is the photon polarization vector with $\sigma = \pm 1$ being the spin projection of the photon. Notice that the coefficients a_l in Eq. (2.25) are not independent, because $\vec{D}_{jm}(\vec{k})$ must satisfy the transversality condition

$$\vec{D}_{jm}(\vec{k}) \cdot \vec{k} = 0, \quad (2.27)$$

here we denote with $\vec{a} \cdot \vec{c}$ the scalar product of vectors \vec{a} and \vec{c} . Therefore, there are only two different photon states with given quantum numbers j and m . We denote them $\vec{D}_{jm}^{(0)}(\vec{k})$ and $\vec{D}_{jm}^{(1)}(\vec{k})$. These functions are (cf. Ref. [Akhiezer 1965])

$$\vec{D}_{jm}^{(1)}(\vec{k}) = i\vec{D}_{jjm}(\vec{k}) \times \vec{k} = \frac{1}{\sqrt{j(j+1)}} \left(\frac{\partial}{\partial \vec{k}} - \vec{k} \left(\vec{k} \cdot \frac{\partial}{\partial \vec{k}} \right) \right) Y_{jm}(\vec{k}), \quad (2.28)$$

$$\vec{D}_{jm}^{(0)}(\vec{k}) = \vec{D}_{jjm}(\vec{k}) = -\frac{i}{\sqrt{j(j+1)}} \vec{k} \times \frac{\partial}{\partial \vec{k}} Y_{jm}(\vec{k}), \quad (2.29)$$

here we denote with $\vec{a} \times \vec{c}$ the cross product of vectors \vec{a} and \vec{c} . It can be shown that $\vec{D}_{jm}^{(1)}(\vec{k})$ and $\vec{D}_{jm}^{(0)}(\vec{k})$ have parities $(-1)^j$ and $(-1)^{j+1}$ and correspond to states of electric and magnetic type. The expressions that we will derive are cumbersome, however, we find them easier to read using the following notations for the dot and cross products $\vec{a} \cdot \vec{c} \rightarrow (\vec{a}\vec{c})$ and $\vec{a} \times \vec{c} \rightarrow [\vec{a}\vec{c}]$, which we use everywhere below.

To write the helicity amplitude it is enough to have projections of these wave functions onto the states with definite helicity. To obtain them, we take the scalar product of $\vec{D}_{jm}^{(1)}(\vec{k})$ ($\vec{D}_{jm}^{(0)}(\vec{k})$) and $\vec{\varepsilon}_{\sigma}^*$, i.e.,

$$\left(\vec{\varepsilon}_{\sigma}^* \vec{D}_{jm}^{(1)}(\vec{k}) \right) = \frac{1}{\sqrt{j(j+1)}} \left(\vec{\varepsilon}_{\sigma}^* \frac{\partial}{\partial \vec{k}} \right) Y_{jm}(\vec{k}), \quad (2.30)$$

$$\left(\vec{\varepsilon}_{\sigma}^* \vec{D}_{jm}^{(0)}(\vec{k}) \right) = \frac{1}{\sqrt{j(j+1)}} \left(i[\vec{k}\vec{\varepsilon}_{\sigma}^*] \frac{\partial}{\partial \vec{k}} \right) Y_{jm}(\vec{k}). \quad (2.31)$$

From now on instead of $\vec{D}_{jm}^{(1)}(\vec{k})$ and $\vec{D}_{jm}^{(0)}(\vec{k})$ we use $(\vec{\varepsilon}_{\sigma}^* \vec{D}_{jm}^{(1)}(\vec{k}))$ and $(\vec{\varepsilon}_{\sigma}^* \vec{D}_{jm}^{(0)}(\vec{k}))$.

Allowed transitions. Clearly, not all transitions from j to j' can be realized in nature. Therefore, to write down a meaningful $L^{\lambda\lambda}$, we need to establish transitions allowed by the parity and total angular momentum conservation laws. The rules of addition of angular momenta connect

the quantum numbers J , j' and j in the following way

$$J = j + 1/2 = j' + 1/2, \quad J = j - 1/2 = j' - 1/2, \quad (2.32)$$

$$J = j + 1/2 = j' - 1/2, \quad J = j - 1/2 = j' + 1/2. \quad (2.33)$$

The parity conservation gives another relation between j' and j . For instance, when the initial and final photons are in electric modes (below called the EE transition), then the parity conservation law is $(-1)^j = (-1)^{j'}$. This law implies that $j' = j + 2n$, where n is an integer. Therefore, this scenario is realised only for J given in Eq. (2.32)

$$EE \quad (-1)^j = (-1)^{j'}, \quad J = j + 1/2 = j' + 1/2, \quad J = j - 1/2 = j' - 1/2. \quad (2.34)$$

Similar arguments applied to other transitions yield

$$\begin{aligned} EM \quad & (-1)^j = (-1)^{j'+1}, \quad J = j + 1/2 = j' - 1/2, \quad J = j - 1/2 = j' + 1/2, \\ ME \quad & (-1)^{j+1} = (-1)^{j'}, \quad J = j + 1/2 = j' - 1/2, \quad J = j - 1/2 = j' + 1/2, \\ MM \quad & (-1)^{j+1} = (-1)^{j'+1}, \quad J = j + 1/2 = j' + 1/2, \quad J = j - 1/2 = j' - 1/2. \end{aligned} \quad (2.35)$$

Below we derive the operator \hat{L} for the EE and EM transitions. The results for the other transitions can be obtained in a similar way.

EE transition. According to Eq. (2.34) the conservation of the total angular momentum and parity in the photon-proton system leads to the following relation between the angular momentum of initial and final photons

$$j' = j, \quad (2.36)$$

which allows us to write the function $L^{\lambda\lambda}$ from Eq. (2.21) as

$$\begin{aligned} L_{EE}^{\lambda\lambda} &= \frac{1}{j(j+1)} \left(\vec{\varepsilon}' \frac{\partial}{\partial \vec{k}'} \right)^* G_{EE}^{\lambda\lambda}, \quad \text{where} \\ G_{EE}^{\lambda\lambda} &\equiv \sum_M C_{jM-\lambda', \frac{1}{2}\lambda'}^{JM} C_{jM-\lambda, \frac{1}{2}\lambda}^{JM} \left(\vec{\varepsilon}' \frac{\partial}{\partial \vec{k}'} \right) Y_{jM-\lambda'}(\vec{k}') Y_{jM-\lambda}^*(\vec{k}). \end{aligned} \quad (2.37)$$

Here we omit the subscript σ' (σ) of vector $\vec{\varepsilon}'$ ($\vec{\varepsilon}$) for simplicity. Inserting these expressions in Eq. (2.23), we write down the angular operator,

$$\begin{aligned} \hat{L}_{EE} &= \frac{1}{j(j+1)} \left(\vec{\varepsilon}' \frac{\partial}{\partial \vec{k}'} \right)^* G_{EE} \equiv \frac{1}{j(j+1)} \left(\vec{\varepsilon}' \frac{\partial}{\partial \vec{k}'} \right)^* \times \\ &\left[\frac{1}{2}(1 + \sigma_z) G_{EE}^{\frac{1}{2}\frac{1}{2}} + \frac{1}{2}(\sigma_x + i\sigma_y) G_{EE}^{\frac{1}{2}-\frac{1}{2}} + \frac{1}{2}(\sigma_x - i\sigma_y) G_{EE}^{-\frac{1}{2}\frac{1}{2}} + \frac{1}{2}(1 - \sigma_z) G_{EE}^{-\frac{1}{2}-\frac{1}{2}} \right]. \end{aligned} \quad (2.38)$$

The EE transition assumes two possible values of j , i.e., $j = J - 1/2$ and $j = J + 1/2$ (see Eq. (2.34)), which will yield two elements in the scattering matrix. Therefore, to proceed further, we need calculate the G_{EE} function for both values of j . For this we assume, that $\vec{k}' = (0, 0, 1)$ and $\vec{k} = (\sin \theta \cos \phi, \sin \theta \sin \phi, \cos \theta)$ (later we show, that this assumption does not affect the generality of the final results). Then $Y_{jM-\lambda'}(\vec{k}') \neq 0$ only if $M = \lambda'$. Furthermore, in this case $M - \lambda = \lambda' - \lambda = 0, \pm 1$, and, therefore, only the following spherical harmonics should be taken into account

$$\begin{aligned} Y_{j0}^*(\vec{k}) &= \sqrt{2j+1} P_j(\cos \theta), & Y_{j1}^*(\vec{k}) &= -\sqrt{\frac{2j+1}{j(j+1)}} \sin \theta P'_j(\cos \theta) e^{-i\varphi}, \\ Y_{j-1}^*(\vec{k}) &= \sqrt{\frac{2j+1}{j(j+1)}} \sin \theta P'_j(\cos \theta) e^{i\varphi}, & Y_{j0}(\vec{k}) &= \sqrt{2j+1}, \end{aligned} \quad (2.39)$$

where $P_j(\cos \theta)$ is the j th Legendre polynomial, and the derivative of $P_j(\cos \theta)$ is taken with respect to its argument. After straightforward but tedious calculations we obtain G_{EE} for $j = J - 1/2$,

$$G_{EE} = \left\{ (J + 1/2) (\vec{k}' \vec{\varepsilon}) - i (\vec{\sigma} [\vec{k}' \vec{\varepsilon}]) \right\} P'_{J-1/2} - i (\vec{k}' \vec{\varepsilon}) (\vec{\sigma} [\vec{k}' \vec{k}]) P''_{J-1/2}, \quad (2.40)$$

and G_{EE} for $j = J + 1/2$,

$$G_{EE} = \left\{ (J + 1/2) (\vec{k}' \vec{\varepsilon}) + i (\vec{\sigma} [\vec{k}' \vec{\varepsilon}]) \right\} P'_{J+1/2} + i (\vec{k}' \vec{\varepsilon}) (\vec{\sigma} [\vec{k}' \vec{k}]) P''_{J+1/2}, \quad (2.41)$$

where the argument of the Legendre polynomials is $(\vec{k}' \vec{k})$. Note that expressions in (2.40) do not depend on the direction of \vec{k}' individually, but on its relative position with respect to \vec{k} and $\vec{\varepsilon}$. Therefore, we can always rotate the system to direct \vec{k}' along the z-axis as the rotation of the whole system does not change G_{EE} . This means that the assumption we made above about the direction of \vec{k}' does not affect the result for the function G_{EE} but simplifies the calculation. Finally, we substitute Eq. (2.40) into Eq. (2.38), and take the derivative with respect to \vec{k}' . This yields

$$\begin{aligned} \hat{L}_{EE}^{J-1/2} &= \frac{1}{(J-1/2)(J+1/2)} \left\{ \left[(J+1/2) (\varepsilon^{\vec{k}'} \vec{\varepsilon}) - i (\vec{\sigma} [\varepsilon^{\vec{k}'} \vec{\varepsilon}]) \right] P'_{J-1/2} + \left[(J+1/2) (\vec{k}' \vec{\varepsilon}) (\varepsilon^{\vec{k}'} \vec{k}) \right. \right. \\ &- i (\vec{\sigma} [\vec{k}' \vec{\varepsilon}]) (\varepsilon^{\vec{k}'} \vec{k}) - i (\vec{\sigma} [\vec{k}' \vec{k}]) (\varepsilon^{\vec{k}'} \vec{\varepsilon}) - i (\vec{\sigma} [\varepsilon^{\vec{k}'} \vec{k}]) (\vec{k}' \vec{\varepsilon}) \left. \right] P''_{J-1/2} \\ &- i (\vec{\sigma} [\vec{k}' \vec{k}]) (\vec{k}' \vec{\varepsilon}) (\varepsilon^{\vec{k}'} \vec{k}) P'''_{J-1/2} \left. \right\}, \end{aligned}$$

$$\begin{aligned}
 \hat{L}_{EE}^{J+1/2} &= \frac{1}{(J+1/2)(J+3/2)} \left\{ [(J+1/2)(\vec{\varepsilon}^{\vec{s}^*} \vec{\varepsilon}^{\vec{s}}) + i(\vec{\sigma}[\vec{\varepsilon}^{\vec{s}^*} \vec{\varepsilon}^{\vec{s}}])] P'_{J+1/2} + [(J+1/2)(\vec{k}' \vec{\varepsilon}^{\vec{s}})(\vec{\varepsilon}^{\vec{s}^*} \vec{k}) \right. \\
 &+ i(\vec{\sigma}[\vec{k}' \vec{\varepsilon}^{\vec{s}}])(\vec{\varepsilon}^{\vec{s}^*} \vec{k}) + i(\vec{\sigma}[\vec{k}' \vec{k}]) (\vec{\varepsilon}^{\vec{s}^*} \vec{\varepsilon}^{\vec{s}}) + i(\vec{\sigma}[\vec{\varepsilon}^{\vec{s}^*} \vec{k}]) (\vec{k}' \vec{\varepsilon}^{\vec{s}})] P''_{J+1/2} \\
 &\left. + i(\vec{\sigma}[\vec{k}' \vec{k}]) (\vec{k}' \vec{\varepsilon}^{\vec{s}})(\vec{\varepsilon}^{\vec{s}^*} \vec{k}) P'''_{J+1/2} \right\},
 \end{aligned} \tag{2.42}$$

where the superscript of \hat{L}_{EE}^j defines the total angular momentum of the initial photon, j . Note that Eq. (2.42) is written in a slightly different form, compared with the corresponding equation in Ref. [Ritus 1957]. However, we checked that they are equivalent.

EM transition. For the EM transition the function $L^{\lambda\lambda}$ from Eq. (2.21) reads

$$L_{EM}^{\lambda\lambda} = \frac{1}{\sqrt{j'(j'+1)j(j+1)}} \left(i[\vec{k}' \varepsilon^{\vec{s}^*}] \frac{\partial}{\partial \vec{k}'} \right) \left(\vec{\varepsilon}^{\vec{s}} \frac{\partial}{\partial \vec{k}} \right) \sum_M C_{j'M-\lambda', \frac{1}{2}\lambda'}^{JM} C_{jM-\lambda, \frac{1}{2}\lambda}^{JM} Y_{j'M-\lambda'}(\vec{k}') Y_{jM-\lambda}^*(\vec{k}), \tag{2.43}$$

where the conservation of total angular momentum and parity (see Eq. (2.35)) implies that j' can take only the following values

$$\begin{aligned}
 j' &= J - 1/2, & \text{for } j &= J + 1/2, \\
 j' &= J + 1/2, & \text{for } j &= J - 1/2.
 \end{aligned} \tag{2.44}$$

We do the steps similar to the ones we have presented in the *EE* case and obtain the angular operator \hat{L}_{EM}

$$\begin{aligned}
 \hat{L}_{EM}^{J+1/2} &= \frac{i}{(J+1/2)\sqrt{(J-1/2)(J+3/2)}} \left\{ -(J-1/2) [(\vec{\sigma} \vec{s}^{\vec{s}})(\vec{k}' \vec{\varepsilon}^{\vec{s}}) + (\vec{\sigma} \vec{k}')(\vec{s}^{\vec{s}} \vec{\varepsilon}^{\vec{s}})] P'_{J+1/2} \right. \\
 &+ [-(J-3/2)(\vec{\sigma} \vec{k}')(\vec{k}' \vec{\varepsilon}^{\vec{s}})(\vec{s}^{\vec{s}} \vec{k}) - (\vec{\sigma} \vec{\varepsilon}^{\vec{s}})(\vec{s}^{\vec{s}} \vec{k}) - (\vec{\sigma} \vec{k})(\vec{s}^{\vec{s}} \vec{\varepsilon}^{\vec{s}}) + (\vec{\sigma} \vec{s}^{\vec{s}})(\vec{k}' \vec{\varepsilon}^{\vec{s}})(\vec{k}' \vec{k}) \\
 &\left. + (\vec{\sigma} \vec{k}')(\vec{s}^{\vec{s}} \vec{\varepsilon}^{\vec{s}})(\vec{k}' \vec{k})] P''_{J+1/2} - (\vec{s}^{\vec{s}} \vec{k})(\vec{k}' \vec{\varepsilon}^{\vec{s}}) [(\vec{\sigma} \vec{k}) - (\vec{\sigma} \vec{k}')(\vec{k}' \vec{k})] P'''_{J+1/2} \right\}, \\
 \hat{L}_{EM}^{J-1/2} &= \frac{i}{(J+1/2)\sqrt{(J-1/2)(J+3/2)}} \left\{ -(J+3/2) [(\vec{\sigma} \vec{s}^{\vec{s}})(\vec{k}' \vec{\varepsilon}^{\vec{s}}) + (\vec{\sigma} \vec{k}')(\vec{s}^{\vec{s}} \vec{\varepsilon}^{\vec{s}})] P'_{J-1/2} \right. \\
 &+ [-(J+5/2)(\vec{\sigma} \vec{k}')(\vec{k}' \vec{\varepsilon}^{\vec{s}})(\vec{s}^{\vec{s}} \vec{k}) + (\vec{\sigma} \vec{\varepsilon}^{\vec{s}})(\vec{s}^{\vec{s}} \vec{k}) + (\vec{\sigma} \vec{k})(\vec{s}^{\vec{s}} \vec{\varepsilon}^{\vec{s}}) - (\vec{\sigma} \vec{s}^{\vec{s}})(\vec{k}' \vec{\varepsilon}^{\vec{s}})(\vec{k}' \vec{k}) \\
 &\left. - (\vec{\sigma} \vec{k}')(\vec{s}^{\vec{s}} \vec{\varepsilon}^{\vec{s}})(\vec{k}' \vec{k})] P''_{J-1/2} + (\vec{s}^{\vec{s}} \vec{k})(\vec{k}' \vec{\varepsilon}^{\vec{s}}) [(\vec{\sigma} \vec{k}) - (\vec{\sigma} \vec{k}')(\vec{k}' \vec{k})] P'''_{J-1/2} \right\},
 \end{aligned} \tag{2.45}$$

where $\vec{s}^{\vec{s}} \equiv [\vec{k}' \varepsilon^{\vec{s}^*}]$.

The angular operators that correspond to the absorption of a magnetic photon, i.e., the *MM* and *ME* transitions, can be obtained from Eqs. (2.42) and (2.45) by the following replacements

- (i) $\vec{\varepsilon} \rightarrow -i[\vec{k}\vec{\varepsilon}]$ in Eqs. (2.42) and (2.45),
- (ii) $\vec{\varepsilon}^{\vec{\lambda}^*} \rightarrow i[\vec{k}'\vec{\varepsilon}^{\vec{\lambda}^*}]$ in Eq. (2.42),
- (iii) $i[\vec{k}'\vec{\varepsilon}^{\vec{\lambda}^*}] \rightarrow \vec{\varepsilon}^{\vec{\lambda}^*}$ in Eq. (2.45).

2.3.2 Derivation of the Helicity Amplitudes

In this section we derive the helicity amplitude, $T_{H',H}$. Recall that, by definition, it describes the probability of the scattering in the (θ, φ) -direction for the incoming, along the z-axis, flux. In Ref. [Jacob 1959], M. Jacob and G. C. Wick showed that for rotationally and parity invariant systems the helicity amplitudes offer the most convenient way to describe the scattering processes of particles with spin. For Compton scattering this follows from the observation that the operator \hat{L} given in Eq. (2.42) maps an initial state of the photon-proton system with the helicity H to a state with the helicity H' simply times the Wigner d-function. For example, for the EE transition with positive helicities of the initial and final particles (i.e., $H = H' = 1/2$) we have

$$\begin{aligned} \langle \mathcal{Q}_{1/2\,1/2} | \hat{L}_{EE}^{J-1/2} | \mathcal{Q}_{1/2\,1/2} \rangle &= \left(\sin \frac{\theta}{2}, -e^{-i\varphi} \cos \frac{\theta}{2} \right) \hat{L}_{EE}^{J-1/2} \begin{pmatrix} 0 \\ -1 \end{pmatrix} = 1/2 (J - 1/2) e^{-i\varphi} d_{\frac{1}{2}\frac{1}{2}}^J(\theta), \\ \langle \mathcal{Q}_{1/2\,1/2} | \hat{L}_{EE}^{J+1/2} | \mathcal{Q}_{1/2\,1/2} \rangle &= \left(\sin \frac{\theta}{2}, -e^{-i\varphi} \cos \frac{\theta}{2} \right) \hat{L}_{EE}^{J+1/2} \begin{pmatrix} 0 \\ -1 \end{pmatrix} = 1/2 (J + 3/2) e^{-i\varphi} d_{\frac{1}{2}\frac{1}{2}}^J(\theta), \end{aligned} \quad (2.46)$$

where $d_{H'H}^J(\theta)$ is the Wigner d-function [Varshalovich 1988] and the spin functions of the proton in an arbitrary direction (θ, φ) are given by [Landau 1965]

$$\mathcal{Q}_{1/2\,1/2}(\theta, \varphi) = \begin{pmatrix} \cos \frac{\theta}{2} \\ e^{i\varphi} \sin \frac{\theta}{2} \end{pmatrix}, \quad \mathcal{Q}_{1/2\,-1/2}(\theta, \varphi) = \begin{pmatrix} -e^{-i\varphi} \sin \frac{\theta}{2} \\ \cos \frac{\theta}{2} \end{pmatrix}. \quad (2.47)$$

Note that in Eq. (2.46) the initial proton travels in the negative z-direction, whereas the final proton is in the direction $(\pi - \theta, \varphi + \pi)$. The mapping in Eq. (2.46) naturally leads to the so-called partial wave expansion

$$T_{H',H} = \sum_{J=1/2}^{\infty} (2J+1) T_{H',H}^J d_{H',H}^J(\theta), \quad (2.48)$$

where $T_{H',H}^J$ is the partial-wave helicity amplitude related linearly to $S_J^{fi}(\omega)$ (see below).

To establish the amplitude $T_{H',H}^J$ we first connect $T_{H',H}$, with the help of Eq. (2.18), to the already derived operator L

$$\begin{aligned} T_{H',H} &= \sum_J S_J^{fi}(\omega) \int d\vec{k}_f \int d\vec{k}_i \psi_f^*(\vec{k}_f) \langle \mathcal{Q}_{1/2\,\lambda'} | \hat{L} | \mathcal{Q}_{1/2\,\lambda} \rangle \psi_i(\vec{k}_i) \\ &= \sum_J S_J^{fi}(\omega) \langle \mathcal{Q}_{1/2\,\lambda'} | \hat{L} | \mathcal{Q}_{1/2\,\lambda} \rangle, \end{aligned} \quad (2.49)$$

where the wave functions $\psi_f^*(\vec{k}_f)$ and $\psi_i(\vec{k}_i)$ of the initial and final photons are given by δ -functions, i.e., $\psi_f^*(\vec{k}_f) = \delta(\cos \theta_f - \cos \theta) \delta(\varphi_f - \varphi)$ and $\psi_i(\vec{k}_i) = \delta(\cos \theta_i - 1) \delta(\varphi_i)$, thus, the integrations over \vec{k}_f and \vec{k}_i are trivial. The expectation value $\langle Q_{1/2, \lambda'} | \hat{L} | Q_{1/2, \lambda} \rangle$ can be calculated using the results of the previous section for the operator \hat{L} (see Eq. (2.46)). We derive the amplitude $T_{H', H}^J$ by comparing Eqs. (2.48) and (2.49).

The amplitude $T_{H', H}^J$ contains information about different transitions, i.e., EE , EM transition etc., and it is possible to rewrite it in terms of the so-called multipole amplitudes, each of which describes a certain transition. To do this we first note that there are 16 different helicity amplitudes. However, discrete symmetries, such as parity (P) and time-reversal (T) invariance connect different $T_{H', H}$ as

$$\begin{aligned} \text{P} \quad T_{-H', -H} &= (-1)^{H'+H} T_{H', H}, \\ \text{T} \quad T_{H, H'} &= (-1)^{H'+H} T_{H', H}, \end{aligned} \quad (2.50)$$

reducing the number of independent amplitudes to six. Ordinarily, the following set of six independent helicity amplitudes is chosen

$$\begin{aligned} \Phi_1 &= \frac{1}{8\pi\sqrt{s}} T_{\frac{1}{2}, \frac{1}{2}}, & \Phi_2 &= \frac{1}{8\pi\sqrt{s}} T_{-\frac{1}{2}, \frac{1}{2}}, & \Phi_3 &= \frac{1}{8\pi\sqrt{s}} T_{-\frac{3}{2}, \frac{1}{2}}, \\ \Phi_4 &= \frac{1}{8\pi\sqrt{s}} T_{\frac{3}{2}, \frac{1}{2}}, & \Phi_5 &= \frac{1}{8\pi\sqrt{s}} T_{\frac{3}{2}, \frac{3}{2}}, & \Phi_6 &= \frac{1}{8\pi\sqrt{s}} T_{-\frac{3}{2}, \frac{3}{2}}, \end{aligned} \quad (2.51)$$

where s is the standard Mandelstam variable. Using the derivations above we establish the partial-wave amplitudes (cf. [Pfeil 1974])

$$\begin{aligned} \Phi_2^{L+\frac{1}{2}} &= \frac{1}{4} \left\{ (L+2)^2 (f_{EE}^{(L+1)-} \pm f_{MM}^{(L+1)-}) \pm L^2 (f_{EE}^{L+} \pm f_{MM}^{L+}) \mp 2L(L+2) (f_{EM}^{L+} \pm f_{ME}^{L+}) \right\}, \\ \Phi_3^{L+\frac{1}{2}} &= \frac{1}{4} \sqrt{L(L+2)} \left\{ (L+2) (f_{EE}^{(L+1)-} \mp f_{MM}^{(L+1)-}) \pm L (f_{EE}^{L+} \mp f_{MM}^{L+}) \mp 2 (f_{EM}^{L+} \mp f_{ME}^{L+}) \right\}, \\ \Phi_5^{L+\frac{1}{2}} &= \frac{1}{4} L(L+2) \left\{ (f_{EE}^{(L+1)-} \pm f_{MM}^{(L+1)-}) \pm (f_{EE}^{L+} \pm f_{MM}^{L+}) \pm 2 (f_{EM}^{L+} \pm f_{ME}^{L+}) \right\}, \end{aligned} \quad (2.52)$$

where $L = J - 1/2$, and we use the standard multipole amplitudes $f_{\varrho\varrho'}^{j\pm}$ with $\varrho, \varrho' = E, M$, e.g., f_{EE}^{j+} corresponds to the amplitude of the process with the electric initial and final photons, the superscript j indicates the total angular momentum of the initial photon j , whereas the plus sign means that the total angular momentum of the system is $J = j + 1/2$ (the minus sign corresponds to $J = j - 1/2$). By definition $f_{EE}^{0+} = f_{MM}^{0+} = f_{EM}^{0+} = f_{ME}^{0+} = 0$. One should notice, that the multipole amplitudes $f_{EM}^{(L+1)-}$ and $f_{ME}^{(L+1)-}$ are not shown in Eq. (2.52), because, due to the time reflection

invariance, they are connected to f_{ME}^{L+} and f_{EM}^{L+} , i.e.,

$$f_{EM}^{(L+1)-} = f_{ME}^{L+}, \quad f_{ME}^{(L+1)-} = f_{EM}^{L+}. \quad (2.53)$$

Finally, we write how the amplitudes $f_{\rho\rho'}^{j\pm}$ are connected to the energy-dependent part of the amplitude S_j^{fi} ,

$$\begin{aligned} f_{EE}^{L+} &= \frac{1}{L(L+1)} S_{j+1/2}^{EE}(\omega), & f_{EE}^{(L+1)-} &= \frac{1}{(L+1)(L+2)} S_{j-1/2}^{EE}(\omega), \\ f_{MM}^{L+} &= \frac{1}{L(L+1)} S_{j+1/2}^{MM}(\omega), & f_{MM}^{(L+1)-} &= \frac{1}{(L+1)(L+2)} S_{j-1/2}^{MM}(\omega), \\ f_{EM}^{L+} &= \frac{1}{(L+1)\sqrt{L(L+2)}} S_{j+1/2}^{EM}(\omega), & f_{ME}^{L+} &= \frac{1}{(L+1)\sqrt{L(L+2)}} S_{j+1/2}^{ME}(\omega). \end{aligned} \quad (2.54)$$

It is important to note that the multipole amplitudes that we have derived are functions of the photon energy in the CM frame.

2.3.3 Relation between the Polarizabilities and Multipoles

In this section we connect the introduced polarizabilities to the multipoles $f_{\rho\rho'}^{\ell\pm}$. In order to do this, we divide the multipoles into the Born and the non-Born parts, i.e., $f = f^{(B)} + \bar{f}$. The Born part is related to \mathcal{L}_0 and \mathcal{L}_1 , and, hence, depends only on M , e and κ (see Chapter 4). The non-Born part is related to \mathcal{L}_{pol} , and can be written in terms of the dynamical polarizabilities [Guasu 1979, Hildebrandt 2004, Griesshammer 2002],

$$\begin{aligned} \bar{f}_{EE}^{1+}(\omega) &= \frac{\omega^2}{3} [\alpha_{E1}(\omega) + \omega \gamma_{E1E1}(\omega)], & \bar{f}_{MM}^{1-}(\omega) &= \frac{\omega^2}{3} [\beta_{M1}(\omega) - 2\omega \gamma_{M1M1}(\omega)], \\ \bar{f}_{EE}^{1-}(\omega) &= \frac{\omega^2}{3} [\alpha_{E1}(\omega) - 2\omega \gamma_{E1E1}(\omega)], & \bar{f}_{EM}^{1+}(\omega) &= \frac{\omega^3}{6} \gamma_{E1M2}(\omega), \\ \bar{f}_{MM}^{1+}(\omega) &= \frac{\omega^2}{3} [\beta_{M1}(\omega) + \omega \gamma_{M1M1}(\omega)], & \bar{f}_{ME}^{1+}(\omega) &= \frac{\omega^3}{6} \gamma_{M1E2}(\omega). \end{aligned} \quad (2.55)$$

where ω is the photon energy in the CM frame (see Supplementary Material 3.11). At low energies these equations connect the multipoles to the static polarizabilities, as the low-energy expansions of the dynamical polarizabilities are (cf. Ref. [Lensky 2015])

$$\begin{aligned} \alpha_{E1}(\omega) &= \alpha_{E1} + \frac{\omega \beta_{M1}}{M} + O(\omega^2), \\ \beta_{M1}(\omega) &= \beta_{M1} + \frac{\omega \alpha_{E1}}{M} + O(\omega^2), \\ \gamma_{E1E1}(\omega) &= \gamma_{E1E1} + \omega \left(\frac{4\gamma_{E1E1} + 7\gamma_{M1E2} + 5\gamma_{M1M1}}{8M} + \frac{\beta_{M1}}{16M^2} \right) + O(\omega^2), \end{aligned}$$

$$\begin{aligned}
\gamma_{M1M1}(\omega) &= \gamma_{M1M1} + \omega \left(\frac{5\gamma_{E1E1} + 7\gamma_{E1M2} + 4\gamma_{M1M1}}{8M} + \frac{\alpha_{E1}}{16M^2} \right) + O(\omega^2), \\
\gamma_{E1M2}(\omega) &= \gamma_{E1M2} + \omega \left(\frac{2\gamma_{E1M2} + 3\gamma_{M1E2} + 3\gamma_{M1M1}}{4M} - \frac{\beta_{M1}}{8M^2} \right) + O(\omega^2), \\
\gamma_{M1E2}(\omega) &= \gamma_{M1E2} + \omega \left(\frac{3\gamma_{E1E1} + 3\gamma_{E1M2} + 2\gamma_{M1E2}}{4M} - \frac{\alpha_{E1}}{8M^2} \right) + O(\omega^2). \tag{2.56}
\end{aligned}$$

Later, in Chapter 4, we develop an approach based on the MEX that uses these relations to establish the polarizabilities.

2.4 Summary

In this chapter we discussed the low-energy expansion and the multipole expansion of CS amplitudes. For the LEX we introduced the effective Lagrangian that characterizes the electromagnetic structure of the proton at low energies. Here we presented the terms that describe the interaction of the photon with a pointlike proton and yield the Born part of the Feynman CS amplitude, and the terms that define the scalar and spin polarizabilities and yield the non-Born part of the amplitude. Subsequently, we found the contributions of the scalar and spin polarizabilities to the invariant amplitudes $\mathcal{A}_1, \dots, \mathcal{A}_8$, see Eqs. (2.11) and (2.16). These formulae comprise the original part of this chapter. For the MEX we derived the multipole expansion of the helicity amplitudes in terms of the conventional multipoles $f_{\rho\rho'}^{\ell\pm}$ and the polarizabilities.

2.5 Supplementary Material

Derivation of Feynman Rules

To derive Feynman rules from our Lagrangian, we rewrite \mathcal{L} as a sum of the non-interacting and interaction terms, i.e., $\mathcal{L} = \mathcal{L}_0 + \mathcal{L}_{\text{int}}$, where $\mathcal{L}_{\text{int}} = \mathcal{L}_1 + \mathcal{L}_2 + \dots$. Now, following the standard procedure (see, e.g., Ref. [Peskin 1995]) we obtain propagators from the former, and the vertices from the latter.

In order to do this, we write \mathcal{L}_0 as

$$\mathcal{L}_0 = \frac{1}{2} \phi_i P_{ij}^{\text{boson, real}} \phi_j + \chi_i^* P_{ij}^{\text{boson, complex}} \chi_j + \bar{\psi}_i P_{ij}^{\text{fermion}} \psi_j, \quad (\text{SM2.57})$$

where ϕ_i denotes real boson fields (in our case the photon field), χ_i denotes complex boson fields (we do not have this term in our effective Lagrangian, but we write it here for the sake of generality), ψ_i denotes fermion fields (in our case the proton field). The matrix operator P here is hermitian, and the corresponding inverse operator P^{-1} satisfies the equation

$$\sum_j P_{ij}(x) P_{jl}^{-1}(x-y) = \delta_{il} \delta^4(x-y). \quad (\text{SM2.58})$$

The propagator $\Delta_F(k)$ in momentum space is given by the Fourier transform of $P_{ij}^{-1}(x)$ multiplied by i , i.e.,

$$\Delta_F(k) = i \tilde{P}_{ij}^{-1}(k). \quad (\text{SM2.59})$$

Following this prescription we obtain the propagators from \mathcal{L}_0 in Eq. (2.4) for photons

$$\Delta_F(k) = -i \frac{g^{\mu\nu}}{k^2}, \quad (\text{SM2.60})$$

and for protons

$$\Delta_F(p) = i \frac{\not{p} + M}{p^2 - M^2}. \quad (\text{SM2.61})$$

To derive Feynman rules for the vertices, we write the interaction Lagrangian \mathcal{L}_{int} as

$$\mathcal{L}_{\text{int}} = \sum_{n \geq 3} \int d^4x_1 \dots d^4x_n v_{i_1 \dots i_n}(x, x_1, \dots, x_n) \phi_{i_1}(x_1) \dots \phi_{i_n}(x_n), \quad (\text{SM2.62})$$

where $v_{i_1 \dots i_n}(x, x_1, \dots, x_n)$ describes interactions and, therefore, defines a vertex in coordinate space, n is the number of fields (ϕ_i) in this vertex (in our case $n = 3$ for the $NN\gamma$ vertex interaction in \mathcal{L}_1 and $n = 4$ for the $NN\gamma\gamma$ vertex in \mathcal{L}_2 and \mathcal{L}_3). The vertex in momentum space

is

$$i \sum_{P_f} (-1)^{\sigma(P_f)} \tilde{v}_{i_1 \dots i_n}(k_1, \dots, k_n), \quad (\text{SM2.63})$$

where $\tilde{v}_{i_1 \dots i_n}(k_1, \dots, k_n)$ is the Fourier transform of $v_{i_1 \dots i_n}(x, x_1, \dots, x_n)$, the sum is taken over the all possible permutations P_f of the identical field operators, and $\sigma(P_f)$ is the parity of the permutation P_f with respect to the fermionic fields.

Using the presented algorithm and \mathcal{L}_1 from Eq. (2.5), we first derive the Feynman rule for the vertex $NN\gamma$ with a pointlike proton

$$i\Gamma^\mu(p', p+k) = ie\gamma^\mu - \frac{ie}{2M} \kappa (\gamma^{\mu\rho} p'_\rho - \gamma^{\mu\delta} (p+k)_\delta), \quad (\text{SM2.64})$$

and then for the $NN\gamma\gamma$ vertex

$$\begin{aligned} i\Gamma_{(2)}^{\mu\nu}(k, k', p, p') &= 4\pi i \left[\beta_{M1} (k \cdot k' g^{\mu\nu} - k^\mu k'^\nu) \right. \\ &\quad \left. - \frac{\alpha_{E1} + \beta_{M1}}{2M^2} (p'_\alpha p_\beta + p_\alpha p'_\beta) (k'^\alpha k^\beta g^{\mu\nu} - k'^\alpha k^\mu g^{\nu\beta} - k'^\nu k^\beta g^{\mu\alpha} + k \cdot k' g^{\mu\alpha} g^{\nu\beta}) \right], \end{aligned} \quad (\text{SM2.65})$$

which quantifies the contribution of the scalar polarizabilities to the amplitude. We note that this rule is easier to derive after rewriting \mathcal{L}_2 in Eq. (2.6) as

$$\mathcal{L}_2 = \pi\beta_{M1} \bar{N} N F^2 - \frac{2\pi(\alpha_{E1} + \beta_{M1})}{M^2} (\partial_\alpha \bar{N})(\partial_\beta N) F^{\alpha\mu} F^{\beta\nu} g_{\mu\nu}. \quad (\text{SM2.66})$$

Finally, we use the third-order Lagrangian, \mathcal{L}_3 to obtain the contribution of the spin polarizabilities to the $NN\gamma\gamma$ vertex that we presented in Eq. (2.14).

Low-energy Expansion of Observables

This chapter presents the low-energy expansion of the observables of interest, and discusses how it can be used to determine the scalar and spin polarizabilities of the proton. In particular, it shows that the magnetic polarizability can be determined from the low-energy measurement of the beam asymmetry. To support this statement, it presents the results of the proof-of-the-principle experiment that was recently carried out in Mainz.

3.1 Introduction

Here we discuss the proton polarizabilities, introduced in Chapter 2, in more detail, and connect them to the four Compton scattering observables, the unpolarized cross section, $d\sigma/d\Omega$, the beam asymmetry, Σ_3 , and the beam-target asymmetries, Σ_{2x} and Σ_{2z} . In order to do so, we calculate the low-energy Compton scattering amplitude using the effective Lagrangian given in Eq. (2.2), i.e., we compute the Feynman diagrams presented in Fig. 3.1. Here graphs 3.1a and 3.1b depict the Born contribution, which can be calculated exactly (for details see Supplementary Material 3.11), and graph 3.1c illustrates the non-Born (NB) contribution. The former does not contain the polarizabilities, therefore, in this chapter we only work with the latter, which in lowest orders contains the two scalar and four spin polarizabilities.

The chapter is organized as follows. Firstly, we introduce the Compton scattering observables. Secondly, we express these observables in terms of the invariant response functions. Thirdly, we use the obtained expressions to study the beam asymmetry, Σ_3 , and to derive the main result of this chapter – Eq. (3.24) for the low-energy expansion of Σ_3 . This equation allows us to suggest that the low-energy measurement of Σ_3 can be used for the precision determination of the proton magnetic polarizability β_{M1} . Fourthly, we present the low-energy expansions of Σ_{2x} and Σ_{2z} , for which the leading order non-Born terms depend on the spin polarizabilities.

3.2 CS Cross Section and Spin Asymmetries

Observables measured in Compton scattering experiments can be divided into two categories — unpolarized and polarized [Babusci 1998a]. In the former the initial and final states do not have definite polarizations, and in calculations one needs to sum over the all possible polarizations of

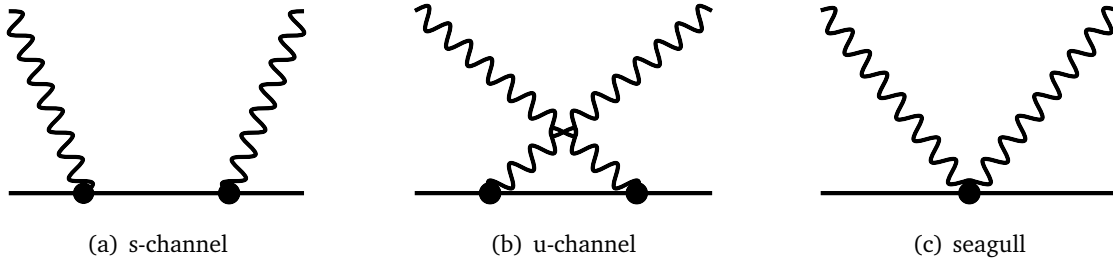


Figure 3.1: Feynman diagrams for low-energy Compton scattering off a nucleon.

the outgoing particles and average over the polarization of the incoming particles; in the latter the system is polarized, these observables can be further divided into the single polarized (either the initial photon or the nucleon is polarized) and doubly polarized (both – the photon and the nucleon – are polarized). In this thesis, we work with one unpolarized, one single-polarized and two doubly-polarized observables. However, before we write them down, we introduce the variables on which they depend, the 4-momentum, k (k'), the polarization vector, ε_σ ($\varepsilon'_{\sigma'}$), the helicity $\sigma = \pm 1$ ($\sigma' = \pm 1$) of the incoming (outgoing) photon, the helicity of the incoming (outgoing) proton, $\lambda = \pm 1/2$ ($\lambda' = \pm 1/2$), and the scattering angle in the laboratory frame, θ_{lab} (cf. Supplementary Material 3.11). Note that for the circularly-polarized photon, ε_σ is

$$\varepsilon_{(\sigma)} = \frac{1}{\sqrt{2}}(0, -\sigma, -i, 0), \quad (3.1)$$

whereas for a linearly-polarized photon with the polarization vector that makes the angle ϕ with the scattering plane, it is

$$\varepsilon_{(\sigma)} = (0, \cos \phi, \sin \phi, 0). \quad (3.2)$$

Finally, we can introduce the observables relevant for our investigation

- (i) The unpolarized cross section,

$$\frac{d\sigma}{d\Omega} = \frac{1}{4} \sum_{\sigma', \lambda', \sigma, \lambda} \frac{d\sigma_{\sigma', \lambda', \sigma, \lambda}}{d\Omega}, \quad (3.3)$$

where $d\sigma_{\sigma', \lambda', \sigma, \lambda}/d\Omega$ is the cross section that corresponds to definite helicities of the incoming and outgoing particles, the factor $1/4$ appears here due to the averaging over the all possible polarizations of the incoming particles.

- (ii) The beam asymmetry, $\Sigma_3(\phi)$, for the processes in which the photons with linear polarization (cf. Eq. (3.2)), are scattered off the unpolarized target

$$\Sigma_3(\phi) \equiv \frac{d\sigma_\phi - d\sigma_{\phi+\pi/2}}{d\sigma_\phi + d\sigma_{\phi+\pi/2}}, \quad (3.4)$$

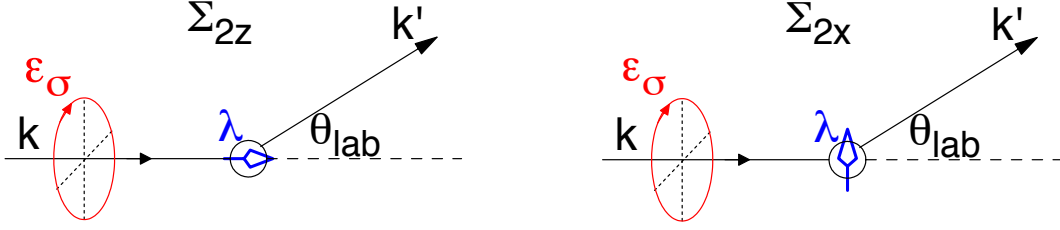


Figure 3.2: The schematics of the scattering process in which circularly polarized photons are scattered off a target polarized either longitudinally (left figure) or transversely (right figure). The variables $k, k', \varepsilon_\sigma, \lambda$ and θ_{lab} are defined in the text.

where $d\sigma_\phi = 1/2 \sum_{\sigma', \lambda', \lambda} d\sigma_{\sigma', \lambda', \phi, \lambda}$, i.e., the sum over the all possible polarizations of the outgoing particles, and the average over the polarization of the proton target, note that the polarization of the incoming photon is fixed. For the sake of generality, in this chapter we do not specify the angle ϕ . However, later, we choose to work with $\phi = 0$ (see chapter 3.6).

- (iii) The beam-target asymmetries for the processes in which the circularly-polarized photons are scattered off the target polarized in the scattering plane (xz -plane). In this dissertation we study the processes with the target polarized either along the z -axis or x -axis (see Fig. 3.2 for illustration), and the two corresponding beam asymmetries,

(a) i.e., for the longitudinal polarization (the target is polarized along the z -axis) we work with the following beam-target asymmetry

$$\Sigma_{2z} \equiv \frac{d\sigma_{1, \frac{1}{2}} - d\sigma_{-1, \frac{1}{2}}}{d\sigma_{1, \frac{1}{2}} + d\sigma_{-1, \frac{1}{2}}}, \quad (3.5)$$

(b) and for the transversal polarization (the target is polarized along the x -axis) we work with

$$\Sigma_{2x} \equiv \frac{d\sigma_{1, x} - d\sigma_{-1, x}}{d\sigma_{1, x} + d\sigma_{-1, x}}. \quad (3.6)$$

Note, that besides these four observables, there are other single and doubly polarized observables (see, e.g., Ref. [Babusci 1998a]). We do not include them in our analysis because they are negligibly small at the energies of our interest, i.e., below the pion production threshold. However, for the sake of completeness, we write a few other observables in terms of the invariant response functions in the Supplementary Material 3.11. The expressions in this Supplementary Material together with the ones in Eqs. (3.3)-(3.6) form a minimal closed set of observables in CS with a polarized initial state (cf. Ref. [Babusci 1998a]).

3.3 Invariant Response Functions

To obtain expressions for the above defined observables, we need to find the cross section for a given initial helicity, $d\sigma_H$. To find it we first calculate the sum of¹ $|T_{H',H}|^2$, taken over the all possible polarizations of the final state – the observables of interest describe the processes with unpolarized outgoing particles, hence the sum. If the sum is known, then $d\sigma_H$ is easily obtained (see, e.g., Ref. [Itzykson 1980])

$$d\sigma_H = \Gamma \sum_{H'} |T_{H',H}|^2 \quad \text{with} \quad \Gamma = \frac{4\pi}{(s - M^2)^2} dt, \quad (3.7)$$

where $s = (p + k)^2$ and $t = (k - k')^2$ are the standard Mandelstam invariants.

To find $\sum |T_{H',H}|^2$, we write the helicity amplitude as

$$T_{H',H} = \bar{u}_{\lambda'}(p') \mathcal{M}^{\rho\nu} u_{\lambda}(p) \varepsilon_{(\sigma')\rho}^* \varepsilon_{(\sigma)\nu}, \quad (3.8)$$

where $\mathcal{M}^{\rho\nu}$ is the Feynman amplitude for Compton scattering (the diagrams are sketched in Fig. 3.1), u_{λ} is the normalized helicity spinor, i.e., $\bar{u}_{\lambda'} u_{\lambda} = 2M$. Now, we use the sums over the final states $\sum_{\lambda'} u_{\lambda'}(p') \bar{u}_{\lambda'}(p') = \not{p}' + M$ and $\sum_{\sigma'} \varepsilon_{(\sigma')\rho}^* \varepsilon_{(\sigma)\delta} = -g_{\rho\delta}$ to obtain (cf. Ref. [Peskin 1995])

$$\sum_{H'=-3/2}^{3/2} |T_{H',H}|^2 = -\bar{u}_{\lambda}(\vec{p}) \left[\overline{\mathcal{M}}^{\rho\mu} (\not{p}' + M) \mathcal{M}_{\rho}^{\nu} \right] u_{\lambda}(\vec{p}) \varepsilon_{(\sigma)\mu}^* \varepsilon_{(\sigma)\nu}, \quad (3.9)$$

where M is the proton mass. Note that this expression is Lorentz invariant, therefore, any reference frame can be used for the analysis. We choose to work in the laboratory frame (i.e., $p = (M, \vec{0})$), where some calculations are simpler. For instance, such a choice implies that $\bar{u}(0) \gamma_5 u(0) = 0$. Note also that the phase-space factor, Γ , here can be expressed in terms of the solid angle Ω_{lab} using that $dt = \frac{(v')^2}{\pi} d\Omega_{lab}$, here v' is the energy of the outgoing photon (see Supplementary Material 3.11).

We see that to calculate the $d\sigma_H$, we need to know the $\mathcal{M}^{\rho\nu}$. For the low-energy scattering we obtain the latter in the next section using the Feynman rules. In the rest of this section, we would like to present the general structure of $\sum_{H'} |T_{H',H}|^2$, i.e., we write down the all possible structures that can appear after inserting $\mathcal{M}^{\rho\nu}$ into Eq. (3.9), and express the observables in terms of these structures. These expressions will be used later to simplify the discussion.

¹Recall that $T_{H',H}$ denotes the helicity amplitude, defined in Chapter 2, here H', H are the helicities of the outgoing and incoming particles, p (k) and p' (k') are the initial and final 4-momenta of the proton (photon).

The most general form of $\sum_{H'} |T_{H',H}|^2$ is

$$\begin{aligned} \sum_{H'} |T_{H',H}|^2 = & 4 \left\{ R_0 + |n' \cdot \varepsilon_{(\sigma)}|^2 R_1 + \bar{u}_\lambda(0) \gamma^{\mu\nu} u_\lambda(0) \left[\varepsilon_{(\sigma)\mu}^* \varepsilon_{(\sigma)\nu} R_2 \right. \right. \\ & + (n_\mu \varepsilon_{(\sigma)\nu} - n_\mu \varepsilon_{(\sigma)\nu}^*) n' \cdot \varepsilon_{(\sigma)} R_3 + (n'_\mu \varepsilon_{(\sigma)\nu} - n'_\mu \varepsilon_{(\sigma)\nu}^*) n' \cdot \varepsilon_{(\sigma)} R_4 \\ & + i(n_\mu \varepsilon_{(\sigma)\nu} + n_\mu \varepsilon_{(\sigma)\nu}^*) n' \cdot \varepsilon_{(\sigma)} R_5 + i(n'_\mu \varepsilon_{(\sigma)\nu} + n'_\mu \varepsilon_{(\sigma)\nu}^*) n' \cdot \varepsilon_{(\sigma)} R_6 \\ & \left. \left. + i n_\mu n'_\nu |n' \cdot \varepsilon_{(\sigma)}|^2 R_7 \right] \right\}, \end{aligned} \quad (3.10)$$

where $R_i = R_i(s, t)$ are scalar functions which depend only on the Mandelstam invariants. The 4-momenta $n = \frac{k}{|k|} = (1, 0, 0, 1)$ and $n' = \frac{k'}{|k'|} = (1, \sin \theta_{lab}, 0, \cos \theta_{lab})$ show, respectively, the directions of the incoming and outgoing photon in the laboratory frame (see Supplementary material 3.11).

To proceed further we establish $\bar{u}_\lambda(0) \gamma^{\mu\nu} u_\lambda(0)$ in terms of the arbitrary 4-vectors \tilde{k} and \tilde{q} ,

$$\bar{u}_{\pm z}(0) \tilde{k} \cdot \gamma \cdot \tilde{q} u_{\pm z}(0) \equiv \bar{u}_{\pm z}(0) \gamma^{\mu\nu} u_{\pm z}(0) \tilde{k}_\mu \tilde{q}_\nu = \pm i(\tilde{k}_2 \tilde{q}_1 - \tilde{k}_1 \tilde{q}_2), \quad (3.11)$$

$$\bar{u}_{\pm x}(0) \tilde{k} \cdot \gamma \cdot \tilde{q} u_{\pm x}(0) = \pm i(\tilde{k}_3 \tilde{q}_2 - \tilde{k}_2 \tilde{q}_3), \quad (3.12)$$

here the spinors $u_{\pm z}$ are used for the longitudinal polarization of the target (the polarization along the z-direction ($\lambda = \pm 1/2$)), whereas the spinors $u_{\pm x}$ are used for the transverse polarization of the target (i.e., along the x-axis), thus, they are connected to u_λ as

$$u_{\pm x}(\vec{p}) = \frac{1}{\sqrt{2}} \left[u_{-1/2}(\vec{p}) \pm u_{1/2}(\vec{p}) \right]. \quad (3.13)$$

By inserting these identities into Eq. (3.10) we write the cross sections in terms of the functions R_0, \dots, R_6 ,

$$\begin{aligned} d\sigma_{\sigma, \pm z} &= \Gamma \left[R_0 + \frac{1}{2} R_1 \sin^2 \theta_{lab} \pm \sigma (R_2 - R_4 \sin^2 \theta_{lab}) \right], \\ d\sigma_{\sigma, \pm x} &= \Gamma \left[R_0 + \frac{1}{2} R_1 \sin^2 \theta_{lab} \pm \sigma \sin \theta_{lab} (R_3 + R_4 \cos \theta_{lab}) \right], \\ d\sigma_{\phi, \pm x} &= \Gamma \left[R_0 + R_1 \sin^2 \theta_{lab} \cos^2 \phi \pm \sin \theta_{lab} \sin 2\phi (R_5 + R_6 \cos \theta_{lab}) \right], \\ d\sigma_{\phi, \pm z} &= \Gamma \left[R_0 + R_1 \sin^2 \theta_{lab} \cos^2 \phi \mp R_6 \sin^2 \theta_{lab} \sin 2\phi \right], \end{aligned} \quad (3.14)$$

here the subscript defines the initial helicity – the first symbol is the polarization of the photon, either circular with $\sigma = \pm 1$ or linear at angle ϕ (cf. Eq. (3.2)), and the second one is the polarization of the proton. Using these equations we establish $d\sigma$ (cf. Eq. (3.3))

$$d\sigma = \frac{1}{4} \sum_{\sigma=\pm 1} (d\sigma_{\sigma, +z} + d\sigma_{\sigma, -z}), \quad (3.15)$$

and $d\sigma_\phi$ which determines $\Sigma_3(\phi)$ (cf. Eq. (3.4)),

$$d\sigma_\phi = \frac{1}{2}(d\sigma_{\phi,+z} + d\sigma_{\phi,-z}) = \Gamma \left[R_0 + R_1 \sin^2 \theta_{lab} \cos^2 \phi \right]. \quad (3.16)$$

Now we use the established polarized cross sections to obtain the unpolarized cross section and the asymmetries in terms of the functions R_i

$$\frac{d\sigma}{d\Omega_{lab}} = \left(\frac{2v'}{s - M^2} \right)^2 \left[R_0 + \frac{1}{2} R_1 \sin^2 \theta_{lab} \right]. \quad (3.17)$$

$$\Sigma_{2z} = \frac{R_2 - R_4 \sin^2 \theta_{lab}}{R_0 + \frac{1}{2} R_1 \sin^2 \theta_{lab}}, \quad (3.18)$$

$$\Sigma_{2x} = \frac{\sin \theta_{lab} (R_3 + R_4 \cos \theta_{lab})}{R_0 + \frac{1}{2} R_1 \sin^2 \theta_{lab}}, \quad (3.19)$$

$$\Sigma_3(\phi) = \frac{R_1 \sin^2 \theta_{lab} \cos 2\phi}{2R_0 + R_1 \sin^2 \theta_{lab}}, \quad (3.20)$$

$$\Sigma_3 \equiv \Sigma_3(0) = \frac{R_1 \sin^2 \theta_{lab}}{2R_0 + R_1 \sin^2 \theta_{lab}}. \quad (3.21)$$

Below we use these expressions² to obtain the low-energy expansions of the corresponding observables.

3.4 Low-energy Expansion. Contribution of Scalar Polarizabilities

In this subsection we obtain the low-energy expansion (LEX) of the R_i functions, i.e., here we compute the leading order non-Born (NB) terms that contain the scalar polarizabilities. In order to do so, we decompose the Feynman amplitude in Eq. (3.9) into the Born and non-Born parts, $\mathcal{M}^{\mu\nu} = \mathcal{M}_B^{\mu\nu} + \mathcal{M}_{NB(2)}^{\mu\nu}$. The subscript (2) on the NB amplitude indicates that here we are interested only in the contribution of α_{E1} and β_{M1} , and, hence, we disregard the higher-order polarizabilities, such as spin, quadrupole polarizabilities etc., which are also contained in $\mathcal{M}_{NB}^{\mu\nu}$.

The Born part, $\mathcal{M}_B^{\mu\nu}$, is well-known and we give the expression for it in the Supplementary Material 3.11. The non-Born part, $\mathcal{M}_{NB(2)}^{\mu\nu}$, can be obtained using the effective Lagrangian, see Eq. (2.8) and chapter 2. Now we insert $\mathcal{M}_B^{\mu\nu} + \mathcal{M}_{NB(2)}^{\mu\nu}$ in Eq. (3.9), and compare the result with Eq. (3.10). Such a comparison allows us to obtain the energy expansions of the functions R_i , which determine the observables of interest, see Eqs. (3.17)-(3.21). We present the Born

²See Supplementary Material 3.11 for the expressions of a few other important observables which, however, are not relevant at the energies of interest. See also the discussion in Section 3.2.

contribution in the Supplementary Material 3.11, and the leading order NB terms here³

$$\begin{aligned}
 R_0^{\text{NB}(2)} &= \frac{\pi e^2}{8M} \alpha_{E1} (v^2 + v'^2) [-8M^2 - (1 + \kappa)^2 t (1 + z_{lab}) + 2t] \\
 &+ \frac{\pi e^2}{8M} \beta_{M1} (t + v^2 + v'^2) [-8M^2 - (1 + \kappa)^2 t (1 + z_{lab}) + 2t] \\
 &+ \frac{\pi M^2}{2} \alpha_{E1} \beta_{M1} (v^2 + v'^2) (t + v^2 + v'^2) + \frac{\pi M^2}{4} \alpha_{E1}^2 (v^2 + v'^2)^2 \\
 &+ \frac{\pi M^2}{4} \beta_{M1}^2 (t + v^2 + v'^2)^2 + O(v^5), \\
 R_1^{\text{NB}(2)} &= -\frac{\pi e^2}{4M} \alpha_{E1} v v' [-8M^2 + 3t + \kappa(2 + \kappa)(v^2 + v'^2)] \\
 &- \frac{\pi e^2}{4M} \beta_{M1} v v' [(1 + \kappa)^2 t + 2t + \kappa(2 + \kappa)(v^2 + v'^2)] - \pi M^2 \alpha_{E1}^2 v^2 v'^2 \\
 &+ \pi M^2 \beta_{M1}^2 v^2 v'^2 + O(v^5), \\
 R_2^{\text{NB}(2)} &= \frac{\pi e^2}{4} \alpha_{E1} [-(1 + \kappa)^2 (1 - z_{lab}) + \kappa^2] (v + v') (v^2 + v'^2) \\
 &+ \frac{\pi e^2}{4} \beta_{M1} [-(1 + \kappa)^2 (1 - z_{lab}) + \kappa^2] (v + v') (t + v^2 + v'^2) + O(v^5), \\
 R_3^{\text{NB}(2)} &= -\frac{\pi e^2}{4M} \alpha_{E1} [-M v' (4v^2 - v v' + v'^2) - M \kappa (v^3 + 3v^2 v' + 2v'^3) - \kappa^2 v v'^3 \\
 &- M \kappa^2 (v^3 - v^2 v' + v v'^2 + v'^3) + 2M^2 (1 + \kappa) v (v - v')] \\
 &- \frac{\pi e^2}{4M} \beta_{M1} [-M v' (4v^2 - v v' + v'^2) - M \kappa (v^3 + 5v^2 v' - 2v v'^2 + 2v'^3) - \kappa^2 v v'^3 \\
 &- M \kappa^2 (v^3 + v^2 v' + v v'^2 + v'^3) + 2M^2 (1 + \kappa)^2 (v^2 - v'^2)] + O(v^5), \\
 R_4^{\text{NB}(2)} &= -\frac{\pi e^2}{4M} \alpha_{E1} v' [M(1 + \kappa) (2v^2 + v'^2 + v v') + 2M v v' \kappa - \kappa^2 v^3] \\
 &- \frac{\pi e^2}{4M} \beta_{M1} v' [M(1 + \kappa) (2(1 + \kappa)v^2 + v'^2 + v v') - 2M^2 (1 + \kappa) (v - v') - \kappa^2 v^3] \\
 &+ O(v^5), \\
 R_5^{\text{NB}(2)} &= 0, \\
 R_6^{\text{NB}(2)} &= 0, \\
 R_7^{\text{NB}(2)} &= 0.
 \end{aligned} \tag{3.22}$$

where κ is the anomalous magnetic moment of the proton and $z_{lab} = \cos \theta_{lab}$. Note that we do not include here the spin polarizabilities which start to contribute at the order v^3 , and the fourth-order scalar polarizabilities α_{E2} , β_{M2} , α_{E1v} , and β_{M1v} which are relevant at the order v^4 . In the following sections we use these expressions to write down the LEX of the unpolarized cross section and the beam asymmetry. Certainly, the LEX approach has a limited region of

³It is worthwhile noting that the leading order NB terms (of the order $O(v^2)$) in the sum $\sum_{H'} |T_{H',H}|^2$, and, hence, in observables, come from the interference of $\mathcal{M}_B^{\mu\nu}$ and $\mathcal{M}_{\text{NB}(2)}^{\mu\nu}$.

applicability (well below the pion production threshold), where precision measurements are currently not feasible. However, it can give us an idea of which observable is sensitive to which quantity and motivate future theoretical and experimental studies.

3.5 Low-energy Expansion of $d\sigma/d\Omega$

Here we obtain the LEX of the unpolarized cross section. In order to do this, we insert the expressions in Eq. (3.22) into Eq. (3.17), and obtain the well-known formula (see, e.g., Ref. [Maximon 1989])

$$\frac{d\sigma^{(\text{NB})}}{d\Omega_{lab}} = -\frac{\alpha}{M} \left(\frac{v'}{v}\right)^2 v v' \left[\alpha_{E1} (1 + \cos^2 \theta_{lab}) + 2\beta_{M1} \cos \theta_{lab} \right] + O(v^3), \quad (3.23)$$

where $\alpha = e^2/4\pi$ is the fine-structure constant. We see that the leading order non-Born contribution to $d\sigma/d\Omega$ is determined by a linear combination of α_{E1} and β_{M1} . For instance, at $\theta_{lab} = 0$ the cross section is proportional to $\alpha_{E1} + \beta_{M1}$, and at $\theta_{lab} = \pi$ to $\alpha_{E1} - \beta_{M1}$. Therefore, a precision measurement of $d\sigma/d\Omega_{lab}$ at different angles should allow one to extract α_{E1} and β_{M1} . That is the reason why the unpolarized cross section is commonly considered to be a good observable to determine the scalar polarizabilities. It is important to notice though, that at very low energies the non-Born contribution in Eq. (3.23) is highly suppressed (due to the vv' factor), and $d\sigma/d\Omega_{lab}$ is mainly determined by the Born contribution. This makes it difficult, if at all possible, to measure the effect of the polarizabilities at those energies. At higher energies the sensitivity to the polarizabilities is higher, which motivated experiments done at energies exceeding 100 MeV, i.e., not small compared to the pion mass, m_π . However, at these energies (around the pion-production threshold) the higher-order terms in Eq. (3.23) become substantial. This indicates that the LEX does not work in this energy regime, and, to extract the polarizabilities, one needs to resort to model-dependent approaches. For example, one can use BChPT or dispersion relation (DR) (see [Drechsel 2003, Schumacher 2005] for reviews) which demonstrate their predictive power in many quantum low-energy problems. Note, however, that as these approaches might have very different starting points, their outcomes are not guaranteed to coincide with one another. For instance, the value of the magnetic polarizability, obtained using the DR approach and fitted to the unpolarized Compton scattering data, is not in consistence with calculated in BChPT. In Chapter 4 we show that this discrepancy might be due to the inconsistency of the experimental data used by DR. In any case, as the value of β_{M1} is small, there is a necessity to find an observable sensitive to the magnetic polarizability alone, which would allow one to determine β_{M1} independently of α_{E1} . Below we show that the beam asymmetry, Σ_3 , could serve as such an observable.

3.6 Low-energy Expansion of Σ_3

Now we insert the functions R_i from Eq. (3.22) into Eq. (3.21) to derive the leading order non-Born contribution to Σ_3 ,

$$\Sigma_3^{(\text{NB})} = -\frac{4Mv^2 \cos \theta_{lab} \sin^2 \theta_{lab}}{\alpha(1 + \cos^2 \theta_{lab})^2} \beta_{M1} + O(v^3). \quad (3.24)$$

The derived equation shows that the leading (in the LEX) effect of the electric polarizability cancels out, while the effect of the magnetic polarizability remains. Hence, the beam asymmetry should be optimal for a precision measurement of β_{M1} independently of α_{E1} . It is worthwhile noting that Eq. (3.24) retains its form in the Breit (brick-wall) or center-of-mass reference frames. For instance, in the Breit frame we have

$$\Sigma_3^{(\text{NB})} = -\frac{4M\omega_B^2 \cos \theta_B \sin^2 \theta_B}{\alpha(1 + \cos^2 \theta_B)^2} \beta_{M1} + O(\omega_B^4), \quad (3.25)$$

where ω_B and θ_B are the energy and the angle in the Breit frame (see Supplementary Material 3.11).

One should keep in mind that Eq. (3.24) is valid only at low energies. Unfortunately, as we have already mentioned in the previous section, low-energy Compton experiments on the proton are difficult to analyze, because of small cross sections and overwhelming QED backgrounds. Today, a precision measurement is only feasible for photon-beam energies above 60 MeV and scattering angles greater than 40 degrees. For instance, the recent experiments at MAMI were carried out at photon energies between 80 and 150 MeV. At these energies the effect of higher-order terms may become substantial, and one must check the applicability of the leading LEX term. One way to do that is to compare Eq. (3.24) with the corresponding results of the dispersion relation or chiral perturbation theory calculations. We demonstrate a comparison to the latter calculations in Fig. 3.3, where the leading-LEX and the next-next-to-leading order (NNLO) BChPT (cf. Ref. [Lensky 2010]) terms of Σ_3 are plotted for different values of β_{M1} . From Fig. 3.3 one sees that for the beam energy of 100 MeV and forward directions (upper left panel) the LEX is in a good agreement with BChPT. At the same time the results for the beam energy of 135 MeV (lower panels) suggest that the leading LEX result does not apply at such energies.

Figure 3.3 shows that Σ_3 depends strongly on β_{M1} . This observation together with the fact that many systematic errors tend to cancel out for the beam asymmetry, suggests that it should be feasible to obtain an accurate value of β_{M1} from Σ_3 .

To find the optimal kinematic parameters that will allow experimentalists to determine β_{M1} by measuring Σ_3 , one should know the kinematic region where the higher-order terms are small,

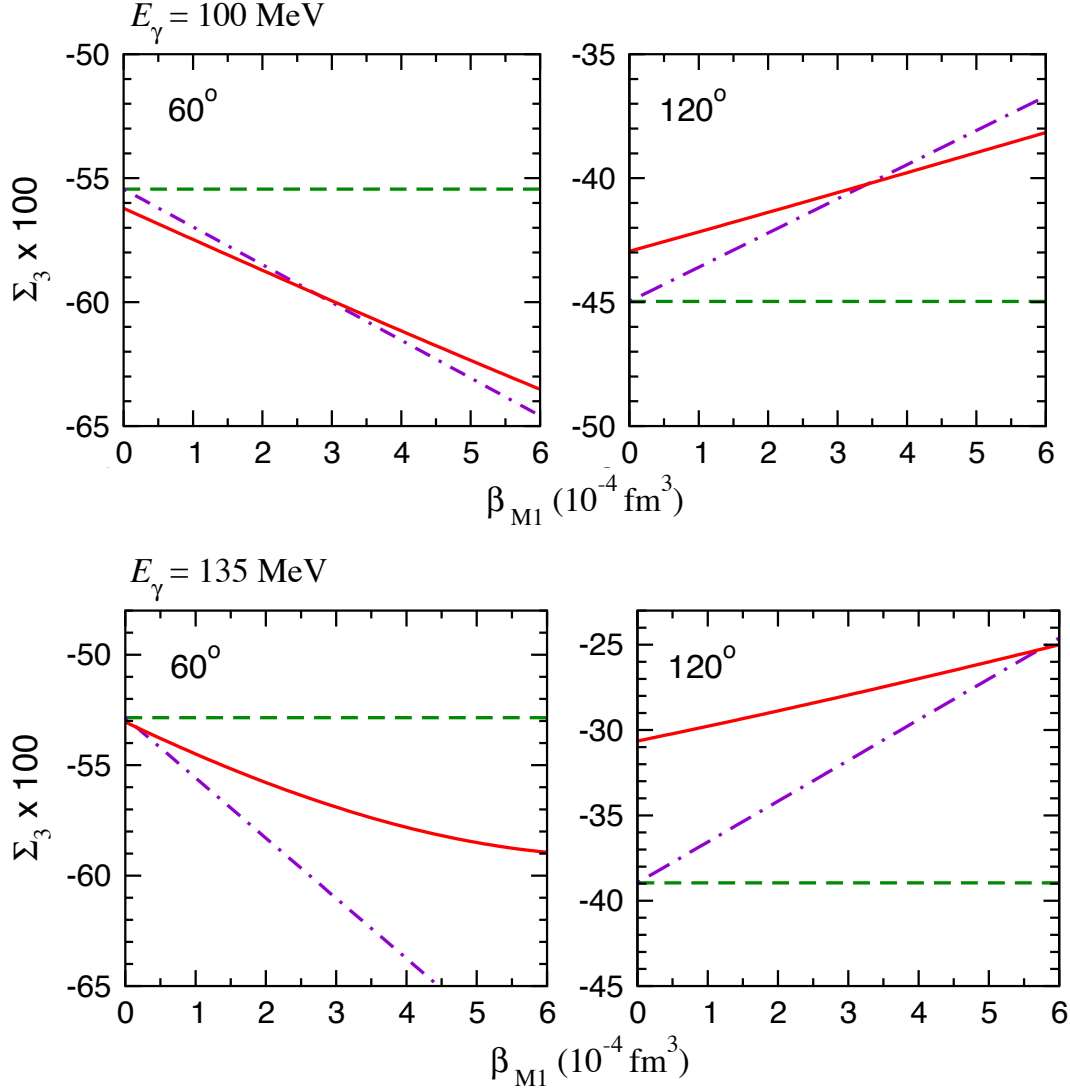


Figure 3.3: The beam asymmetry Σ_3 shown as a function of β_{M1} for the fixed photon energies of 100 MeV (upper panel) and 135 MeV (lower panel) and scattering angles of 60 (left panels) and 120 (right panels) degrees. The dashed green curve corresponds the Born contribution, the dash-dotted magenta — leading LEX formula (3.24) and the red solid curve — NNLO BChPT [Lensky 2010].

and $\Sigma_3^{(\text{NB})}$ is given by Eq. (3.24). To provide this information we take the contributions of the order of $O(v^3)$ and $O(v^4)$ to $\Sigma_3^{(\text{NB})}$ to the beam asymmetry into consideration

$$\begin{aligned}
 \Sigma_3^{(\text{NB})} &= -\frac{4 \cos \theta_{lab} \sin^2 \theta_{lab}}{(1 + \cos^2 \theta_{lab})^2} \frac{M^3 \beta_{M1}}{\alpha} \left(\frac{v}{M}\right)^2 \left\{ 1 + \frac{v}{M} (-1 + \cos \theta_{lab}) \right. \\
 &+ \left. \left(\frac{v}{M}\right)^2 \left[a_1(\cos \theta_{lab}) + \frac{M^3 \alpha_{E1}}{\alpha} \right] \right\} + \frac{\sin^2 \theta_{lab}}{(1 + \cos^2 \theta_{lab})^2} \left(\frac{v}{M}\right)^4 \left[a_2(\cos \theta_{lab}) \frac{M^3 \alpha_{E1}}{\alpha} \right. \\
 &+ \left. a_3(\cos \theta_{lab}) \left(\frac{M^3 \beta_{M1}}{\alpha}\right)^2 \right] + O(v^5),
 \end{aligned} \tag{3.26}$$

where the dimensionless coefficients depend on the angle as

$$\begin{aligned}
 a_1(z_{lab}) &= \frac{1}{4z_{lab}(1+z_{lab}^2)} \left[-1 - 4z_{lab} + 7z_{lab}^2 + z_{lab}^3 - 8z_{lab}^4 + 5z_{lab}^5 + 2z_{lab}(-8 + 16z_{lab} \right. \\
 &\quad \left. - 7z_{lab}^2 + z_{lab}^4) \kappa + z_{lab}(-32 + 40z_{lab} + z_{lab}^2 + z_{lab}^4) \kappa^2 + 4z_{lab}(-5 + 4z_{lab} + 3z_{lab}^2) \kappa^3 \right. \\
 &\quad \left. + z_{lab}(-5 + 3z_{lab}^2) \kappa^4 \right], \\
 a_2(z_{lab}) &= 2 - z_{lab} - z_{lab}^2 + 2(2 - 4z_{lab} + z_{lab}^2) \kappa + (7 - 10z_{lab} - 2z_{lab}^2) \kappa^2 + 4(1 - z_{lab} - z_{lab}^2) \kappa^3 \\
 &\quad + (1 - z_{lab}^2) \kappa^4, \\
 a_3(z_{lab}) &= \frac{2(1 - 6z_{lab}^2 + z_{lab}^4)}{1 + z_{lab}^2}
 \end{aligned} \tag{3.27}$$

with $z_{lab} = \cos \theta_{lab}$. To obtain these equations we have used the functions R_i from Eq. (3.22) in Eq. (3.21). We remind the reader that here we do not include contributions of the higher-order polarizabilities that appear at the orders ν^3 and ν^4 . For instance, we disregard the spin polarizabilities (at ν^3 and ν^4) and the fourth-order scalar polarizabilities⁴ α_{E2} , β_{M2} , and $\beta_{M1\nu}$ (at ν^4). Note, however, that the contribution of the fourth-order scalar polarizabilities can be recovered by the following replacement in the $O(\nu^2)$ term

$$\beta_{M1} \rightarrow \beta_{M1} + \nu^2 \left(\beta_{M\nu} - \frac{1}{12} \alpha_{E2} + \frac{1}{6} \beta_{M2} \cos \theta_{lab} \right). \tag{3.28}$$

The spin polarizabilities⁵ and the $O(\nu^4)$ part of the scalar polarizabilities (cf. Fig. 3.4) are important only in the backward scattering. We demonstrate this fact in Fig. (3.4). Here the curve that depicts the $O(\nu^2)$ terms differs for the backward scattering from the curve that shows the $O(\nu^4)$ contribution. On the other hand, we see that the curves practically coincide at angles below 60 degrees, demonstrating a negligible effect of the $O(\nu^3)$ and $O(\nu^4)$ terms at these kinematics. Therefore, to extract β_{M1} , we propose to study only the forward scattering, i.e., $\theta_{lab} \lesssim 60$ degrees, (see Fig. 3.4). It is worthwhile noting that at $\theta_{lab} = 60$ degrees the leading-order LEX result is also very close to the BChPT result (see Fig. 3.3), confirming the near-perfect cancellation of higher-order terms.

3.7 Measurement of Σ_3

As argued in the previous section, the optimal way to determine the magnetic polarizability from CS is to measure the beam asymmetry at low energies. To date, this observable has only been measured well above the pion-production threshold where the LEX is not expected to hold.

⁴Note that we do not consider here the dispersive polarizability $\alpha_{E1\nu}$ as it starts to contribute to Σ_3 only at ν^6 .

⁵See the corresponding expressions in Section 3.8

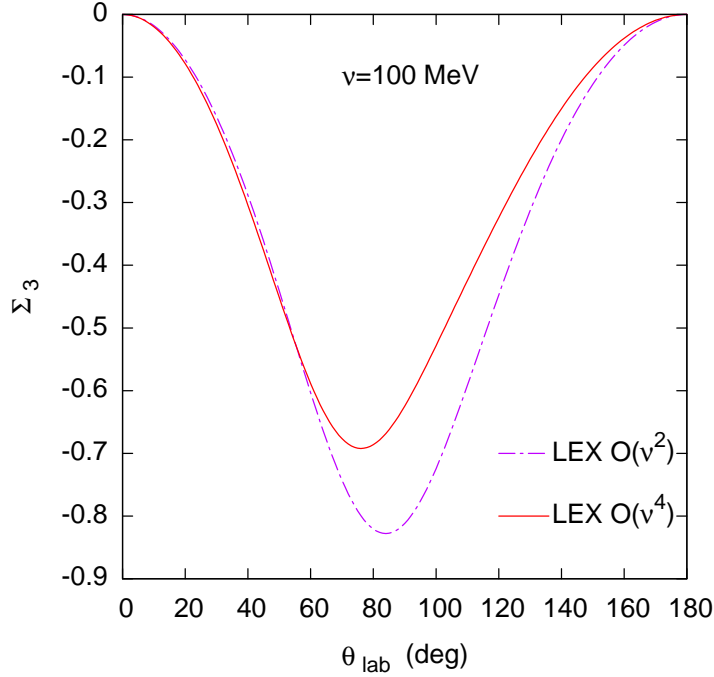


Figure 3.4: The beam asymmetry Σ_3 as a function of the scattering angle for the photon energy of 100 MeV. The dot-dashed purple curve corresponds to the leading LEX formula (3.24) and the red solid curve is the sum of the contributions $O(v^2)$, $O(v^3)$ and $O(v^4)$. The latter curve contains the contributions of the scalar dipole polarizabilities (cf. Eq. (3.26)), spin (cf. Eq. (3.35)) and fourth-order scalar polarizabilities (cf. Eq. (3.28)). The values of the scalar polarizabilities in the analysis are taken from PDG [Olive 2014], $\alpha_{E1} = 11.2 [10^{-4}\text{fm}^3]$ and $\beta_{M1} = 2.5 [10^{-4}\text{fm}^3]$, and the spin and fourth-order scalar polarizabilities from BChPT [Lensky 2015], $\gamma_{E1E1} = -3.3 [10^{-4}\text{fm}^4]$, $\gamma_{E1M2} = 0.2 [10^{-4}\text{fm}^4]$, $\gamma_{M1E2} = 1.1 [10^{-4}\text{fm}^4]$, $\gamma_{M1M1} = 2.9 [10^{-4}\text{fm}^4]$, $\alpha_{E2} = 17.3 [10^{-4}\text{fm}^5]$, $\beta_{M2} = -15.5 [10^{-4}\text{fm}^5]$ and $\beta_{Mv} = 7.1 [10^{-4}\text{fm}^5]$.

However, very recently, inspired by our suggestion [Krupina 2013], the A2 collaboration at the Mainz Microtron (MAMI) has provided the very first proof-of-principle measurements of the beam asymmetry below the threshold. In this section we discuss this experiment. In particular, we will argue that its characteristic energies are beyond the range of the applicability of the LEX, and analyze the data using ChPT. We will also sum up the implication of these results for the LEX-based approach.

The A2 experiment starts with an electron beam which passes through a diamond radiator producing coherent linearly-polarized photons in the three energy ranges $\nu = 76 - 98$, $98 - 119$, $119 - 139$ MeV. These photons are then shoot to the unpolarized liquid hydrogen target and those which undergo an elastic scattering with the proton are detected in the Crystal Ball detector [Starostin 2001]. The beam asymmetry is obtained by counting the number of events for given scattering angles θ and ϕ [Sokhoyan 2016]. The dependence of the beam asymmetry on the azimuthal angle ϕ , which defines the angle between the photon polarization vector and

the scattering plane, see Eq. (3.4), is simply factorized (cf. Eqs. (3.20) and (3.21)),

$$\Sigma_3(\phi) = \Sigma_3 \cos 2\phi. \quad (3.29)$$

Here $\Sigma_3 \equiv \Sigma_3(0) = \frac{d\sigma_{\parallel} - d\sigma_{\perp}}{2d\sigma}$, where σ_{\parallel} , σ_{\perp} are the cross sections with the photon polarization either parallel or perpendicular to the scattering plane. In the experiment the scattering plane, and hence $\phi = 0$, cannot be fixed, thus, we obtain Σ_3 by fitting the ϕ -distributions using Eq. (3.29), see Fig. 3.5. Note that the collected data are divided into 30 degree-wide bins in the azimuthal angle ϕ bringing an additional factor of $6/\pi \sin \pi/6$ to Eq. (3.29) due to the averaging over the bin width.

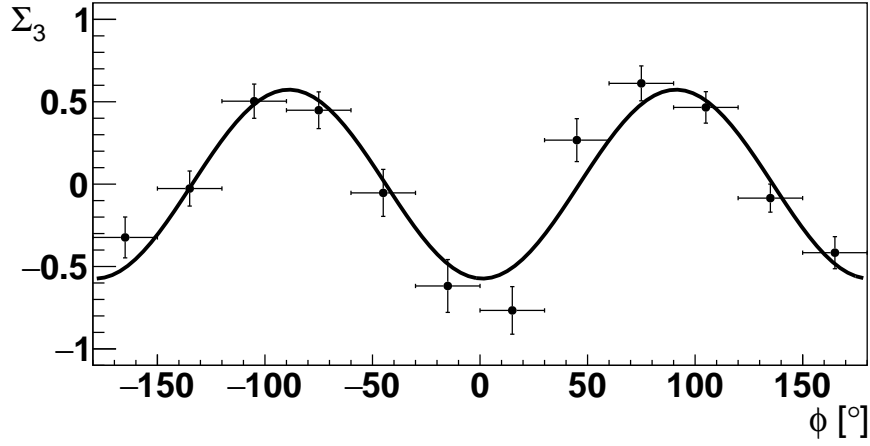


Figure 3.5: The ϕ -dependence of the beam asymmetry. The black points are the experimental data collected at the MAMI [Sokhoyan 2016], and the black curve shows the fit of these data to Eq. (3.29).

The obtained data are divided into seven bins in the polar angle with the central values at $\theta_{lab} = 35, 50, 70, 90, 110, 130, 147.5$ degrees, and presented in Fig. 3.6. The figure clearly indicates the importance of the polarizability contributions by showing the deviation of the data from the Born terms. Note, however, that in most cases the data points lie outside the region of the applicability of the LO [$O(\nu^2)$] low-energy result from Eq. (3.24). This statement can be proved by comparing the LO contribution with the fourth-order terms⁶ [$O(\nu^4)$] in the LEX. In particular, the leading-order of the LEX at $\nu = 119 - 139$ MeV deviates significantly from the fourth-order contribution. Moreover, we notice that even at $\nu = 76 - 98$ MeV and $\theta_{lab} > 60$ deg the $O(\nu^4)$ term is at least as important as the LO contribution. Therefore, we conclude that for these parameters the LEX converges slow, and, thus, we cannot extract the magnetic polarizability from the data using the LEX. Ideally, we could do that at $\nu = 76 - 98$ MeV and $\theta_{lab} \lesssim 60$ deg,

⁶Here we include the contributions of the scalar polarizabilities from Eq. (3.26), as well as the contributions of the spin polarizabilities from Eq. (3.35) and fourth-order scalar polarizabilities from Eq. (3.28).

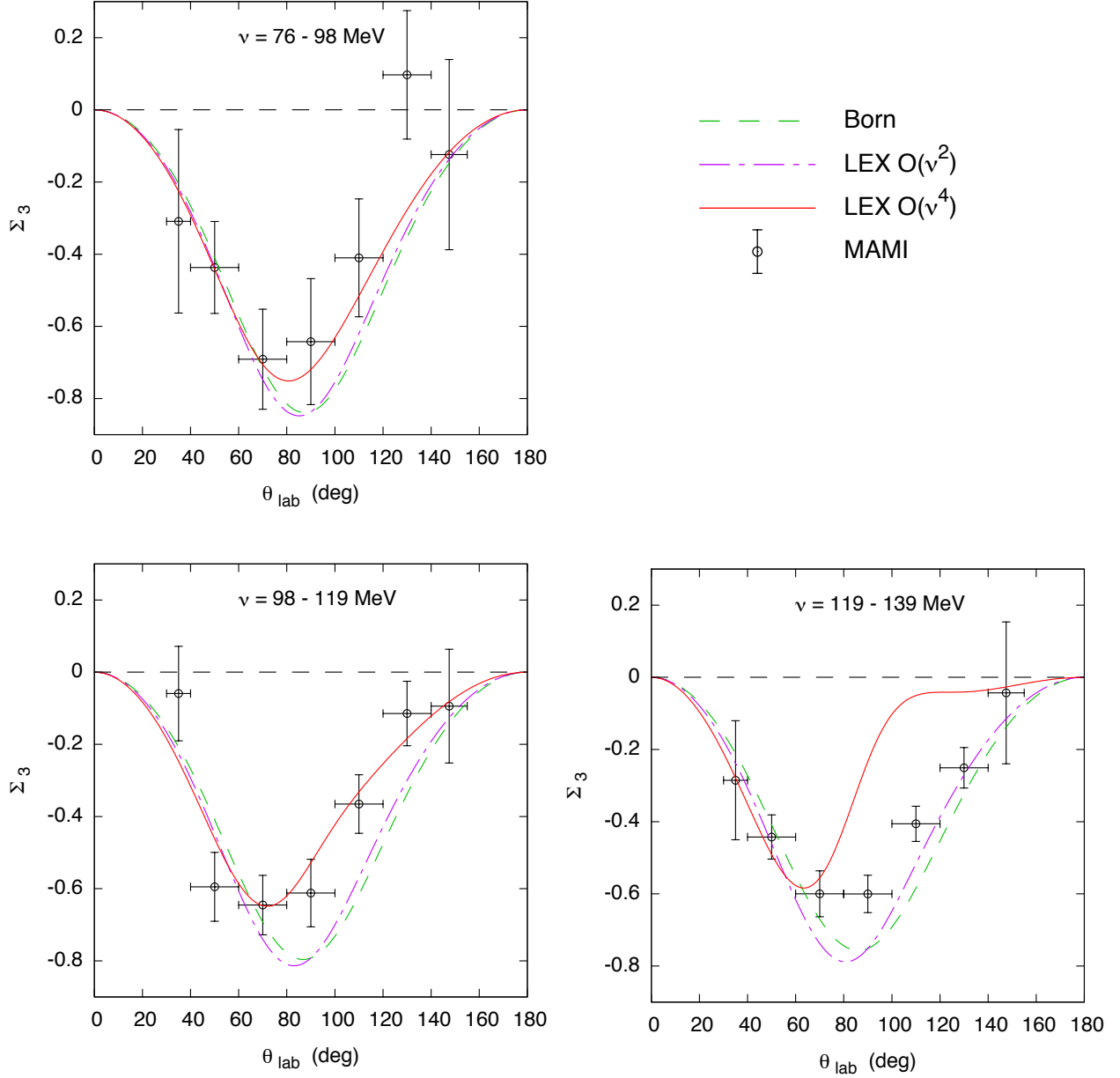


Figure 3.6: The beam asymmetry Σ_3 as a function of the scattering angle for the three photon energy bins. The black points are the experimental data from MAMI [Sokhoyan 2016]. The green dashed curve corresponds to the Born contribution, the dot-dashed purple curve represents the leading LEX formula (3.24), and the red solid curve corresponds to the contribution of the order of $O(v^4)$ from Eqs. (3.26), (3.35) and (3.28). The values of the scalar polarizabilities are taken from PDG [Olive 2014], $\alpha_{E1} = 11.2 [10^{-4} \text{fm}^3]$ and $\beta_{M1} = 2.5 [10^{-4} \text{fm}^3]$, and the spin and fourth-order scalar polarizabilities from BChPT [Lensky 2015], $\gamma_{E1E1} = -3.3 [10^{-4} \text{fm}^4]$, $\gamma_{E1M2} = 0.2 [10^{-4} \text{fm}^4]$, $\gamma_{M1E2} = 1.1 [10^{-4} \text{fm}^4]$, $\gamma_{M1M1} = 2.9 [10^{-4} \text{fm}^4]$, $\alpha_{E2} = 17.3 [10^{-4} \text{fm}^5]$, $\beta_{M2} = -15.5 [10^{-4} \text{fm}^5]$ and $\beta_{Mv} = 7.1 [10^{-4} \text{fm}^5]$.

where, as we discussed in the previous section, the LEX converges fast. However, the figure

clearly shows that it is not feasible at the moment as the current data have too large error bars. Therefore, Eq. (3.24) cannot be used to extract β_{M1} . Instead, we will utilize ChPT which includes the pion production physics.

Both BChPT and HBChPT can be used for our purposes⁷. We use the results of the BChPT calculation [Lensky 2014, Lensky 2015] which contains the Born, π^0 -anomaly contributions, chiral loops, $\Delta(1232)$ -excitation, and the contact term (see graph 3.1c). In this framework one could either treat both α_{E1} and β_{M1} as free parameters and perform a two-parameter fit, or fix their sum using its empirically known value [Gryniuk 2015],

$$\alpha_{E1} + \beta_{M1} = (14.0 \pm 0.2) \times 10^{-4} \text{ fm}^3, \quad (3.30)$$

and fit only β_{M1} . We choose to perform a one-parameter fit. To do so we calculate the chi-square

$$\chi^2 = \sum_{i=1}^{21} \left(\frac{(\Sigma_3^{\text{exp}})_i - (\Sigma_3^{\text{th}})_i}{\delta_i^{\text{exp}}} \right)^2, \quad (3.31)$$

where the sum is held over the 21 experimental data points, $(\Sigma_3^{\text{exp}})_i$, here $(\Sigma_3^{\text{th}})_i$ are the corresponding theoretical prediction, and δ_i^{exp} is the error of the i th observation. Note that due to the relative broadness of the energy and polar angle bins, we average the theoretical result for the cross sections over the bin width. The value of β_{M1} is then obtained from χ^2 at its minimum value, $\chi_{\min}^2 = 19.2$,

$$\beta_{M1} = 2.8_{-2.1}^{+2.3} [10^{-4} \text{ fm}^3], \quad (3.32)$$

where the error is defined from the $(\chi_{\min}^2 + 1)$ interval, see Fig. 3.7. Recall that the minimum value of χ^2 represents the level of agreement between the measurements and the fitted function, hence, we can conclude that our fit describes the data well as we have χ_{\min}^2 per point ≈ 1 .

Figure 3.8 shows the result of this fit. The band corresponds to the errors on β_{M1} given in Eq. (3.32), demonstrating the sensitivity of the beam asymmetry to the magnetic polarizability β_{M1} .

For completeness, we present also the value extracted from the same data set using HBChPT at fourth order [Sokhoyan 2016]

$$\beta_{M1} = 3.7_{-2.3}^{+2.5} [10^{-4} \text{ fm}^3]. \quad (3.33)$$

Thus, this method gives the value for β_{M1} compatible (within the large error bars) with the BChPT fit presented above. Note that the spin polarizabilities in BChPT and HBChPT are consistent with one another. However, the error bars are large and prevent a conclusive determination

⁷Differences between the BChPT and HBChPT calculations are reviewed in Ref. [Lensky 2012].

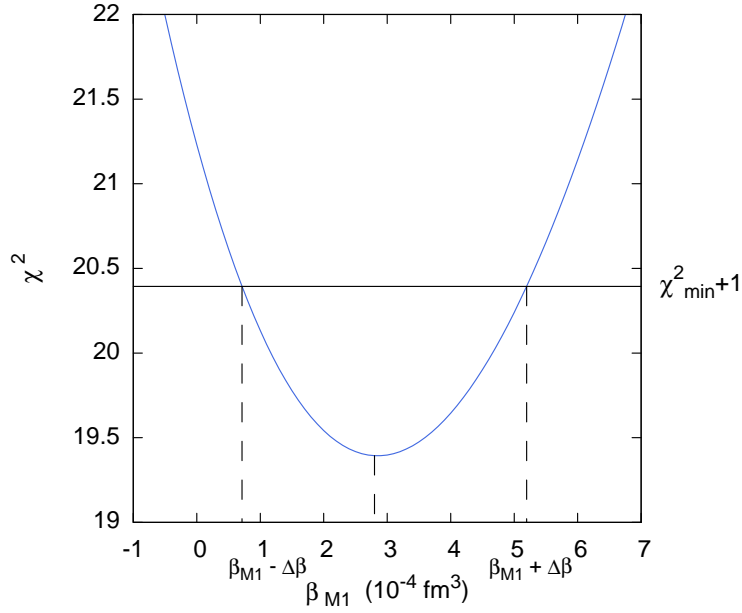


Figure 3.7: Chi-squared as a function of β_{M1} . The minimum of functions χ^2 defines the fitted parameter, β_{M1} . The corresponding error bars are obtained from the intersection of the χ^2 and $\chi^2_{\min} + 1$ curves.

of their values, e.g., the former gives $\gamma_0 = -0.9 \pm 1.4 [10^{-4} \text{fm}^4]$, whereas the value in the latter is $\gamma_0 = -2.6 \pm 1.9 [10^{-4} \text{fm}^4]$. We have checked that if we fix in our calculations the central values of the spin polarizabilities to the HBChPT values the minimum of chi-squared changes marginally.

Due to the large error bars the present extraction does not improve the accuracy of the global value of β_{M1} . Despite of that, we find these experimental data very exciting as they correspond to a pioneering measurement of Σ_3 at these energies. We expect that further measurements of this observable should pin down the value of β_{M1} . Such experiments are planned at MAMI with the aim to achieve a much higher accuracy by increasing the statistics and improving the control over systematic effects. According to our estimate, decreasing the error bars on experimental data by a factor of four, decreases the uncertainty on β_{M1} by the same factor. This would be already enough to impact the global determination of β_{M1} , as a single experiment should not compete with the accuracy of the global value, but with the accuracy of other experiments, in our case with the results of Olmos de Leon et al. [Olmos de Leon 2001].

At this moment one important comment is in order. In this subsection, we demonstrated that the LEX does not allow us to extract the magnetic polarizability from the new Σ_3 data. However, more importantly, we also showed that the LEX can help us to find the observables that are the best candidates for disentangling various polarizabilities, and, hence, guide ChPT calculations and experiments.

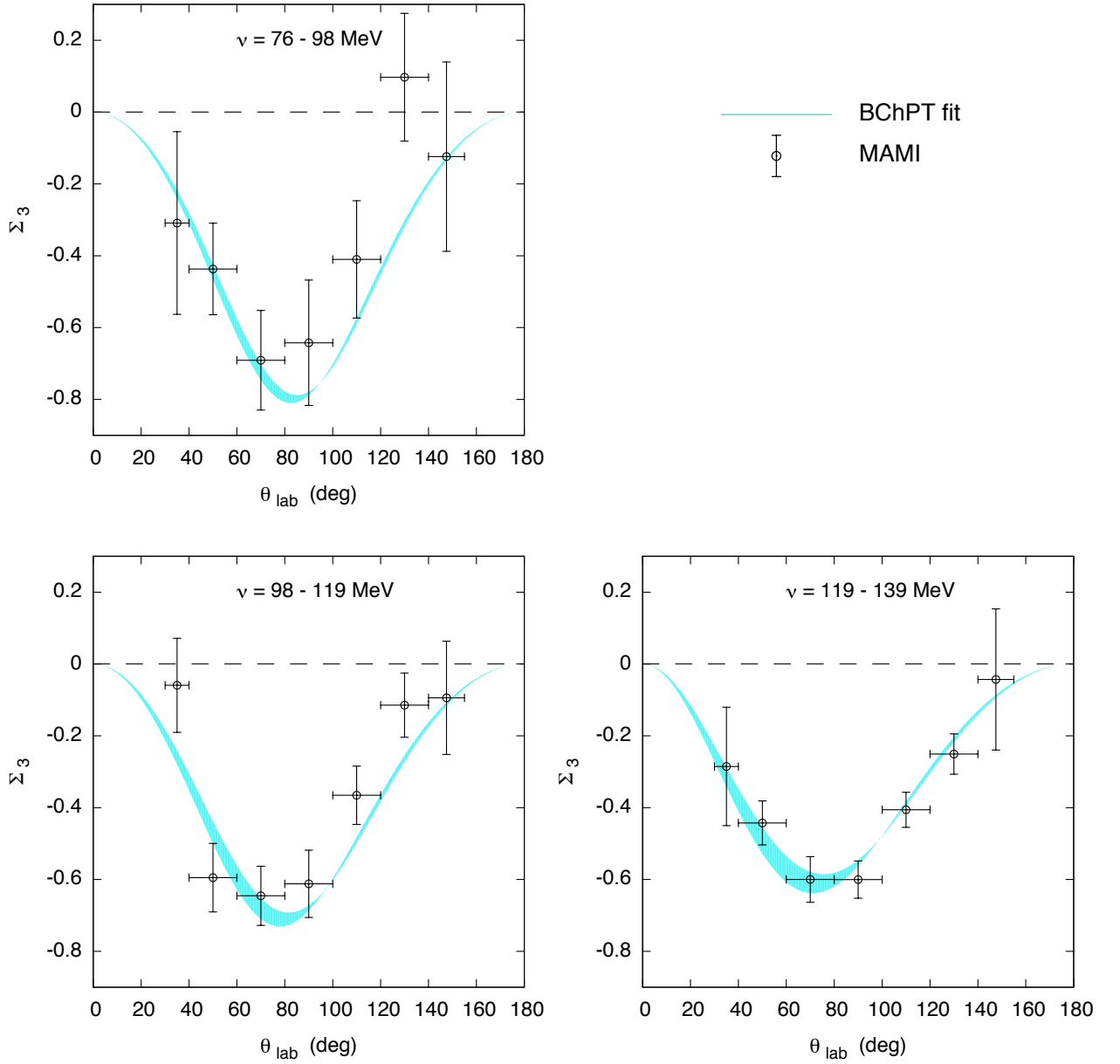


Figure 3.8: The beam asymmetry Σ_3 as a function of the scattering angle for the three photon energy bins. The black points are the experimental data from MAMI [Sokhoyan 2016], and the cyan band corresponds to the fit to BChPT [Lensky 2014, Lensky 2015].

3.8 Contribution of Spin Polarizabilities to R_i Functions and Σ_3

In this section we obtain the leading-order contribution of the spin polarizabilities to the functions R_i . To this end, we embrace the route developed for the scalar polarizabilities in Section 3.4. First the Feynman amplitude is decomposed into the Born and the non-Born parts,

$\mathcal{M}_B^{\mu\nu} + \mathcal{M}_{\text{NB}(3)}^{\mu\nu}$. The term $\mathcal{M}_B^{\mu\nu}$ is written in Supplementary Material 3.11, and $\mathcal{M}_{\text{NB}(3)}^{\mu\nu}$ is in Eq. (2.14). Note that the subscript (3) here indicates that we consider only the contribution of the spin polarizabilities to the non-Born amplitude. Second the expression for $\mathcal{M}_B^{\mu\nu} + \mathcal{M}_{\text{NB}(3)}^{\mu\nu}$ is inserted in Eq. (3.9). Then we obtain the functions R_i by comparing the result with Eq. (3.10),

$$\begin{aligned}
 R_0^{\text{NB}(3)} &= -\pi e^2 \gamma_{E1E1} \frac{(v+v')^2}{4vv'} \left[\frac{1}{2} (1-\kappa^2) t vv' - \kappa^2 v^2 v'^2 + \frac{1}{4} (1+\kappa) t^2 \right] \\
 &- \frac{\pi e^2}{4} \gamma_{E1M2} \left[-\left(\frac{1}{2} + \kappa\right) t + \kappa^2 vv' \right] (v^2 - 2t - 6vv' + v'^2) \\
 &+ \pi e^2 \gamma_{M1E2} \frac{1}{4vv'} \left[-\frac{1}{2} (1+\kappa) t^3 + 4\kappa^2 v^3 v'^3 + 4(-1+2\kappa)(1+\kappa) M^2 (v-v')^2 vv' \right. \\
 &- \left. 4(1+2\kappa)^2 M (v-v') v^2 v'^2 \right] \\
 &- \pi e^2 \gamma_{M1M1} \frac{(v+v')^2}{4vv'} \left[\frac{1}{4} (1+\kappa)^2 t^2 + \frac{1}{2} (3+6\kappa+2\kappa^2) vv' t - \kappa^2 v^2 v'^2 \right] + O(v^5), \\
 R_1^{\text{NB}(3)} &= \frac{\pi e^2}{4} \left[\gamma_{E1E1} - \gamma_{E1M2} + \gamma_{M1E2} (1+\kappa)^2 - \gamma_{M1M1} (1+\kappa)^2 \right] vv' (v+v')^2 + O(v^5), \\
 R_2^{\text{NB}(3)} &= \pi e^2 \gamma_{E1E1} \frac{(v+v')^2}{4vv'} \left[-2Mv^2 v' + \left(\frac{1}{2} + \kappa\right) vv' t + \frac{1}{4} (1+\kappa) t^2 \right] \\
 &+ \frac{\pi e^2}{4} \gamma_{E1M2} \left[-M(v+v')^3 + (1+2\kappa) t^2 + 4(1+2\kappa) vv' t \right] \\
 &- \pi e^2 \gamma_{M1E2} \frac{1}{4vv'} \left\{ -\frac{1}{2} (1+\kappa) t^3 - M^2 (2+5\kappa+3\kappa^2) (v-v')(v+v')^3 \right. \\
 &+ \left. 2M^2 (v-v') \left[\kappa(1+\kappa) v'^3 - (4-5\kappa-7\kappa^2) v^2 v' + (8+14\kappa+4\kappa^2) vv'^2 \right] \right. \\
 &+ \left. Mvv' \left[(3+6\kappa+2\kappa^2) (v+v')^3 + 2\kappa(2+3\kappa) v^3 + 4\kappa(-6-5\kappa) v^2 v' \right. \right. \\
 &- \left. \left. 2(8+14\kappa+\kappa^2) vv'^2 \right] \right\} + \pi e^2 \gamma_{M1M1} \frac{(v+v')}{4vv'} \left\{ M^2 (v-v') \left[(1+\kappa)^2 (v^2 - v'^2) \right. \right. \\
 &+ \left. \left. 4vv' \right] - Mvv' \left[(1+4\kappa+\kappa^2) (v^2 - v'^2) + 4vv' - 2(1+\kappa^2) v'(v'-v) \right] \right\} + O(v^5), \\
 R_3^{\text{NB}(3)} &= -\frac{\pi e^2}{8M} \gamma_{E1E1} v' (v+v') \left[-M(1+5\kappa+\kappa^2) v(v+v') - 2Mv(\kappa^2 v + v') \right. \\
 &- \left. (1+\kappa) Mt \right] - \frac{\pi e^2}{8M} \gamma_{E1M2} v \left[-4M^2 t - 4M^2 v'(v+v') - M(2+\kappa)(v+v') t \right. \\
 &- \left. 8M\kappa v' t - 4M(2+3\kappa) vv'^2 + 4M\kappa^2 vv'^2 \right] + \frac{\pi e^2}{8M} \gamma_{M1E2} \left\{ 8(1+\kappa) M^3 (v-v')^2 \right. \\
 &- \left. 4M^2 v(v-v') \left[\kappa(1+\kappa)v + (4+5\kappa)v \right] + 2Mv^2 v' \left[\kappa(1+3\kappa)v + (4+9\kappa-\kappa^2) v' \right] \right\} \\
 &+ \frac{\pi e^2}{8M} \gamma_{M1M1} (v+v') \left\{ Mv' (-6Mv - v^2 + 2Mv' + 5vv') + \kappa M [vv'(v+5v') \right. \\
 &- \left. 4M(v^2 - v'^2)] + \kappa^2 [4Mvv'^2 - 2M^2(v^2 - v'^2)] \right\} + O(v^5),
 \end{aligned}$$

$$\begin{aligned}
 R_4^{\text{NB}(3)} &= -\frac{\pi e^2}{8M} \gamma_{E1E1} v' (v + v') \left[2M^2 (v + v') + M(1 + \kappa) v^2 + M(3 + 5\kappa) v v' \right] \\
 &\quad - \frac{\pi e^2}{8M} \gamma_{E1M2} v v' \left[16M^2 v' - 2M(2 + 2\kappa + \kappa^2) t + 4M\kappa v^2 + 4M(2 - \kappa^2) v v' \right] \\
 &\quad + \frac{\pi e^2}{8M} \gamma_{M1E2} v' \left\{ 8M^3 (v - v') - 2M(1 + \kappa) v^2 [3\kappa v - (-4 + \kappa) v'] \right. \\
 &\quad \left. + 4M^2 v [(1 + \kappa) v - (3 + \kappa) v'] \right\} \\
 &\quad - \frac{\pi e^2}{8M} \gamma_{M1M1} v' (v + v') \left\{ -2M^2(1 + \kappa)(v - v') + Mv \left[(-1 + \kappa + \kappa^2) v \right. \right. \\
 &\quad \left. \left. + (5 + \kappa - \kappa^2) v' \right] \right\} + O(v^5), \\
 R_5^{\text{NB}(3)} &= 0, \\
 R_6^{\text{NB}(3)} &= 0, \\
 R_7^{\text{NB}(3)} &= 0.
 \end{aligned} \tag{3.34}$$

Using these expressions and Eqs. (3.17)-(3.21) we can calculate the contribution of the spin polarizabilities to the observables of interest. For instance, for the beam asymmetry we obtain

$$\begin{aligned}
 \Sigma_3^{\text{NB}(3)} &= -\frac{2 \sin^2 \theta_{lab} v^4}{(1 + \cos^2 \theta_{lab})^2 \alpha} \left[b_1(\cos \theta_{lab}) \gamma_{E1E1} + b_2(\cos \theta_{lab}) \gamma_{E1M2} + b_3(\cos \theta_{lab}) \gamma_{M1E2} \right. \\
 &\quad \left. + b_4(\cos \theta_{lab}) \gamma_{M1M1} \right] + O(v^5),
 \end{aligned} \tag{3.35}$$

where the dimensionless coefficients are

$$\begin{aligned}
 b_1(z_{lab}) &= -1 + \kappa + z_{lab}^2 (1 + \kappa) - z_{lab} (1 + \kappa)^2, \\
 b_2(z_{lab}) &= 1 - z_{lab} (1 + \kappa)^2 + z_{lab}^2 (1 + 2\kappa), \\
 b_3(z_{lab}) &= z_{lab} \left[\kappa + z_{lab}^2 (1 + \kappa) - 2z_{lab} (1 + \kappa)^2 \right], \\
 b_4(z_{lab}) &= z_{lab} + 2z_{lab} \kappa - (1 + \kappa)^2 + z_{lab}^2 (1 + \kappa)^2.
 \end{aligned} \tag{3.36}$$

Note that the presented expression is the leading-order contribution of the spin polarizabilities to the beam asymmetry. The inclusion of this term is necessary when considering the scattering at $\theta_{lab} > 60$ degrees. We have discussed this fact already in Section 3.6, and here we support this statement by plotting $\Sigma_3^{\text{NB}(3)}$ in Fig. 3.9. We see that at $\theta_{lab} \lesssim 60$ degrees $\Sigma_3^{\text{NB}(3)}$ is small and can be neglected, however, at larger angles it should be included, as, for example, at $\theta \approx 100$ degrees it amounts to about 10% of the LO non-Born contribution given in Eq. (3.24) (cf. Fig. 3.4).

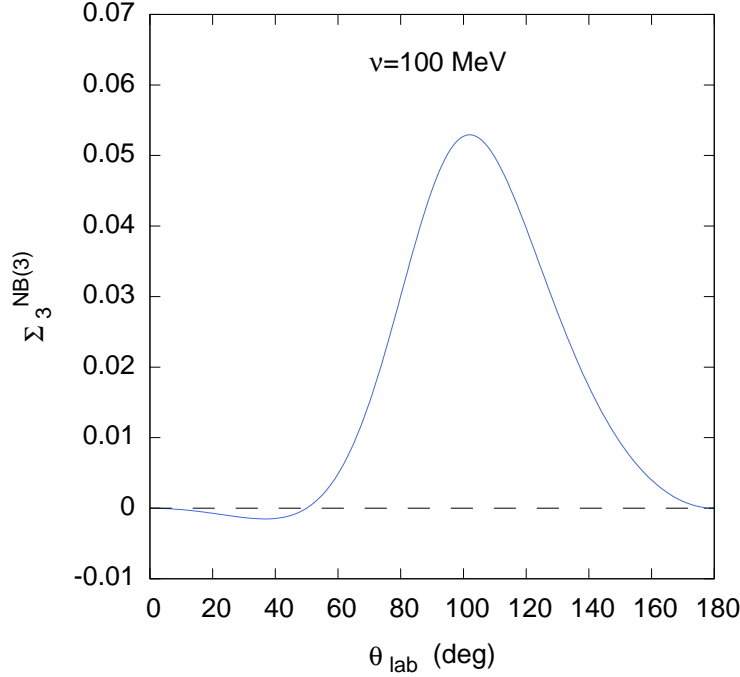


Figure 3.9: The leading-order contribution of the spin polarizabilities to the beam asymmetry Σ_3 given by Eq. (3.35) as a function of the scattering angle for the photon energy of 100 MeV.

3.9 Low-energy Expansion of Σ_{2x} and Σ_{2z}

In this section we study the beam-target asymmetries Σ_{2z} and Σ_{2x} . In particular we show that they can be used to measure experimentally the effect of the spin polarizabilities.

To calculate Σ_{2z} and Σ_{2x} we insert Eq. (3.34) into Eqs. (3.18) and (3.19), see the discussion in the previous chapter, and obtain the leading order non-Born contribution to these observables,

$$\begin{aligned} \Sigma_{2x}^{(NB)} &= -\frac{\sin \theta_{lab} v^3}{(1+z_{lab}^2)\alpha} \{\alpha_{E1}[(1+\kappa)^2 - (1+2\kappa)z_{lab}] \\ &+ \frac{\beta_{M1}}{1+z_{lab}^2} [\kappa + 3(1+\kappa)^2 z_{lab} - 3(1+2\kappa)z_{lab}^2 - (1+\kappa)^2 z_{lab}^3 + (1+\kappa)z_{lab}^4] \\ &+ 2[\gamma_{M1M1} + z_{lab}(\gamma_{E1E1} + \gamma_{E1M2}) + z_{lab}^2 \gamma_{M1E2}]\} + O(v^4), \end{aligned} \quad (3.37a)$$

$$\begin{aligned} \Sigma_{2z}^{(NB)} &= -\frac{v^3}{(1+z_{lab}^2)\alpha} \{\alpha_{E1}[-\kappa + 2(1+\kappa)^2 z_{lab} - (2+3\kappa)z_{lab}^2] \\ &+ \frac{\beta_{M1}}{1+z_{lab}^2} [-(1+\kappa)^2 + (1-\kappa)z_{lab} + 6(1+\kappa)^2 z_{lab}^2 - 2(3+4\kappa)z_{lab}^3 - (1+\kappa)^2 z_{lab}^4 + (1+\kappa)z_{lab}^5] \\ &+ 2[(1+z_{lab}^2)(\gamma_{E1E1} + z_{lab} \gamma_{M1E2}) + 2z_{lab}(\gamma_{M1M1} + z_{lab} \gamma_{E1M2})]\} + O(v^4). \end{aligned} \quad (3.37b)$$

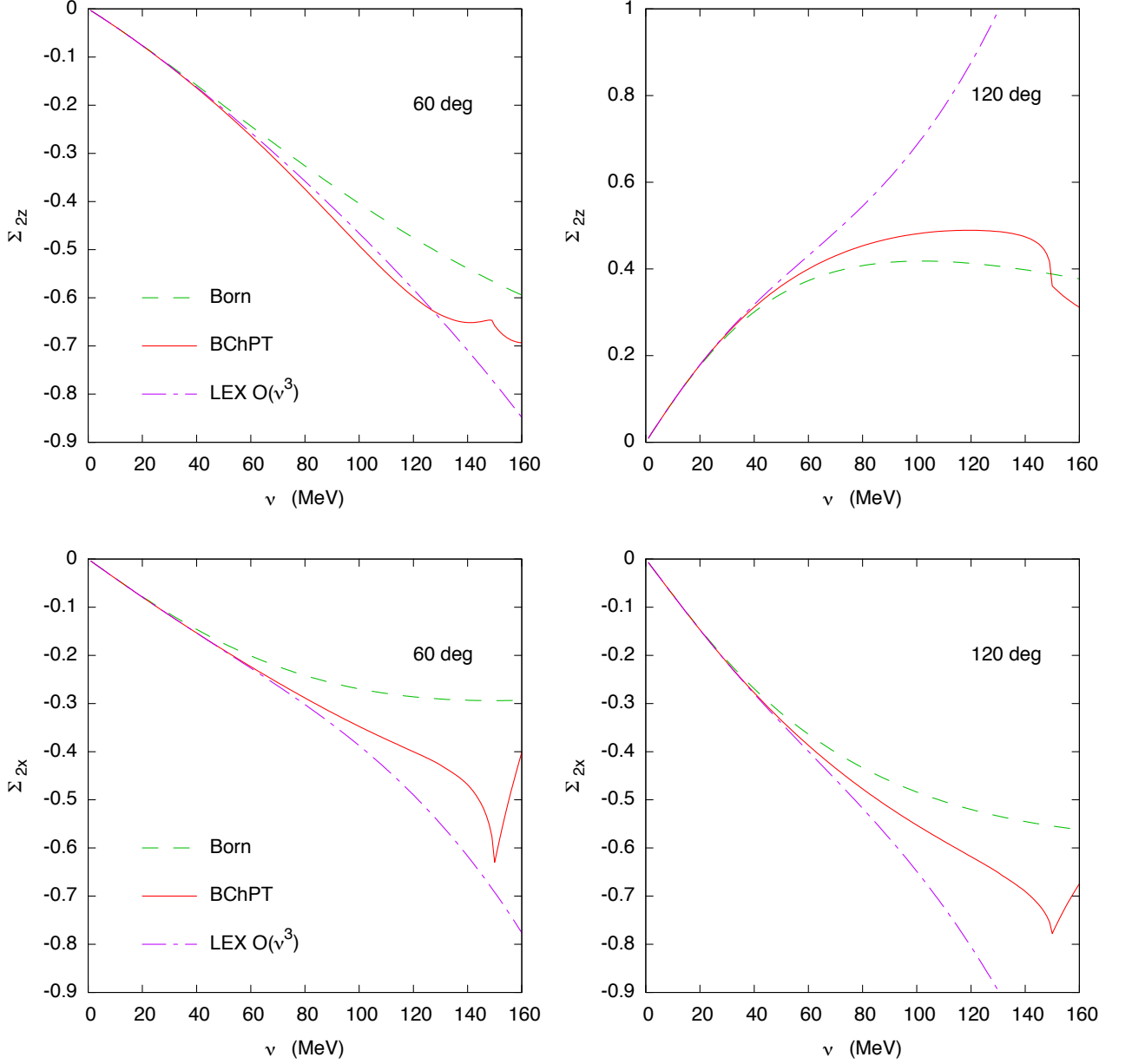


Figure 3.10: The beam-target asymmetries Σ_{2z} (upper panel) and Σ_{2x} (lower panel) as functions of the incident photon energy for scattering angles of 60 (left panel) and 120 (right panel) degrees. The dashed green curves correspond to the Born contribution, red solid to the NNLO BChPT, and dot-dashed purple to the leading LEX formulas from Eq. (3.37).

To demonstrate the limits of applicability of Eq. (3.37), we follow the strategy outlined for Σ_3 , i.e., we compare the LEX expressions with the predictions of BChPT. We illustrate this comparison in Fig. 3.10. In particular, it shows that for $\theta_{lab} = 60 \text{ deg}$ Eq. (3.37) is applicable only for photon energies below $\nu \approx 80 \text{ MeV}$, and for $\theta_{lab} = 120 \text{ deg}$ only below $\nu \approx 50 \text{ MeV}$, as there the LEX and BChPT curves coincide implying that the higher-order corrections to Eq. (3.37) are

suppressed.

It is worthwhile noting that the spin polarizabilities enter in the $O(\nu^3)$ terms, and, hence, their effect is believed to be measurable only at relatively high energies. For example, modern experiments [Martel 2015] designed for this purpose operate at energies around the $\Delta(1232)$ -resonance. At these energies Eq. (3.37) does not apply, cf. Fig. 3.10, and, to extract the polarizabilities, model-dependent approaches should be used. The expressions we derive here provide valuable reference points at low energies for testing and developing these techniques. Once they are tested, we will use them to describe the current experiments that aim to extract the spin polarizabilities.

3.10 Summary

In this chapter we used the LEX to study low-energy Compton scattering and the observables that can be used to measure the proton polarizabilities. First, we addressed the magnetic dipole polarizability, β_{M1} . In particular, we showed that it determines the leading order non-Born contribution to the beam asymmetry. This result together with the observation that the next-to-leading corrections are suppressed at forward scattering angles allowed us to argue that a precise and model-independent determination of β_{M1} is feasible through a precision measurement of Σ_3 at forward scattering angles and beam energies below 100 MeV [Krupina 2013].

Our results inspired the A2 collaboration at MAMI to measure the beam asymmetry for the first time below the pion-production threshold [Sokhoyan 2016]. In this chapter we presented and discussed their preliminary results. In particular, we examined the LEX in the kinematical region of the experiment and concluded that it should not be used in the upper energy range. Also we noted that in the lower energy range, i.e., $\nu = 79 - 98$ MeV, where the LEX can be applied, the extraction of β_{M1} is at present not possible due to large error bars on the data. To overcome the LEX limitations and extract β_{M1} we used the BChPT analysis that yielded

$$\beta_{M1} = 2.8_{-2.1}^{+2.3} [10^{-4} \text{fm}^3]. \quad (3.38)$$

The error bars on this value are too large to make this experiment conclusive. However, we have estimated that decreasing the errors on the data by a factor of four, decreases the uncertainty on β_{M1} by the same factor. Therefore, we believe that the new more accurate measurements scheduled at MAMI will help us to extract the value of the magnetic dipole polarizability more precisely.

Finally, we studied the beam-target asymmetries Σ_{2z} and Σ_{2x} , which are sensitive to the spin polarizabilities. We demonstrated that the LEX results for these observables have a very limited region of the applicability, i.e., the beam energy below 80 MeV for $\theta_{lab} = 60 \text{ deg}$ and even lower

energies for larger angles, where the effect of the spin polarizabilities cannot be measured. Note that even though these LEX results cannot be used to extract the polarizabilities from the existent CS data, they allow us to understand the behavior of observables at low energies. This, in turn, shall guide further theoretical and experimental investigations.

3.11 Supplementary Material

Born Contribution to R_i Functions

Here we obtain the Born contribution⁸ to the R_i functions and, hence, to the observables (cf. Eqs. (3.17) - (3.21)). In order to do this, we first use the Lagrangian from Eq. (2.5) to write down the Feynman amplitude (for details see Chapter 2)

$$\mathcal{M}_B^{\mu\nu} = -\Gamma^\mu(p', p+k) \frac{\not{p} + \not{k} + M}{s - M^2} \Gamma^\nu(p+k, p) - \Gamma^\nu(p', p'-k) \frac{\not{p}' - \not{k} + M}{u - M^2} \Gamma^\mu(p' - k, p), \quad (\text{SM3.39})$$

where $\Gamma^\mu(p', p+k) = e\gamma^\mu - \frac{e}{2M}\kappa(\gamma^{\mu\rho}p'_\rho - \gamma^{\mu\delta}(p+k)_\delta)$ is the electromagnetic vertex [Peskin 1995]. Then by inserting $\mathcal{M}_B^{\mu\nu}$ into $\sum_{H'} |T_{H',H}|^2$ (Eq. (3.9)) and by matching the result to Eq. (3.10), we obtain the following expressions for the R_i functions

$$\begin{aligned} R_0^B &= e^4 \left[1 - \frac{(v-v')^2}{2vv'} (\kappa^2 - 1) \left(1 + 2\kappa + \frac{1}{2}\kappa^2 \right) + \frac{v-v'}{M} 3\kappa^2 \left(1 + \kappa + \frac{1}{6}\kappa^2 \right) + \frac{vv'}{4M^2} \kappa^4 \right], \\ R_1^B &= e^4 \left[-1 - \frac{vv'}{M^2} \kappa^2 \left(1 + \kappa + \frac{1}{4}\kappa^2 \right) \right], \\ R_2^B &= e^4 \left[\left(\frac{v}{v'} - \frac{v'}{v} \right) \left(\frac{1}{2} + \kappa \right) + \left(\frac{v}{v'} - \frac{v}{M} - 1 \right) \kappa^2 + \frac{(v-v')^2}{4vv'} \kappa^2 \left(1 + 4\kappa + \kappa^2 \right) \right. \\ &\quad \left. - \frac{(v-v')}{M} \kappa^2 \left(1 + 2\kappa + \frac{1}{2}\kappa^2 \right) \right], \\ R_3^B &= e^4 \left[\frac{1}{2} \left(\frac{v}{v'} - \frac{v}{M} - 1 \right) (1 + \kappa) - \frac{v'}{2M} (1 + \kappa)^2 - \frac{v-v'}{4M} \kappa^2 (3 + 4\kappa + \kappa^2) \right. \\ &\quad \left. + \frac{vv'}{4M^2} \kappa^2 (1 + 3\kappa + \kappa^2) \right], \\ R_4^B &= e^4 \left[\frac{v+v'}{2M} (1 + \kappa) + \frac{v}{2M} \kappa + \frac{v-v'}{4M} \kappa^2 (3 + \kappa) - \frac{vv'}{4M^2} \kappa^2 (1 + \kappa) \right], \\ R_5^B &= 0, \\ R_6^B &= 0, \\ R_7^B &= 0. \end{aligned} \quad (\text{SM3.40})$$

There is another piece in the amplitude which can be calculated exactly. It is the so called

⁸Recall that the Born term is given by the tree-level graphs 3.1a and 3.1b, where the proton is assumed to be a structureless object with mass M , electric charge e and anomalous magnetic moment κ .

π^0 -anomaly term, which describes the t-channel exchange of a neutral pion. There is no conventional choice whether to treat this term together with the Born or include it in the non-Born part. We choose the former⁹ approach. Below we present the contribution of the π^0 -anomaly using the Feynman amplitude

$$\mathcal{M}_{(\pi^0)}^{\mu\nu} = A \gamma^{\alpha\beta\mu\nu} k'_\alpha k_\beta, \quad (\text{SM3.41})$$

where $A = \frac{g_A}{(2\pi f_\pi)^2} \frac{M^2}{t - m_{\pi^0}^2}$. For the R_i functions it yields

$$\begin{aligned} R_0^{(\pi^0)} &= \frac{1}{2} e^2 A (\nu - \nu')^2 [(1 - z_{lab})(1 + \kappa) + \kappa(2 + \kappa)] + \frac{1}{2} A^2 M (\nu - \nu')^3, \\ R_1^{(\pi^0)} &= 0, \\ R_2^{(\pi^0)} &= -\frac{1}{2} e^2 A (1 - z_{lab}) \left\{ (\nu'^2 - \nu^2) + \frac{2\nu^2\nu'}{M} (1 + z_{lab})\kappa^2 + \left[(\nu + \nu')^2 + \frac{2\nu\nu'}{M} (\nu + \nu') \right. \right. \\ &\quad \left. \left. + \frac{4\nu^2}{M} (\nu' - M) \right] \kappa \right\} + (A \nu\nu')^2 (1 - z_{lab}^2), \\ R_3^{(\pi^0)} &= \frac{1}{4} e^2 A \left\{ -2\nu' (\nu - \nu') + 2 \left[(\nu + \nu')^2 + \frac{2\nu\nu'}{M} (\nu + \nu') - 4\nu^2 \right] \kappa + \nu [-4(\nu - \nu') \right. \\ &\quad \left. + \frac{\nu'}{M} (\nu + \nu') + \frac{2\nu\nu'}{M} \right] \kappa^2 \right\} - (A \nu\nu')^2 z_{lab}, \\ R_4^{(\pi^0)} &= e^2 A \left[\frac{1}{2} \nu' (\nu - \nu') - \frac{\nu\nu'}{M} (\nu + \nu')\kappa - \frac{\nu\nu'}{4M} (3\nu + \nu')\kappa^2 \right] + (A \nu\nu')^2, \\ R_5^{(\pi^0)} &= 0, \\ R_6^{(\pi^0)} &= 0, \\ R_7^{(\pi^0)} &= 0. \end{aligned} \quad (\text{SM3.42})$$

We have used the algebraic manipulation program FORM [Kuipers 2013] to obtain these equations.

Kinematics

Here we review the kinematics of Compton scattering in the laboratory, the center-of-mass and the Breit (brick-wall) frames. Additionally, we present useful formulae, which relate the scattering angles and the photon energies in different reference systems.

Let us first introduce the aforementioned reference frames, which are often used to describe Compton scattering. They are

- (i) The laboratory frame – the frame in which the proton is initially at rest. Here the incoming photon propagates along the z -direction and has the energy ν . After the scattering event, the particles move in the xz -plane along the directions defined by the energies and the

⁹Note that if the latter approach is chosen, then the spin polarizabilities are usually redefined to absorb the π^0 -anomaly.

scattering angle θ_{lab} . The energy of the outgoing photon is ν' and of the proton is $E' = M + \nu - \nu'$. The corresponding 4-momenta of the incoming and outgoing particles are summarized below

Incoming particles	Outgoing particles
$p = (M, 0, 0, 0)$	$p' = (E', -\nu' \sin \theta_{lab}, 0, \nu - \nu' \cos \theta_{lab})$
$k = (\nu, 0, 0, \nu)$	$k' = (\nu', \nu' \sin \theta_{lab}, 0, \nu' \cos \theta_{lab})$

Using the Mandelstam variables s and t in this frame we write ν and $\cos \theta_{lab}$ as

$$\begin{aligned} \nu &= \frac{s - M^2}{2M}, \\ \cos \theta_{lab} &= 1 + \frac{t}{2\nu\nu'}. \end{aligned} \quad (\text{SM3.43})$$

Note also the following standard expressions, which are useful in derivations

$$\begin{aligned} \nu - \nu' &= \frac{\nu\nu'}{M}(1 - \cos \theta_{lab}) = -\frac{t}{2M}, \\ \frac{\nu}{\nu'} - \frac{\nu'}{\nu} &= \frac{\nu + \nu'}{M}(1 - \cos \theta_{lab}), \\ \frac{\nu}{\nu'} - \frac{\nu}{M} - 1 &= -\frac{\nu \cos \theta_{lab}}{M}. \end{aligned} \quad (\text{SM3.44})$$

- (ii) The center-of-mass frame – the frame in which the total 3-momentum of the system vanishes. Here initially the photon has the energy ω and propagates along the z -direction. At the same time, the proton moves along the negative z -direction with the energy $E = \sqrt{M^2 + \omega^2}$. After the scattering event, the energies are conserved and the particles move in the xz -plane along the directions defined by the scattering angle θ . The 4-momenta of the incoming and outgoing particles are shown below.

Incoming particles	Outgoing particles
$p = (E, 0, 0, -\omega)$	$p' = (E, -\omega \sin \theta, 0, -\omega \cos \theta)$
$k = (\omega, 0, 0, \omega)$,	$k' = (\omega, \omega \sin \theta, 0, \omega \cos \theta)$

Using the variables s and t , we obtain the following useful expressions

$$\begin{aligned} \omega &= \frac{s - M^2}{2\sqrt{s}}, \\ \cos \theta &= 1 + \frac{t}{2\omega^2}. \end{aligned} \quad (\text{SM3.45})$$

- (iii) The Breit frame – the frame in which the energy transfer is zero (hence $\vec{p} + \vec{p}' = 0$). Here the incoming proton moves along the z -direction with the energy $E_B = \sqrt{M^2 + \omega_B^2 \sin^2 \theta_B/2}$, whereas the photon propagates along the direction¹⁰ $(\frac{\pi+\theta_B}{2}, 0)$ and has the energy ω_B . The scattering event reverses the z -components of 3-momenta as if the particles are reflected from a wall (that is why, the reference system is called also the brick-wall frame). The corresponding 4-momenta of the particles are presented in the table below.

Incoming particles	Outgoing particles
$p = (E_B, 0, 0, -\omega_B \sin \theta_B/2)$	$p' = (E_B, 0, 0, \omega_B \sin \theta_B/2)$
$k = (\omega_B, \omega_B \cos \theta_B/2, 0, \omega_B \sin \theta_B/2)$	$k' = (\omega_B, \omega_B \cos \theta_B/2, 0, -\omega_B \sin \theta_B/2)$

Using the variables s and t we write ω_B and $\cos \theta_B$ as

$$\begin{aligned}\omega_B &= \frac{s - M^2 + \frac{t}{2}}{\sqrt{4M^2 - t}}, \\ \cos \theta_B &= 1 + \frac{t}{2\omega_B^2}.\end{aligned}\tag{SM3.46}$$

We recall, that the Mandelstam variables are invariant under the Lorentz transformation. Therefore, using Eqs. (SM3.43), (SM3.45) and (SM3.46), we establish the following useful relations, which connect the photon energies, and the scattering angles in different reference frames,

$$\begin{aligned}\cos \theta_B &= 1 - (1 - \cos \theta_{lab}) \frac{v v'}{\omega_B^2} = 1 - (1 - \cos \theta) \frac{\omega^2}{\omega_B^2}, \\ \omega_B &= \frac{2Mv + \frac{t}{2}}{\sqrt{4M^2 - t}} = \frac{2\sqrt{s}\omega + \frac{t}{2}}{\sqrt{4M^2 - t}}, \\ v &= \frac{\omega_B \sqrt{4M^2 - t} - \frac{t}{2}}{2M}, \\ v' &= \frac{\omega_B \sqrt{4M^2 - t} + \frac{t}{2}}{2M}, \\ \omega_B &= \frac{(v + v')M}{\sqrt{4M^2 - t}}.\end{aligned}\tag{SM3.47}$$

Other Observables in Terms of R_i

Besides the observables that we have introduced and considered in this chapter, there are other independent single and double polarized observables, such as Σ_y , Σ_{1x} , Σ_{1z} and Σ_{3y} . Their definitions can be found in Ref. [Babusci 1998a]. Let us present the expressions for these observables

¹⁰Here the direction is defined by the polar and azimuthal angles.

in terms of the invariant response functions

$$\begin{aligned}
\Sigma_y &= -\frac{\sin \theta_{lab} \left(R_5 + R_6 \cos \theta_{lab} - \frac{1}{2} R_7 \sin^2 \theta_{lab} \right)}{R_0 + \frac{1}{2} R_1 \sin^2 \theta_{lab}}, \\
\Sigma_{1x} &= \frac{\sin \theta_{lab} (R_5 + R_6 \cos \theta_{lab})}{R_0 + \frac{1}{2} R_1 \sin^2 \theta_{lab}}, \\
\Sigma_{1z} &= -\frac{R_6 \sin^2 \theta_{lab}}{R_0 + \frac{1}{2} R_1 \sin^2 \theta_{lab}}, \\
\Sigma_{3y} &= \frac{\Sigma_3 + \Sigma_y}{1 + \Sigma_y} \cos 2\phi. \tag{SM3.48}
\end{aligned}$$

The functions R_5 , R_6 and R_7 at the energies of interest are much smaller than the functions $R_1 - R_4$. Therefore these observables are not relevant for our analysis. However, these expressions are important since they complement the observables in Eqs. (3.3)-(3.6) to a minimal closed set of observables in CS with a polarized initial state.

Multipole Expansion of Observables

This chapter introduces the MEX-based fitting procedure that determines the polarizabilities using the existing experimental data.

4.1 Introduction

Here we introduce a model-independent approach based on the MEX from Chapter 2, which can be used to determine the polarizabilities without employing the LEX. An advantage of the MEX over the LEX is that the former can be successfully applied at relatively high energies, i.e., while the LEX is accurate only for photon energies smaller than 100 MeV, the MEX does not have such limitations. On the downside, the number of non-vanishing parameters¹ (multipole amplitudes $f_{\rho\rho'}^{\ell\pm}$, defined in chapter 2) in the MEX depends on the energy region, i.e., the larger the energy, the larger the number of multipoles that should be taken into account.

In this chapter we limit ourselves to the energies below the pion production threshold, i.e., $\nu < 150$ MeV. At these energies to a good approximation one can truncate the series in the MEX at angular momentum $J = 3/2$, hence, any Compton scattering observable can be parametrized by the 10 parameters

$$f_{EE}^{1+}, f_{EE}^{1-}, f_{MM}^{1+}, f_{MM}^{1-}, f_{EM}^{1+}, f_{ME}^{1+}, f_{EE}^{2+}, f_{EE}^{2-}, f_{MM}^{2+}, f_{MM}^{2-}. \quad (4.1)$$

Each of these multipoles consists of the Born and non-Born parts, i.e., $f = f^B + \bar{f}$. The former part can be calculated exactly (see Section 4.2), however, since it does not contain the polarizabilities, we are mainly after the latter piece. To obtain it, we first anchor the four multipoles \bar{f}_{EE}^{2+} , \bar{f}_{EE}^{2-} , \bar{f}_{MM}^{2+} , \bar{f}_{MM}^{2-} to the values predicted by BChPT at NNLO [Lensky 2015]. This reduces the number of parameters without affecting the outcome, because the BChPT results tell us that these multipoles are small, and contribute only marginally to observables. To find the other non-Born multipoles which are related to the two scalar, α_{E1} and β_{M1} , and four spin, γ_{E1E1} ,

¹We remind the reader (see Chapter 2) that, within the MEX approach, observables can be calculated using the six independent helicity amplitudes, e.g., $\Phi_1 - \Phi_6$ given by Eq. (2.51). These amplitudes can be expanded in partial waves (see Eq. (2.48)), which can be further decomposed into the sum of multipole amplitudes, $f_{\rho\rho'}^{\ell\pm}$, given by Eq. (2.52). Therefore, the multipoles $f_{\rho\rho'}^{\ell\pm}$ fully characterize the MEX.

γ_{M1M1} , γ_{E1M2} , and γ_{M1E2} , polarizabilities, we develop a fitting procedure which uses the existing experimental data as an input, see Section 4.3.

We structure this chapter as follows. In Section 4.2 we first calculate the Born contribution and discuss the non-Born contribution to the multipole amplitudes. After that we discuss the method and its main ingredient — the relation between the non-Born multipoles from Eq. (4.1) and the static polarizabilities. This relation, shown below in Eq. (4.10), is the cornerstone of our analysis which allows us to find directly the polarizabilities that fit experimental data. In Section 4.3 we explain all the details of the employed fitting procedure, i.e., we show the used data, we discuss the constraints that we have implemented to reduce the number of fitted parameters etc. Finally, in Section 4.4 we discuss the results obtained with the existing unpolarized CS data.

4.2 Description of the Method

4.2.1 Born Contribution to $f_{\rho'\rho}^{\ell\pm}$

Here we demonstrate that the Born contributions to the multipole amplitudes can be calculated exactly. To do so, we use the fact that the d -functions are orthogonal to invert the formulae in Eq. (2.52),

$$\begin{aligned}
 f_{MM}^{L+} &= \frac{1}{(L+1)^2} \left\{ \frac{1}{2} \left(\Phi_1^{L+\frac{1}{2}} \mp \Phi_2^{L+\frac{1}{2}} \right) \pm \frac{L+2}{\sqrt{L(L+2)}} \left(\Phi_3^{L+\frac{1}{2}} \mp \Phi_4^{L+\frac{1}{2}} \right) \right\} \\
 &+ \frac{L+2}{2L} \left(\Phi_5^{L+\frac{1}{2}} \mp \Phi_6^{L+\frac{1}{2}} \right), \\
 f_{MM}^{(L+1)-} &= \frac{1}{(L+1)^2} \left\{ \frac{1}{2} \left(\Phi_1^{L+\frac{1}{2}} \pm \Phi_2^{L+\frac{1}{2}} \right) \pm \frac{L}{\sqrt{L(L+2)}} \left(\Phi_3^{L+\frac{1}{2}} \pm \Phi_4^{L+\frac{1}{2}} \right) \right\} \\
 &+ \frac{L}{2(L+2)} \left(\Phi_5^{L+\frac{1}{2}} \pm \Phi_6^{L+\frac{1}{2}} \right), \\
 f_{ME}^{L-} &= \frac{1}{(L+1)^2} \left\{ -\frac{1}{2} \left(\Phi_1^{L+\frac{1}{2}} \mp \Phi_2^{L+\frac{1}{2}} \right) \mp \frac{1}{\sqrt{L(L+2)}} \left(\Phi_3^{L+\frac{1}{2}} \mp \Phi_4^{L+\frac{1}{2}} \right) \right\} \\
 &+ \frac{1}{2} \left(\Phi_5^{L+\frac{1}{2}} \mp \Phi_6^{L+\frac{1}{2}} \right),
 \end{aligned} \tag{4.2}$$

where the partial amplitudes are defined as follows

$$\Phi_i^J(\nu) = \frac{1}{2} \int_{-1}^{+1} \Phi_i(\nu, \theta) d_{\sigma_i' - \lambda_i' \sigma_i - \lambda_i}^J(\theta) d \cos \theta, \quad i = 1, \dots, 6. \tag{4.3}$$

Therefore, to compute the Born part of the multipole amplitudes, one can first calculate the Born contribution to the helicity amplitudes $\Phi_i^{(B)}$, and then simply use Eqs. (4.2) and (4.3). To calculate $\Phi_i^{(B)}$, we use the manifestly Lorentz- and gauge invariant CS amplitude written in terms

of the eight invariant amplitudes $\mathcal{A}_1, \dots, \mathcal{A}_8$ [Pascalutsa 2003],

$$T_{H',H} = 4\pi\alpha \bar{u}_{\lambda'}(p') \sum_{i=1}^8 \mathcal{A}_i(s, t) O_i^{\mu\nu} \mathcal{E}_{(\sigma')\mu}^* \mathcal{E}_{(\sigma)\nu} u_{\lambda}(p), \quad (4.4)$$

where $\mathcal{E}_{(\sigma)\mu}$ is the modified photon polarization vector,

$$\mathcal{E}_{(\sigma)\mu} = \varepsilon_{(\sigma)\mu} - \frac{P \cdot \varepsilon_{(\sigma)}}{P \cdot k} k_{\mu}, \quad (4.5)$$

with $P = p + p'$. The tensors O_i have the following expressions

$$\begin{aligned} O_1^{\mu\nu} &= -g^{\mu\nu}, \\ O_2^{\mu\nu} &= k^{\mu} k'^{\nu}, \\ O_3^{\mu\nu} &= -\gamma^{\mu\nu}, \\ O_4^{\mu\nu} &= g^{\mu\nu} (k' \cdot \gamma \cdot k), \\ O_5^{\mu\nu} &= k^{\mu} k'_{\alpha} \gamma^{\alpha\nu} - \gamma^{\alpha\mu} k_{\alpha} k'^{\nu}, \\ O_6^{\mu\nu} &= k^{\mu} k_{\alpha} \gamma^{\alpha\nu} - \gamma^{\alpha\mu} k'_{\alpha} k'^{\nu}, \\ O_7^{\mu\nu} &= k^{\mu} k'^{\nu} (k' \cdot \gamma \cdot k), \\ O_8^{\mu\nu} &= -i\gamma_5 \varepsilon^{\mu\nu\alpha\beta} k'_{\alpha} k_{\beta}, \end{aligned} \quad (4.6)$$

where $k' \cdot \gamma \cdot k \equiv k'_{\mu} \gamma^{\mu\nu} k_{\nu}$. The Born parts of the eight invariant amplitudes are

$$\begin{aligned} \mathcal{A}_1^{(B)} &= -\frac{1}{M} - \frac{(1+\kappa)^2 t^2}{16M^3 v v'}, \\ \mathcal{A}_2^{(B)} &= \frac{\kappa \{-\kappa t^2 + 8M^2[-2\kappa v v' + (2+\kappa)t]\}}{64M^5 v v'}, \\ \mathcal{A}_3^{(B)} &= -\frac{(t+4Mv)[2\kappa^2 v v' + (1+\kappa)^2 t]}{16M^3 v v'}, \\ \mathcal{A}_4^{(B)} &= -\frac{(1+\kappa)^2 (t+4Mv)}{8M^3 v v'}, \\ \mathcal{A}_5^{(B)} &= \frac{(1+\kappa)^2 (t+4Mv)}{8M^3 v v'}, \\ \mathcal{A}_6^{(B)} &= -\frac{(1+\kappa)(t+4Mv)}{8M^3 v v'}, \\ \mathcal{A}_7^{(B)} &= \frac{\kappa^2 (t+4Mv)}{32M^5 v v'}, \\ \mathcal{A}_8^B &= \frac{-2g_A M^4 v v' + f_{\pi}^2 \pi^2 (m_{\pi^0}^2 - t)[2\kappa^2 v v' + (1+\kappa)^2 t]}{8f_{\pi}^2 M^3 \pi^2 (m_{\pi^0}^2 - t) v v'}, \end{aligned} \quad (4.7)$$

where g_A is the axial charge of the nucleon, f_π is the pion decay constant and m_{π^0} is the pion mass. Now we obtain the Born part of the helicity amplitudes, by using the expressions from Eqs. (4.5), (4.6) and (4.7) in Eq. (4.4),

$$\begin{aligned}
 \Phi_1^{(B)} &= -\alpha \frac{\sqrt{\eta} [\eta M + 2\kappa^2 v^2 v' - 2t v (1 + \kappa/2)^2]}{8\sqrt{s} M v^2 v'}, \\
 \Phi_2^{(B)} &= \frac{\alpha \sqrt{-t}}{16\sqrt{s}} \left\{ -\frac{2Mt + 8\kappa(\kappa+2)v^2 v' + \kappa^2 t v}{M v^2 v'} + \frac{g_A M t}{\pi^2 f_\pi^2 (t - m_{\pi^0}^2)} \right\}, \\
 \Phi_3^{(B)} &= \alpha \frac{\sqrt{\eta} t [2M + v\kappa(\kappa+2)]}{16\sqrt{s} M v^2 v'}, \\
 \Phi_4^{(B)} &= \alpha \frac{\sqrt{-t} \eta [2M - v\kappa(\kappa+2)]}{16\sqrt{s} M v^2 v'}, \\
 \Phi_5^{(B)} &= \alpha \frac{\eta^{3/2} (-2M + v\kappa^2)}{16\sqrt{s} M v^2 v'}, \\
 \Phi_6^{(B)} &= -\frac{\alpha (-t)^{3/2}}{16\sqrt{s}} \left\{ \frac{2M + v(\kappa+2)^2}{M v^2 v'} + \frac{g_A M}{\pi^2 f_\pi^2 (t - m_{\pi^0}^2)} \right\},
 \end{aligned} \tag{4.8}$$

where $\eta = \frac{M^4 - su}{M^2}$. Note that Eq. (4.8) allows one to calculate the Born contribution to the multipole amplitudes using Eq. (4.2).

4.2.2 Non-Born Contribution to $f_{\rho\rho'}^{\ell\pm}$

The non-Born, in contrast to the Born, piece of the helicity amplitudes cannot be calculated exactly. However, the MEX approach gives us the opportunity to estimate its contribution to the observables of interest. In this approach we truncate the multipole series in Eq. (2.48) at $J = 3/2$. The point of truncation here is chosen in accordance with the BChPT analysis [Lensky 2015], which remarks that below the pion-production threshold, the partial waves with $J > 3/2$ (or, equivalently, with $L > 1$ in Eq. (2.52)) are very small and can be neglected. Therefore, in our investigation we use the following truncated amplitudes (cf. Ref. [Pfeil 1974])

$$\begin{aligned}
 \Phi_1^{(NB)} &= \cos \frac{\theta}{2} \left\{ 2(f_{EE}^{1-} + f_{MM}^{1-}) + \frac{1}{2}(-1 + 3 \cos \theta)[9(f_{EE}^{2-} + f_{MM}^{2-}) + (f_{EE}^{1+} + f_{MM}^{1+}) \right. \\
 &\quad \left. - 6(f_{EM}^{1+} + f_{ME}^{1+})] + 6\left[1 + 4(-1 + \cos \theta) + \frac{5}{2}(-1 + \cos \theta)^2\right](f_{EE}^{2+} + f_{MM}^{2+}) \right\}, \\
 \Phi_2^{(NB)} &= -\sin \frac{\theta}{2} \left\{ 2(f_{EE}^{1-} - f_{MM}^{1-}) + \frac{1}{2}(1 + 3 \cos \theta)[9(f_{EE}^{2-} - f_{MM}^{2-}) - (f_{EE}^{1+} - f_{MM}^{1+}) \right. \\
 &\quad \left. + 6(f_{EM}^{1+} - f_{ME}^{1+})] - 6\left[3 + 6(-1 + \cos \theta) + \frac{5}{2}(-1 + \cos \theta)^2\right](f_{EE}^{2+} - f_{MM}^{2+}) \right\},
 \end{aligned}$$

$$\begin{aligned}
 \Phi_3^{(\text{NB})} &= \frac{3}{2} \cos \frac{\theta}{2} (1 - \cos \theta) \{3(\bar{f}_{EE}^{2-} - \bar{f}_{MM}^{2-}) + (\bar{f}_{EE}^{1+} - \bar{f}_{MM}^{1+}) - 2(\bar{f}_{EM}^{1+} - \bar{f}_{ME}^{1+}) \\
 &\quad + 2(1 + 5 \cos \theta)(\bar{f}_{EE}^{2+} - \bar{f}_{MM}^{2+})\}, \\
 \Phi_4^{(\text{NB})} &= \frac{3}{2} \sin \frac{\theta}{2} (1 + \cos \theta) \{3(\bar{f}_{EE}^{2-} + \bar{f}_{MM}^{2-}) - (\bar{f}_{EE}^{1+} + \bar{f}_{MM}^{1+}) + 2(\bar{f}_{EM}^{1+} + \bar{f}_{ME}^{1+}) \\
 &\quad - 2(-1 + 5 \cos \theta)(\bar{f}_{EE}^{2+} + \bar{f}_{MM}^{2+})\}, \\
 \Phi_5^{(\text{NB})} &= \frac{3}{2} \cos \frac{\theta}{2} (1 + \cos \theta) \{(\bar{f}_{EE}^{2-} + \bar{f}_{MM}^{2-}) + (\bar{f}_{EE}^{1+} + \bar{f}_{MM}^{1+}) + 2(\bar{f}_{EM}^{1+} + \bar{f}_{ME}^{1+}) \\
 &\quad + 2(-3 + 5 \cos \theta)(\bar{f}_{EE}^{2+} + \bar{f}_{MM}^{2+})\}, \\
 \Phi_6^{(\text{NB})} &= -\frac{3}{2} \sin \frac{\theta}{2} (1 - \cos \theta) \{(\bar{f}_{EE}^{2-} - \bar{f}_{MM}^{2-}) - (\bar{f}_{EE}^{1+} - \bar{f}_{MM}^{1+}) - 2(\bar{f}_{EM}^{1+} - \bar{f}_{ME}^{1+}) \\
 &\quad - 2(3 + 5 \cos \theta)(\bar{f}_{EE}^{2+} - \bar{f}_{MM}^{2+})\}.
 \end{aligned} \tag{4.9}$$

As anticipated these expressions are determined by the ten multipoles from Eq. (4.1).

To proceed further, we note that according to the BChPT analysis the multipoles with multiplicity $\ell = 2$ at the considered energies are much smaller than the ones with $\ell = 1$. Therefore, \bar{f}_{EE}^{2+} , \bar{f}_{EE}^{2-} , \bar{f}_{MM}^{2+} , \bar{f}_{MM}^{2-} are small and practically unable to influence the analysis, and we fix them to the values predicted by BChPT at NNLO [Lensky 2015]. To establish the values of the other non-Born multipoles and, consequently, of the static polarizabilities, there are at least two approaches. In the first approach, one finds the dynamical polarizabilities (cf. Eq. (2.55)) using the six $\ell = 1$ multipoles from Eq. (4.1) that provide the best fit to observables. After that one finds α_{E1} , β_{M1} , γ_{E1E1} , γ_{M1M1} , γ_{E1M2} and γ_{M1E2} , by extrapolating the established dynamical polarizabilities to the zero energy. In this thesis we follow another approach. Firstly, we write down the low-energy behavior of the non-Born multipole amplitudes in terms of the static polarizabilities. To that end, we use the LEX of the dynamical polarizabilities from Eq. (2.56) in Eq. (2.55). In the obtained expressions we isolate the low-energy piece, and parametrize the rest with the so-called residual functions, $f_1^R - f_6^R$,

$$\begin{aligned}
 \bar{f}_{EE}^{1+}(v) &= v^2 \frac{M}{\sqrt{s}} \left[\frac{\alpha_{E1}}{3} + \frac{v}{3} \left(\frac{-\alpha_{E1} + \beta_{M1}}{M} + \gamma_{E1E1} \right) + \left(\frac{v}{M} \right)^2 f_1^R(v) \right], \\
 \bar{f}_{EE}^{1-}(v) &= v^2 \frac{M}{\sqrt{s}} \left[\frac{\alpha_{E1}}{3} + \frac{v}{3} \left(\frac{-\alpha_{E1} + \beta_{M1}}{M} - 2\gamma_{E1E1} \right) + \left(\frac{v}{M} \right)^2 f_2^R(v) \right], \\
 \bar{f}_{MM}^{1+}(v) &= v^2 \frac{M}{\sqrt{s}} \left[\frac{\beta_{M1}}{3} + \frac{v}{3} \left(\frac{-\beta_{M1} + \alpha_{E1}}{M} + \gamma_{M1M1} \right) + \left(\frac{v}{M} \right)^2 f_3^R(v) \right], \\
 \bar{f}_{MM}^{1-}(v) &= v^2 \frac{M}{\sqrt{s}} \left[\frac{\beta_{M1}}{3} + \frac{v}{3} \left(\frac{-\beta_{M1} + \alpha_{E1}}{M} - 2\gamma_{M1M1} \right) + \left(\frac{v}{M} \right)^2 f_4^R(v) \right], \\
 \bar{f}_{EM}^{1+}(v) &= v^3 \frac{M}{\sqrt{s}} \left[\frac{\gamma_{E1M2}}{6} + \frac{v}{6} \left(\frac{-6\gamma_{E1M2} + 3\gamma_{M1E2} + 3\gamma_{M1M1}}{4M} - \frac{\beta_{M1}}{8M^2} \right) + \left(\frac{v}{M} \right)^2 f_5^R(v) \right], \\
 \bar{f}_{ME}^{1+}(v) &= v^3 \frac{M}{\sqrt{s}} \left[\frac{\gamma_{M1E2}}{6} + \frac{v}{6} \left(\frac{-6\gamma_{M1E2} + 3\gamma_{E1M2} + 3\gamma_{E1E1}}{4M} - \frac{\alpha_{E1}}{8M^2} \right) + \left(\frac{v}{M} \right)^2 f_6^R(v) \right].
 \end{aligned} \tag{4.10}$$

Secondly, we use these equations to express the observables in terms of the static polarizabilities (see the next subsection), which are then found by comparing the obtained expressions with the existing experimental data.

We can reduce the number of parameters, by noting that at the scattering angle of $\theta = 0$ the CS cross section and the beam-target asymmetry Σ_{2z} were calculated with high precision [Gryniuk 2015, Gryniuk 2016]. Therefore, we know (for details see Supplementary Material 4.6) the two combinations of the multipoles that correspond to the forward amplitudes (cf. Eq. (SM4.23))

$$\begin{aligned} f(\nu) &= \frac{\sqrt{s}}{2M} (\Phi_1 + \Phi_5)_{\theta=0} = \frac{\sqrt{s}}{2M} \sum_{L=0}^{\infty} (L+1)^2 \left\{ (L+2) \left(f_{EE}^{(L+1)-} + f_{MM}^{(L+1)-} \right) + L \left(f_{EE}^{L+} + f_{MM}^{L+} \right) \right\}, \\ g(\nu) &= \frac{\sqrt{s}}{2M} (\Phi_1 - \Phi_5)_{\theta=0} = \frac{\sqrt{s}}{2M} \sum_{L=0}^{\infty} (L+1) \left\{ (L+2) \left(f_{EE}^{(L+1)-} + f_{MM}^{(L+1)-} \right) - L \left(f_{EE}^{L+} + f_{MM}^{L+} \right) \right. \\ &\quad \left. - 2L(L+2) \left(f_{EM}^{L+} + f_{ME}^{L+} \right) \right\}. \end{aligned} \quad (4.11)$$

Following the discussion above we truncate these sums as

$$\begin{aligned} f(\nu) &= \frac{\sqrt{s}}{M} \left(f_{EE}^{1-} + 2f_{EE}^{1+} + f_{MM}^{1-} + 2f_{MM}^{1+} + 6f_{EE}^{2-} + 9f_{EE}^{2+} + 6f_{MM}^{2-} + 9f_{MM}^{2+} \right), \\ g(\nu) &= \frac{\sqrt{s}}{M} \left(f_{EE}^{1-} - f_{EE}^{1+} - 6f_{EM}^{1+} - 6f_{ME}^{1+} + f_{MM}^{1-} - f_{MM}^{1+} + 3f_{EE}^{2-} - 3f_{EE}^{2+} + 3f_{MM}^{2-} - 3f_{MM}^{2+} \right). \end{aligned} \quad (4.12)$$

These expressions can be rewritten in terms of the six polarizabilities and six residual functions introduced in Eq. (4.10). This rewriting allows one to express any two parameters in terms of the other ten, reducing the total number of unknowns from twelve to ten. We choose to eliminate f_2^R and f_3^R functions in favour of $f(\nu)$ and $g(\nu)$.

4.2.3 Observables in Terms of Multipoles

In this subsection we show how to connect the four observables from Eqs. (3.3)-(3.6) to the six polarizabilities and six energy-dependent residual functions defined in Eq. (4.10). In order to simplify the calculations, we work with² the asymmetries multiplied by the unpolarized cross section, i.e.,

$$\begin{aligned} \frac{d\sigma}{d\Omega} &= \frac{1}{256\pi^2 s} \sum_{H',H} |T_{H',H}|^2 = \frac{1}{2} |\Phi_1|^2 + \frac{1}{2} |\Phi_2|^2 + |\Phi_3|^2 + |\Phi_4|^2 + \frac{1}{2} |\Phi_5|^2 + \frac{1}{2} |\Phi_6|^2, \\ \frac{d\sigma}{d\Omega} \Sigma_3 &= \frac{1}{128\pi^2 s} \sum_{\sigma',\lambda',\lambda} \left(|T_{\sigma',\lambda',\parallel,\lambda}|^2 - |T_{\sigma',\lambda',\perp,\lambda}|^2 \right) = -\text{Re}[(\Phi_1 + \Phi_5)\Phi_3^* + (\Phi_2 - \Phi_6)\Phi_4^*], \end{aligned}$$

²Here and below we use the CM system.

$$\begin{aligned}\frac{d\sigma}{d\Omega}\Sigma_{2z} &= \frac{1}{64\pi^2s} \sum_{\sigma',\lambda'} \left(|T_{\sigma',\lambda',1,\frac{1}{2}}|^2 - |T_{\sigma',\lambda',-1,\frac{1}{2}}|^2 \right) = -1/2 \left(|\Phi_1|^2 + |\Phi_2|^2 - |\Phi_5|^2 - |\Phi_6|^2 \right), \\ \frac{d\sigma}{d\Omega}\Sigma_{2x} &= \frac{1}{64\pi^2s} \sum_{\sigma',\lambda'} \left(|T_{\sigma',\lambda',1,x}|^2 - |T_{\sigma',\lambda',-1,x}|^2 \right) = \text{Re}[(\Phi_1 - \Phi_5)^*\Phi_4 - (\Phi_2 + \Phi_6)\Phi_3^*],\end{aligned}\quad (4.13)$$

where

$$\begin{aligned}T_{\sigma',\lambda',\parallel,\lambda} &= \frac{1}{\sqrt{2}} (T_{\sigma',\lambda',-1,\lambda} - T_{\sigma',\lambda',1,\lambda}), \\ T_{\sigma',\lambda',\perp,\lambda} &= \frac{i}{\sqrt{2}} (T_{\sigma',\lambda',-1,\lambda} + T_{\sigma',\lambda',1,\lambda}), \\ T_{\sigma',\lambda',\pm 1,x} &= \frac{1}{\sqrt{2}} \left(T_{\sigma',\lambda',\pm 1,-\frac{1}{2}} + T_{\sigma',\lambda',\pm 1,\frac{1}{2}} \right).\end{aligned}\quad (4.14)$$

Let us first consider the expression for $d\sigma/d\Omega$. For convenience, we write it as

$$\frac{d\sigma}{d\Omega} = \left(\frac{d\sigma}{d\Omega} \right)^{\text{Born}} + \left(\frac{d\sigma}{d\Omega} \right)^{\text{interf.}} + \left(\overline{\frac{d\sigma}{d\Omega}} \right).\quad (4.15)$$

Here the first term is the Born contribution, and the rest is the non-Born part. The latter includes the interference between the Born and non-Born amplitudes (the second expression), and the interference between the two non-Born amplitudes (the third expression), i.e.,³

$$\begin{aligned}\left(\frac{d\sigma}{d\Omega} \right)^{\text{Born}} &= \frac{1}{2} \left(\Phi_1^{(\text{B})} \right)^2 + \frac{1}{2} \left(\Phi_2^{(\text{B})} \right)^2 + \left(\Phi_3^{(\text{B})} \right)^2 + \left(\Phi_4^{(\text{B})} \right)^2 + \frac{1}{2} \left(\Phi_5^{(\text{B})} \right)^2 + \frac{1}{2} \left(\Phi_6^{(\text{B})} \right)^2, \\ \left(\frac{d\sigma}{d\Omega} \right)^{\text{interf.}} &= \Phi_1^{(\text{B})}\Phi_1^{(\text{NB})} + \Phi_2^{(\text{B})}\Phi_2^{(\text{NB})} + 2\Phi_3^{(\text{B})}\Phi_3^{(\text{NB})} + 2\Phi_4^{(\text{B})}\Phi_4^{(\text{NB})} + \Phi_5^{(\text{B})}\Phi_5^{(\text{NB})} + \Phi_6^{(\text{B})}\Phi_6^{(\text{NB})}, \\ \left(\overline{\frac{d\sigma}{d\Omega}} \right) &= \frac{1}{2} \left(\Phi_1^{(\text{NB})} \right)^2 + \frac{1}{2} \left(\Phi_2^{(\text{NB})} \right)^2 + \left(\Phi_3^{(\text{NB})} \right)^2 + \left(\Phi_4^{(\text{NB})} \right)^2 + \frac{1}{2} \left(\Phi_5^{(\text{NB})} \right)^2 + \frac{1}{2} \left(\Phi_6^{(\text{NB})} \right)^2.\end{aligned}\quad (4.16)$$

We can easily calculate the Born part here using the expressions from Eq. (4.8), and the non-Born part utilising additionally the MEX of the non-Born amplitudes from Eq. (4.9). These calculations can be accomplished via standard computer software, e.g., Mathematica. Therefore, we can obtain the observables in terms of the six polarizabilities and six energy-dependent residual functions by substituting Eqs. (4.8), (4.9) and (4.10) into Eq. (4.13). We refrain from showing the final expressions here, as they are cumbersome and do not offer any further insight into the physics of the problem. We also do not present the expressions for the asymmetries, as they are obtained from Eq. (4.13) by dividing the corresponding observables by the cross section.

³Here we use the fact that below the pion production threshold the functions $\Phi_1 - \Phi_6$ are real.

4.3 Fitting to Experimental Data

In the previous section we demonstrated how to write the observables in terms of the six polarizabilities, four residual functions and forward amplitudes. Note that $f(\nu)$ and $g(\nu)$ are known (see Supplementary Material 4.6), and we list their values at the energies of interest in Table 4.2. In this section we present a fitting procedure that determines the other parameters using the existing experimental data on the unpolarized cross sections⁴, which we summarise in Table 4.1. These data fall into $N_e = 11$ energy bins, i.e.,

$$59, 69, 79, 89, 99, 109, 117, 127, 135, 143 \text{ and } 150 \text{ (MeV)}, \quad (4.17)$$

therefore, the total number of parameters N_p that we need to find is

$$N_p \equiv 6 + 4 N_e = 50, \quad (4.18)$$

here 6 stands for the number of polarizabilities, and 4 for the number of residual functions.

Table 4.1: Experiments on the unpolarized Compton scattering off the proton below the pion production threshold. The column N_{data} indicates the number of the data points from each experiment used in the fitting procedure. The photon energy, ν , and the scattering angle, θ_{lab} , are given in the laboratory frame of reference (see Supplementary Material 3.11).

Author	Reference	ν , (MeV)	θ_{lab} , (deg)	N_{data}	Symbol
Oxley et al.	[Oxley 1958]	60	70-150	4	●
Hyman et al.	[Hyman 1959]	60-128	50, 90	12	◆
Goldansky et al.	[Goldansky 1960]	55	75-150	5	▶
Bernardini et al.	[Bernardini 1960]	120, 139	133	2	▲
Pugh et al.	[Pugh 1957]	59-135	50, 90, 135	16	◆
Baranov et al.	[Baranov 1974]	79, 89, 109	90, 150	7	▶
Federspiel et al.	[Federspiel 1991]	59, 70	60, 135	4	▲
Zieger et al.	[Zieger 1992]	98, 132	180	2	◆
Hallin et al.	[Hallin 1993]	130-150	45, 60, 82, 135	13	■
MacGibbon et al.	[MacGibbon 1995]	73-145	90-135	18	■
Olmos de Leon et al.	[Olmos de Leon 2001]	59-149	59-155	55	◆

The number of parameters is relatively large and precludes the use of standard minimization

⁴Note that some of the experiments in table 4.1 have also data at somewhat larger energies. We do not show them here, because they are not used in the fitting procedure.

Table 4.2: The forward amplitudes $f(\nu)$ and $g(\nu)$ at the energies from Eq. (4.17).

ν (MeV)	$f(\nu)$ ($\mu\text{b} \cdot \text{GeV}$)	$g(\nu)$ ($\mu\text{b} \cdot \text{GeV}$)
59	-2.76	-0.32
69	-2.66	-0.37
79	-2.54	-0.43
89	-2.39	-0.48
99	-2.22	-0.54
109	-2.01	-0.59
117	-1.83	-0.63
127	-1.55	-0.67
135	-1.28	-0.69
143	-0.94	-0.67
150	-0.41	-0.52

software that finds the minimum exactly, e.g., interior point algorithms. Therefore, we propose first to use Monte-Carlo simulations to anchor the residual functions, and then establish the polarizabilities using the minimisation routine from Mathematica. To provide a seed for the Monte-Carlo analysis we make a natural assumption that the residual functions are of the same order as the corresponding first terms in the brackets in Eq. (4.10), i.e., we assume that $f_1^R(\nu)$ is of the order of α_{E1} , and $f_4^R(\nu)$ is of the order of β_{M1} , etc. (for details, see Supplementary Material 4.6). Then we scan the neighborhood of these values for the four residual functions that minimize the chi-square χ^2 .

Now, when the values of the residual functions are established, we are left with the six unknowns, i.e., α_{E1} , β_{M1} , γ_{E1E1} , γ_{M1M1} , γ_{E1M2} , and γ_{M1E2} . To proceed further, we note, that we can reduce this number to four. In order to do this, we use the Baldin sum rule [Gryniuk 2015]

$$\alpha_{E1} + \beta_{M1} = (14.0 \pm 0.2) \times 10^{-4} \text{ fm}^3, \quad (4.19)$$

and the value of the forward spin polarizability [Gryniuk 2016],

$$\gamma_0 = -\gamma_{E1E1} - \gamma_{M1M1} - \gamma_{E1M2} - \gamma_{M1E2} = (-0.929 \pm 0.044) \times 10^{-4} \text{ fm}^4. \quad (4.20)$$

Therefore, we need to establish only four parameters, i.e., $\alpha_{E1} - \beta_{M1}$, γ_{M1M1} , γ_{E1M2} and γ_{M1E2} .

In the next section we present their values obtained from the fit, that we refer to as Fit 2.

For comparison we also make another fit, Fit 1, where we assume that $\gamma_{E1M2} \approx 0$. This assumption is based on the recent extraction of the spin polarizabilities from the measurements of the double-polarized Compton scattering asymmetries [Martel 2015], as well as on the BChPT [Lensky 2015] and fixed-t DR [Babusci 1998a] results, which all yield values of γ_{E1M2} consistent with zero, i.e., the BChPT analysis quotes $\gamma_{E1M2} = 0.2 \pm 0.2 [10^{-4} \text{ fm}^4]$, fixed-t DR gives $\gamma_{E1M2} = 0.3 [10^{-4} \text{ fm}^4]$, and the value in Ref. [Martel 2015] is $\gamma_{E1M2} = -0.7 \pm 1.2 [10^{-4} \text{ fm}^4]$. Therefore, in Fit 1 we deal with only three unknowns, i.e., $\alpha_{E1} - \beta_{M1}$, γ_{E1E1} , and γ_{M1E2} .

In the next section we present the results of six fits, which correspond to Fit 1 and Fit 2 and are obtained by fitting to three experimental data sets. These fits are summarized in the Table 4.3.

4.4 Results and Discussion

In the previous sections we introduced an algorithm to deduce the ten multipole amplitudes, and hence any observable, from the existing unpolarized cross section data. In this section we exploit this algorithm and discuss its outcome for the unpolarized cross section, multipole amplitudes, static and dynamic polarizabilities.

Table 4.3: The six fits that we work with in our analysis. Here the first column shows the name of the fit, the second column indicates which experimental data were used, and the third column states the unknown parameters.

	Data from Table 4.1	Parameters
fit 1	all points	
fit 1'	all but two points ⁵	$\alpha_{E1} - \beta_{M1}, \gamma_{E1E1}, \gamma_{M1E2}$
fit 1''	all but four points ⁶	
fit 2	all points	
fit 2'	all but two points ⁵	$\alpha_{E1} - \beta_{M1}, \gamma_{M1M1}, \gamma_{E1M2}, \gamma_{M1E2}$
fit 2''	all but four points ⁶	

⁵fit 1' (fit 2') are obtained using Fit 1 (Fit 2) procedure with all the points in Table 4.1 but the two points of Oxley et al. at $\nu = 59 \text{ MeV}$ for $\theta_{lab} = 120 \text{ deg}$ and 150 deg .

⁶fit 1'' (fit 2'') are obtained using Fit 1 (Fit 2) procedure with all the points in Table 4.1 but the two points of Oxley et al. at $\nu = 59 \text{ MeV}$ for $\theta_{lab} = 120 \text{ deg}$ and 150 deg , and the two points of Olmos de Leon et al. for $\nu = 89 \text{ MeV}$, $\theta_{lab} = 133 \text{ deg}$ and $\nu = 109 \text{ MeV}$, $\theta_{lab} = 133 \text{ deg}$.

4.4.1 Unpolarized Cross Section

We present the unpolarized cross section in Fig. 4.1 as the blue (fit 1) and red (fit 1'') solid curves. For comparison, in the same figure we show the experimental data from Table 4.1, the Born contribution, and the BChPT results [Lensky 2010]. Both of our curves are obtained using the Fit 1 procedure⁷ with respectively all the points in Table 4.1, and all but

- (i) the two points of Oxley et al. at $\nu = 59$ MeV for $\theta_{lab} = 120$ deg and 150 deg,

and

- (ii) the two points of Olmos de Leon et al. for $\nu = 89$ MeV, $\theta_{lab} = 133$ deg and $\nu = 109$ MeV, $\theta_{lab} = 133$ deg.

The reason for not including these data is that they are not consistent with the other experimental data [Goldansky 1960, MacGibbon 1995] and with the theoretical predictions of our calculations and BChPT. Note also that Fit 2 and Fit 1 (see Section 4.3) produce almost identical curves, therefore we do not show the former here.

Let us now discuss the curves in the figure. As expected, at low energies the dot-dashed curve (the Born contribution) is close to all the other curves, and at higher energies it starts to deviate from them. This indicates the energy region where the contributions that come from the polarizabilities can be measured. The curves fit 1 and fit 1'' are almost everywhere identical and qualitatively agree with the BChPT results. The most noticeable difference between these curves is at $\nu = 109$ MeV. However, even there we cannot dismiss one of the analyses since they both lie within the experimental resolution. At the same time, fit 1, fit 1'' and BChPT imply different values of the polarizabilities, see Table 4.5 and the discussion below. Therefore, there should be an interplay between the polarizabilities, i.e., the unpolarized cross section is sensitive only to certain combinations of the polarizabilities, and, thus, different values of the polarizabilities can lead to the same value of the observable.

To understand this interplay better we zoom in the plots for $d\sigma/d\Omega_{lab}$ at $\nu = 59$ MeV and $\nu = 109$ MeV, see Figure 4.2. We focus on the forward ($\theta_{lab} = 0$) and backward ($\theta_{lab} = \pi$) scatterings which are fully determined by correspondingly $\alpha_{E1} + \beta_{M1}$ and γ_0 , and $\alpha_{E1} - \beta_{M1}$ and γ_π . We observe that at $\nu = 59$ MeV both fits coincide at $\theta_{lab} = 0$ and slightly differ at $\theta_{lab} = \pi$. This observation can be understood from the fact that at this energy the contribution of the spin polarizabilities is negligible, and the curves assume the same values⁸ of $\alpha_{E1} + \beta_{M1}$ and somewhat different values of $\alpha_{E1} - \beta_{M1}$, see Table 4.4. We also note that the fit 1'' and BChPT curves lie on top of each other at $\theta_{lab} = \pi$, as these analyses predict almost identical $\alpha_{E1} - \beta_{M1}$.

⁷We remind the reader that in Fit 1 we have $\gamma_{E1M2} = 0$, see Section 4.3.

⁸Note that as we have fixed $\alpha_{E1} + \beta_{M1}$ and γ_0 , our fitted curves always coincide at $\theta_{lab} = 0$.

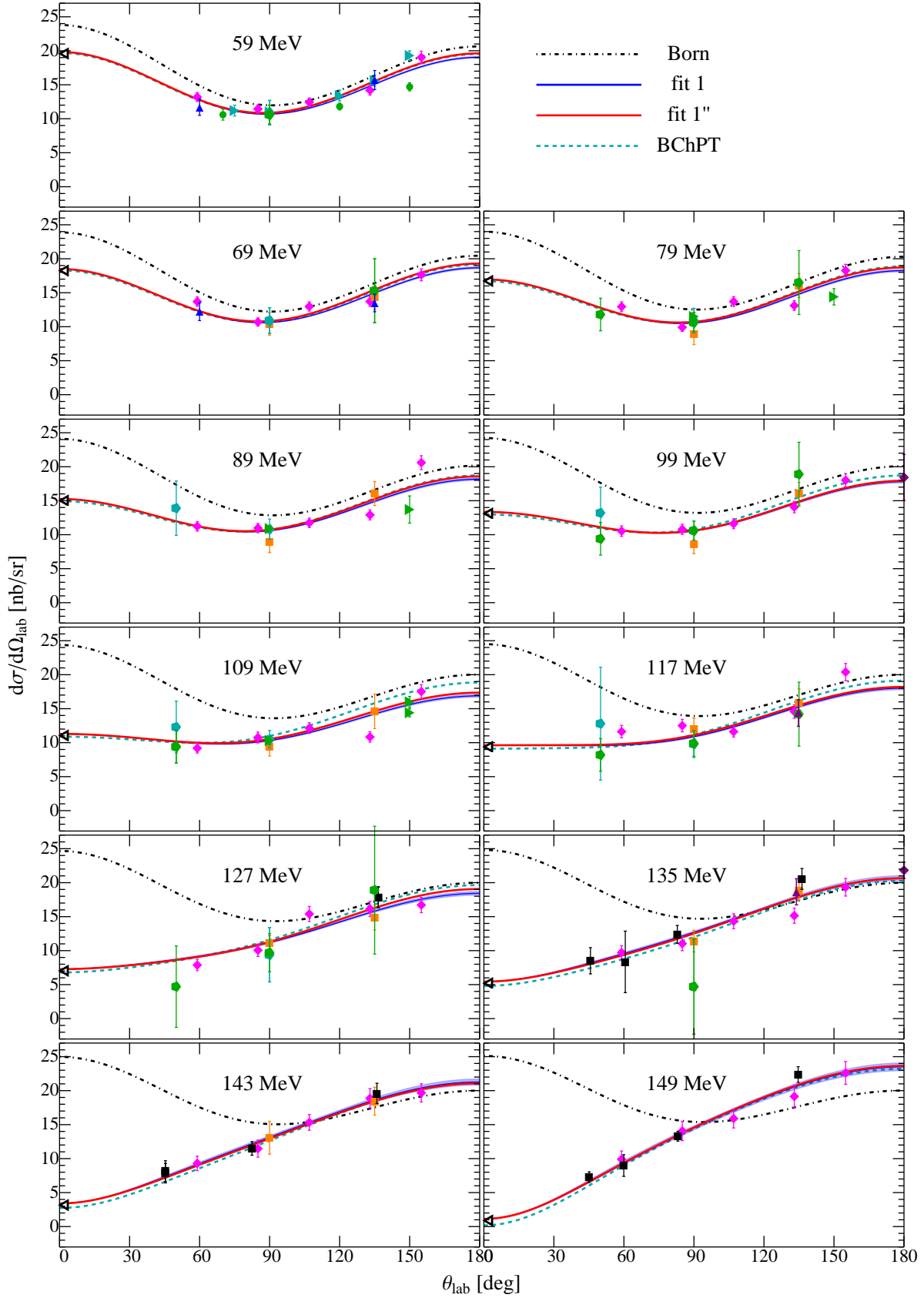


Figure 4.1: The unpolarized cross section as a function of the scattering angle θ_{lab} for the eleven experimentally relevant photon energies, i.e., $\nu = 59, 69, \dots, 149$ MeV. The data points are taken from the various experiments listed in Table 4.1. The symbol \triangleleft at $\theta_{lab} = 0$ corresponds to the empirically known values of $d\sigma/d\Omega_{lab}$. The black dot-dashed curve is the Born contribution, the cyan dashed curve is the BChPT calculation, and the two solid curves are our fits, see the text for details.

At the same time we see that at $\nu = 109$ MeV and $\theta_{lab} = \pi$ the fitted curves lie close to each other even though they have different values of $\alpha_{E1} - \beta_{M1}$ and γ_π . This tells us that in our study the difference in $\alpha_{E1} - \beta_{M1}$ should be somehow compensated by γ_π . Finally, we note that the fit 1'' and BChPT calculations do not coincide any longer, because they have different γ_π .

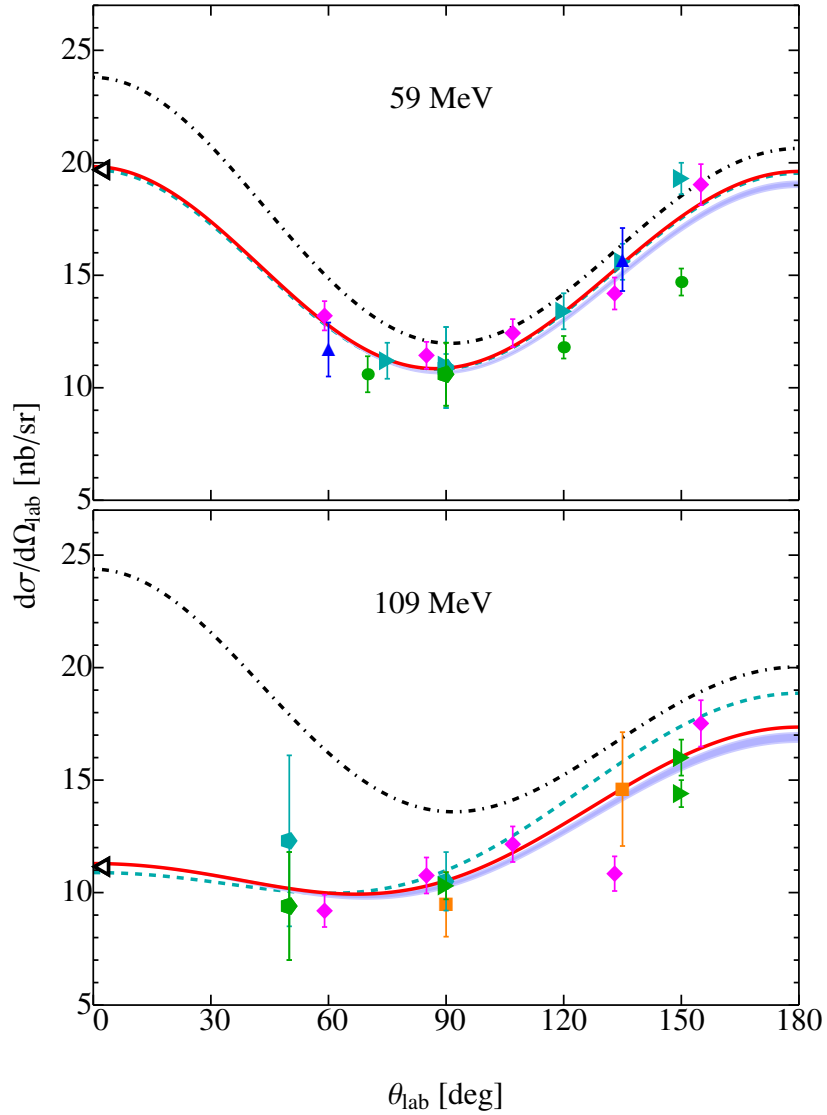


Figure 4.2: The unpolarized cross section as a function of the scattering angle θ_{lab} for the photon energies $\nu = 59$ MeV (top panel) and $\nu = 109$ (bottom panel). The curves and the data points are as in Fig. 4.1.

Our investigation clearly demonstrates that an inconsistent data base cannot be used to estimate the values of the polarizabilities using MEX-based approaches. This fact becomes especially

Table 4.4: Our predictions for $\alpha_{E1} + \beta_{M1}$ and $\alpha_{E1} - \beta_{M1}$ in units 10^{-4} fm^3 , and for γ_0 and γ_π in units 10^{-4} fm^4 , obtained from the fit 1 and fit 1'' procedures. For comparison we also show the values from the BChPT [Lensky 2015] and DR calculations [Olmos de Leon 2001, Babusci 1998a].

	$\alpha_{E1} + \beta_{M1}$	γ_0	$\alpha_{E1} - \beta_{M1}$	γ_π
fit 1	14.0	-0.93	10.5 ± 0.8	7.2 ± 1.3
fit 1''	14.0	-0.93	7.2 ± 0.9	3.0 ± 1.5
BChPT	15.1 ± 1.0	-0.9 ± 1.4	7.3 ± 1.0	7.2 ± 1.7
DR	13.7	-1.5	10.5	7.8

clear after examining Table 4.4. In order to obtain reliable results, we suggest to improve the unpolarized cross section data base especially at $\nu \approx 110 \text{ MeV}$ and backward angles. This, in turn, will allow us to resolve between our solutions and the BChPT prediction, if they still differ, and pin down the values of the polarizabilities.

4.4.2 Multipoles

We present the multipole amplitudes from Eq. (2.55) in Fig. 4.3 in the form of blue (fit 1) and red (fit 1'') points with error bars. The uncertainty here is determined by the errors on the polarizabilities (for details, see Supplementary Material 4.6). Note that at lower energies the error bars are very small, however they increase with energy. This is due to the energy-dependent prefactors in Eq. (4.10), which enter in the calculation of the uncertainties. For comparison, we also show solely the Born contribution, and the results of calculations based on BChPT and DR.

We can see that for all multipoles the Born contribution dominates at energies below 50 MeV. As we go to higher energies the three multipoles, f_{EE}^{1-} , f_{EE}^{1+} and f_{MM}^{1+} , gain a significant non-Born contribution, whereas the other multipoles deviate only slightly from the Born curve. Finally, we note that our results agree well with the predictions of BChPT and DR in which the multipoles are also smooth functions of energy, except of the multipole f_{EE}^{1-} which has a cusp at the pion production threshold.

Our fitting procedure produces only the non-Born part of the multipoles, therefore, we present this part separately in Fig. 4.4. We see that the quality of our results for the largest amplitudes, i.e., f_{EE}^{1-} , f_{EE}^{1+} and f_{MM}^{1+} , is higher than for the other three. To extract the latter more accurately, we need very precise experimental data which can give us the opportunity to

separate the small non-Born parts of these multipoles.

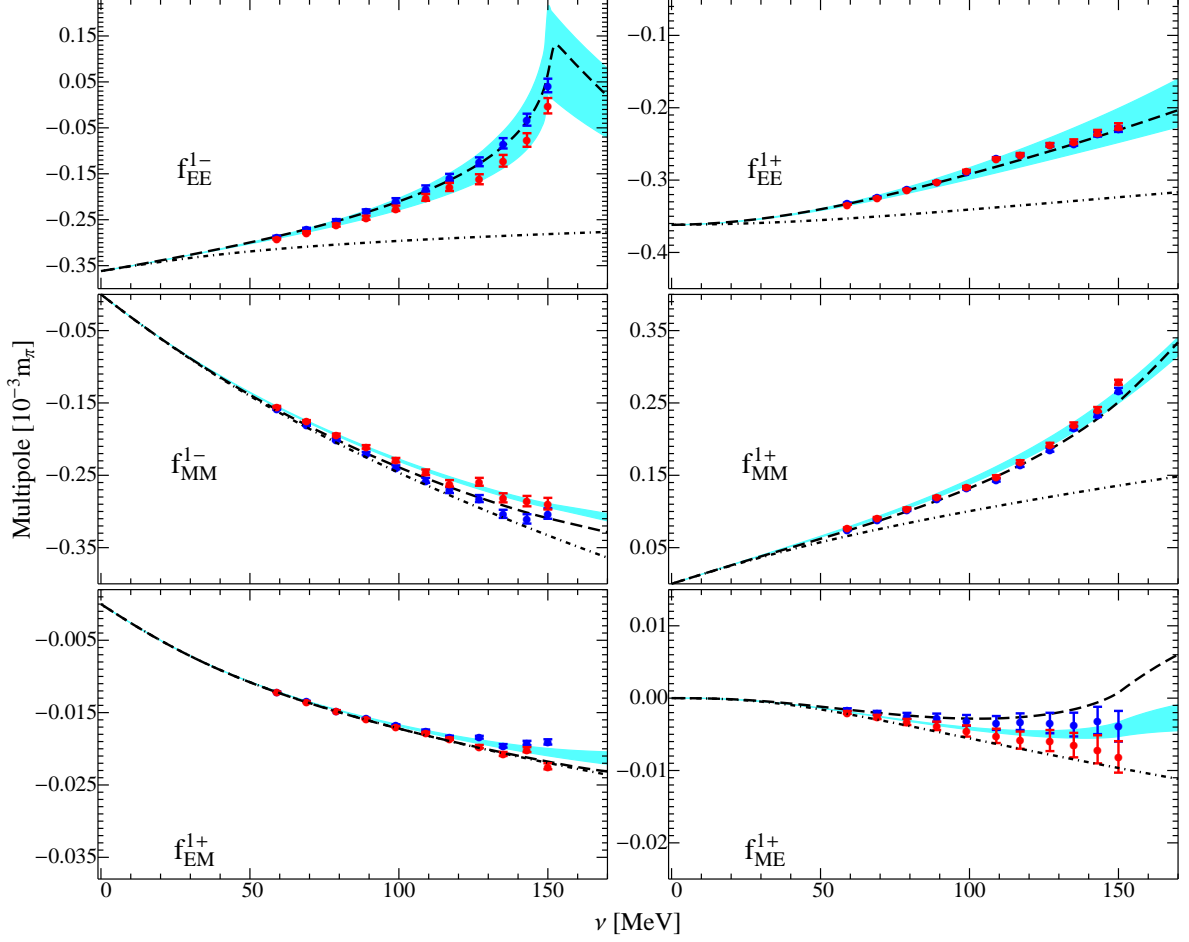


Figure 4.3: The multipole amplitudes as functions of the photon energy ν . The black-dot-dashed curve corresponds to the Born contribution, the black-dashed line is the DR calculation, the cyan band is the BChPT result and the points with error bars correspond to our two fits (fit 1 is blue and fit 1'' is red).

4.4.3 Polarizabilities

Using the multipole amplitudes from the previous subsection, we find the dynamical polarizabilities from Eq. (2.55). We show them in Fig. 4.5 in the form of blue (fit 1) and red (fit 1'') points with error bars. Note that the static polarizabilities are included here as well since they are simply the data at $\nu = 0$. For comparison, in this figure we also show the corresponding BChPT and DR results. Arguably, the most important observation at this point is that the value of β_{M1} suggested⁹ by the fit 1 coincides with the DR result, whereas the value obtained from the fit 1'' matches the BChPT prediction. This information allows us to suggest that the value of β_{M1} in BChPT might differ from the value in the DR approach with the unpolarized CS data,

⁹See the upper right plot in Fig. 4.5 at $\nu = 0$.

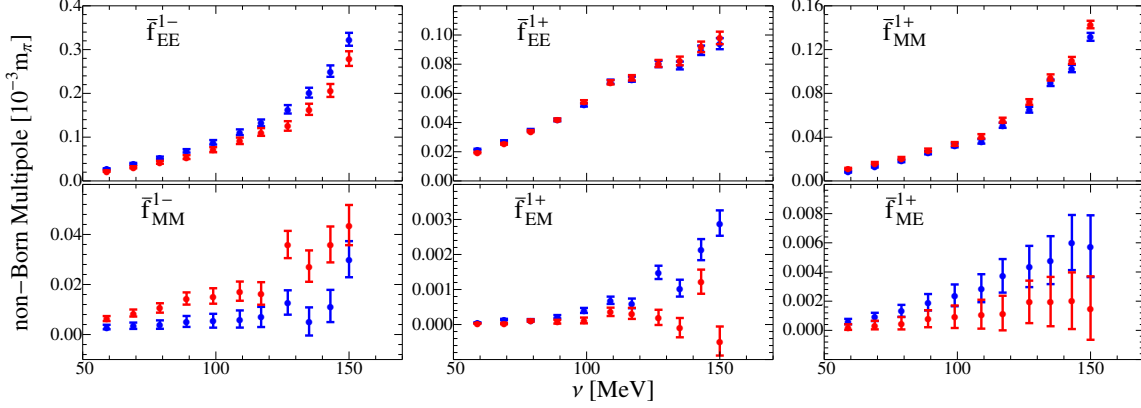


Figure 4.4: The non-Born parts of the multipoles as functions of the photon energy ν . The points with error bars correspond to our two fits, fit 1 is blue and fit 1'' is red. Note that the energy axes here start at $\nu = 50$ MeV.

due to the quoted disagreements in the experimental data base. If this is indeed the case, then this discrepancy will be resolved once the data base is improved.

Let us now discuss the curves in more detail. The fits at $\nu = 0$ and everywhere else are in agreement with BChPT and DR, however, we note that the fit 1 lies closer to the DR curve and the fit 1'' to the BChPT. We also note, that the polarizabilities $\alpha_{E1}(\nu)$ and $\gamma_{E1E1}(\nu)$ are rather smooth functions of energy as they are defined by f_{EE}^{1-} and f_{EE}^{1+} in Fig. 4.4. The other four dynamical polarizabilities are defined by the multipoles f_{MM}^{1-} , f_{EM}^{1+} and f_{ME}^{1+} , for which we obtain less accurate results (see Fig. 4.4), therefore, the fitted points produces the curves that are not smooth functions for energies between 120 and 150 MeV.

Finally, in Table 4.5 we present the scalar and spin polarizabilities obtained using the Fit 1 and Fit 2 procedures (cf. Table 4.3). To this end, we extract the values of the dynamical polarizabilities at zero energy. Recall that fit 1' (fit 2') is obtained using the Fit 1 (Fit 2) procedure with the all (see Table 4.1) but the two points of Oxley et al. at $\nu = 59$ MeV for $\theta_{lab} = 120$ deg and 150 deg. To show the quality of the fits we include values of the χ^2 per point. For example, fit 1'' and fit 2'' are of better quality than fit 1 and fit 2 as they have smaller χ^2 per point. For comparison, in the table we also show the BChPT and DR results as well as the values recently measured at MAMI [Martel 2015].

We see that the Fit 2 procedure always gives larger uncertainties on the values of the spin polarizabilities than the Fit 1, this is due to the fitting of a small γ_{E1M2} . As mentioned before, the polarizabilities obtained from the fit 1 and fit 2 curves are in agreement with the values of DR, whereas the polarizabilities of fit 1'' and fit 2'' agree with the BChPT. This demonstrates how important it is to have a reliable data set and allows to suggest that the difference between the BChPT and DR values of scalar polarizabilities might be due to the inclusion of the inconsistent data points in the DR analysis.

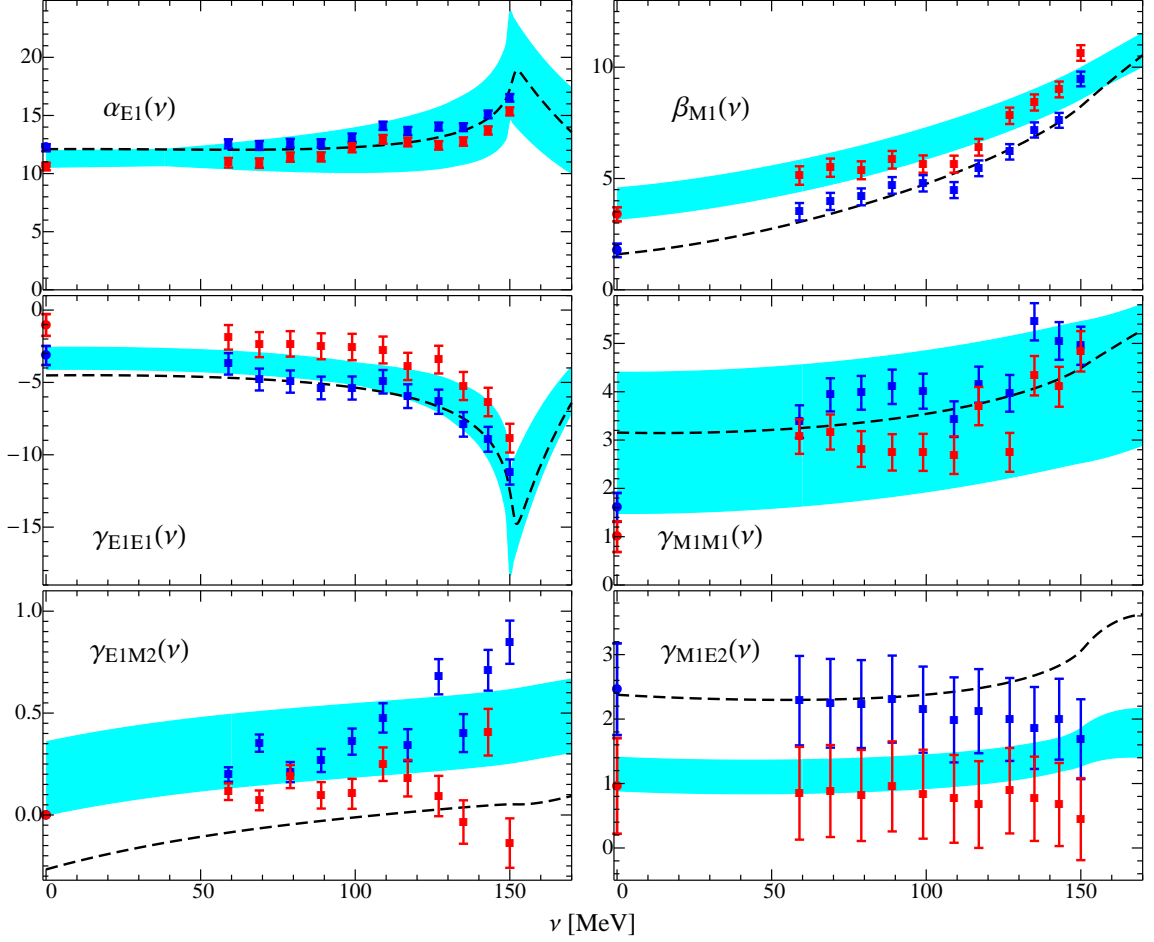


Figure 4.5: The dynamic polarizabilities as functions of the photon energy ν . The black dashed curve corresponds to the DR analysis, the cyan band is the BChPT result and the points with error bars are our fits (fit 1 is blue and fit 1'' is red).

4.4.4 Asymmetries

Using the multipoles from the previous subsection we can calculate any observable below the pion-production threshold. As mentioned in Section 3.2, at these energies there are four important observables, i.e, the unpolarized cross section and the three asymmetries Σ_3 , Σ_{2z} and Σ_{2x} . The former was already demonstrated in Fig. 4.1, and in this subsection we compute the latter. To this end, we utilize Eqs. (4.8), (4.9), (4.13). Before we proceed we note that the parameters obtained using the fit 1 and fit 1'' procedures produce in general different results. Ideally, we would dismiss one of the fits by comparing these results with the existing experimental data. To date, unfortunately, experimental errors do not allow us to do it. Therefore, here we present the outcomes of both fits and compare them, whenever possible, with measured values.

Beam asymmetry We show the beam asymmetry in Figure 4.6. The two solid curves here correspond to the results of fit 1 (blue) and fit 1'' (red). The uncertainties of our results are

Table 4.5: Our predictions for the proton scalar and spin polarizabilities in units 10^{-4} fm^3 and 10^{-4} fm^4 , respectively. For comparison, we include the values from the BChPT [Lensky 2015] and DR calculations [Olmos de Leon 2001, Babusci 1998a] and the recent experimental data from MAMI [Martel 2015]. The last column shows χ^2 per point of our fits.

	α_{E1}	β_{M1}	γ_{E1E1}	γ_{M1M1}	γ_{E1M2}	γ_{M1E2}	χ^2/point
fit 1	12.2 ± 0.3	1.8 ∓ 0.3	-3.1 ± 0.7	1.6 ± 0.3	0.0	2.5 ± 0.7	1.3
fit 1'	11.7 ± 0.3	2.3 ∓ 0.3	-2.6 ± 0.7	1.3 ± 0.3	0.0	2.3 ± 0.7	1.2
fit 1''	10.6 ± 0.3	3.4 ∓ 0.3	-1.0 ± 0.8	1.0 ± 0.3	0.0	1.0 ± 0.7	1.0
fit 2	12.2 ± 0.3	1.8 ∓ 0.3	-1.6 ± 2.6	1.8 ± 1.1	-1.3 ± 3.7	2.0 ± 0.7	1.4
fit 2'	11.9 ± 0.35	2.1 ∓ 0.35	-2.5 ± 2.4	1.7 ± 1.1	-0.6 ± 3.4	2.5 ± 0.7	1.2
fit 2''	11.0 ± 0.36	3.0 ∓ 0.36	-1.4 ± 2.4	1.1 ± 1.3	-0.2 ± 4.0	1.5 ± 0.7	1.0
BChPT	11.2 ± 0.7	3.9 ± 0.7	-3.3 ± 0.8	2.9 ± 1.5	0.2 ± 0.2	1.1 ± 0.3	
DR	12.1	1.6	-3.4	2.7	0.3	1.9	
MAMI 2015			-3.5 ± 1.2	3.16 ± 0.85	-0.7 ± 1.2	1.99 ± 0.29	

shown with the bands. To estimate them, we employ the error propagation method, which uses the error bars on the multipoles as the input (for details, see Supplementary Material 4.6). Besides our results in the figure we also present the experimental data recently collected by the A2 Collaboration at MAMI [Sokhoyan 2016]. Note that these data are the average over photon energy bins. To compare our results with these data, we produce our curves at the central values of the experimental photon energy bins, i.e., $\nu = 89, 109, \text{ and } 129 \text{ MeV}$.

We see that both curves are in agreement with the experimental data. Moreover, at $\nu = 89 \text{ MeV}$ and $\nu = 109 \text{ MeV}$ the curves practically coincide. This observation tells us that the beam asymmetry is sensitive only to some combinations of multipoles that compensate the difference in the values of the individual multipoles. The fact that the curves coincide at $\nu = 89 \text{ MeV}$ and $\nu = 109 \text{ MeV}$ makes it impossible to discriminate between the two solutions (two sets of fitted parameters) at the two lower energies no matter how accurate the data are. At the same time at $\nu = 129 \text{ MeV}$ the curves slightly differ, most noticeably at scattering angles $\theta_{lab} \approx 70\text{--}80$ degrees. Unfortunately, the error bars on the current data are too large to dismiss one of the curves. We will have this opportunity only after the data reaches the accuracy of a few percent.

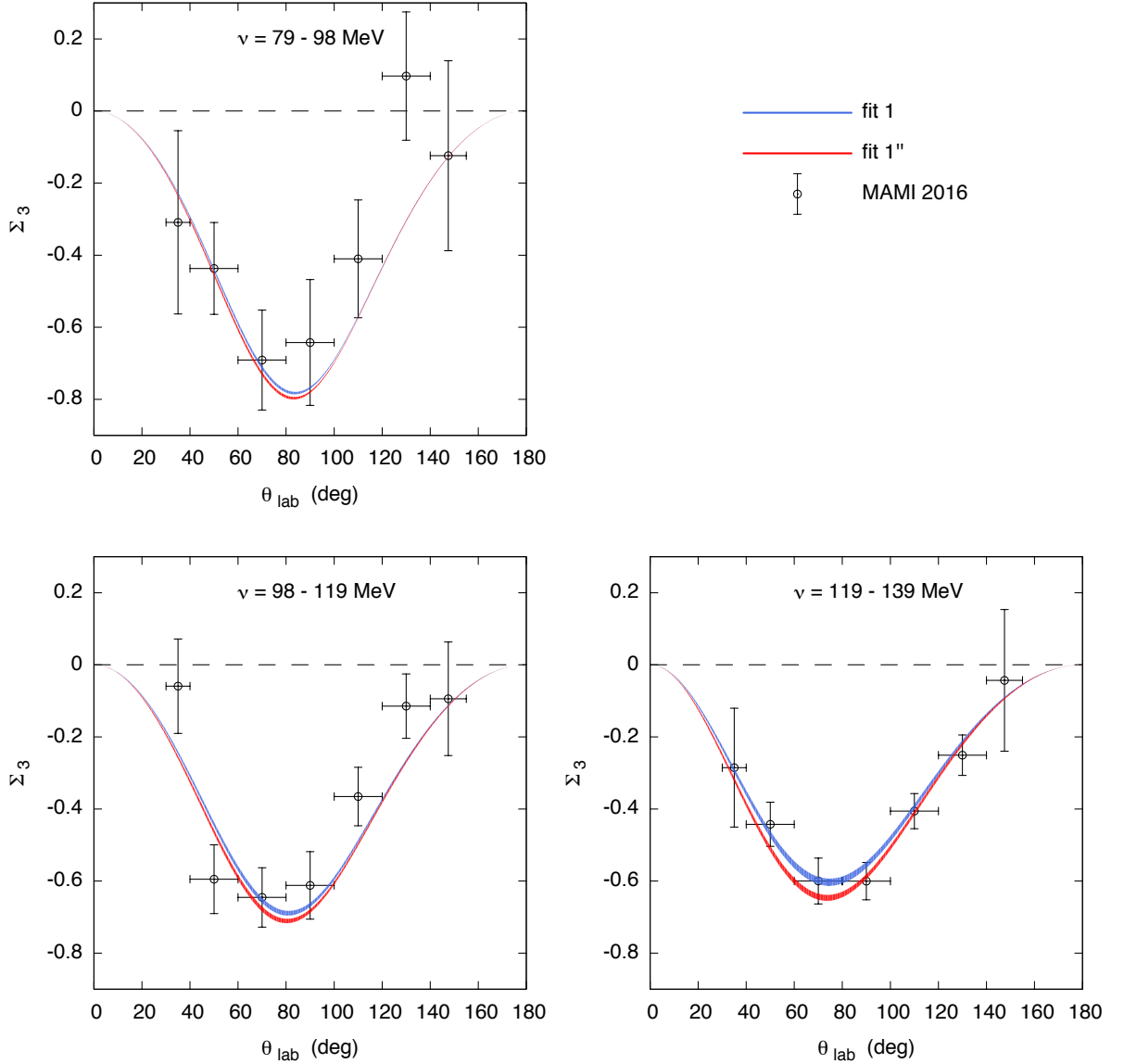


Figure 4.6: The beam asymmetry as a function of the scattering angle for the three experimentally relevant photon energy bins. The black points are the experimental data from MAMI [Sokhoyan 2016], and the curves with uncertainty bands are the calculations of Σ_3 with the multipoles obtained in fit 1 (blue) and fit 1'' (red), see the text for details. Note that the theoretical curves are obtained at the central values of the photon energy bins, i.e., $\nu = 89, 109, 129$ MeV.

Beam-target asymmetries We show the beam-target asymmetry Σ_{2z} in Fig. 4.7. As for the beam asymmetry we plot two curves that correspond to the results of fit 1 (blue) and fit 1'' (red) for $\nu = 89, 109$ and 129 MeV. Note that in the fitting procedures we fix the empirically known values of Σ_{2z} for the forward scattering (see Section 4.2.2 for details), and, therefore, both curves coincide at $\theta_{lab} = 0$. At other angles the curves lie very close to each other, suggesting that the

differences in values of the multipoles cancel out (just as for the unpolarized cross section at most of the considered energies, and for Σ_3 at $\nu = 89$ and 109 MeV). To date, no experimental data on Σ_{2z} exist below the threshold, so we plot only the results of our calculations. It is worthwhile noting that to claim that one of the fits is wrong we need very precise measurements that are not feasible at the moment.

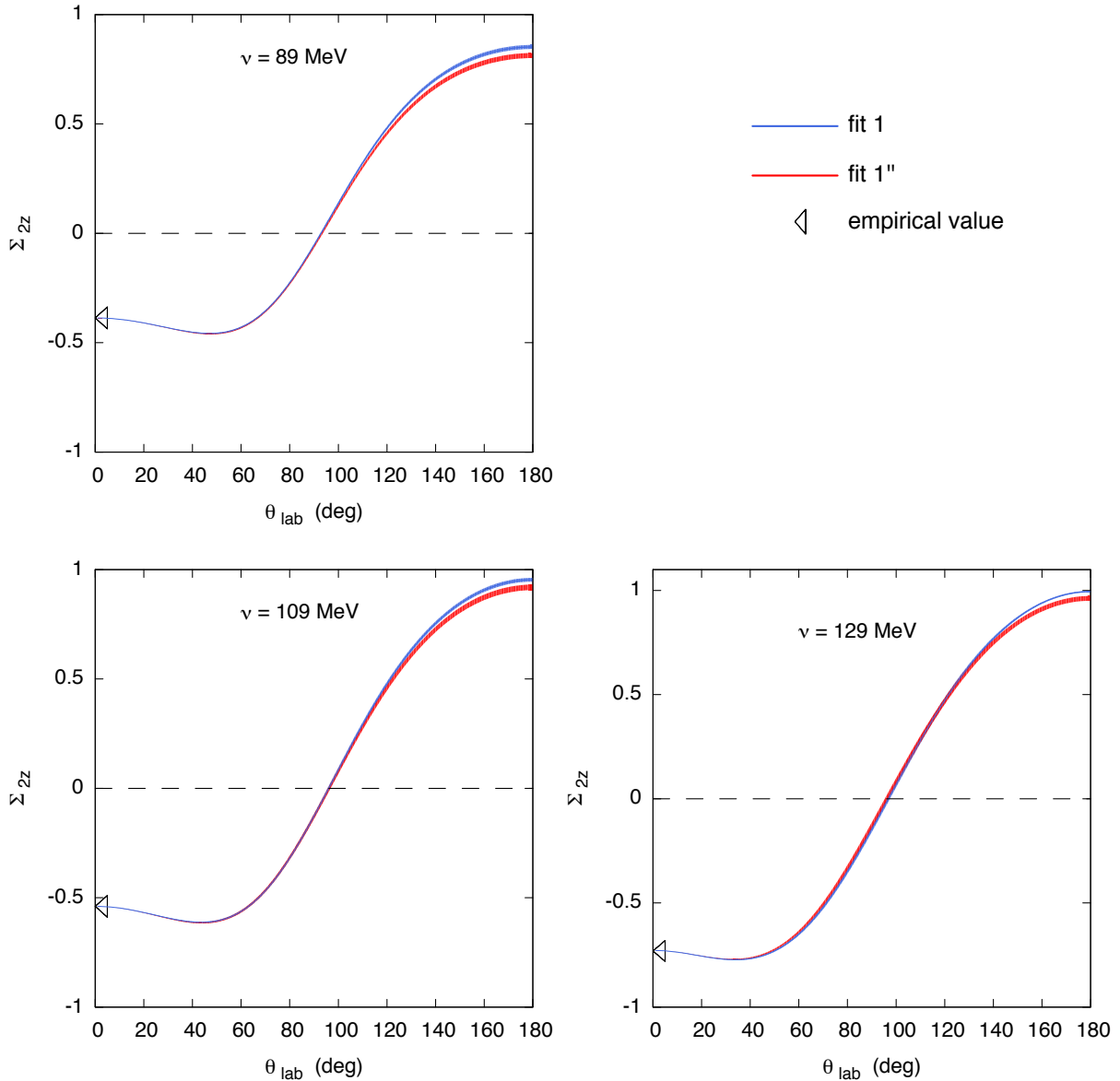


Figure 4.7: The beam-target asymmetry Σ_{2z} as a function of the scattering angle for $\nu = 89, 109$ and 129 MeV. The curves with uncertainty bands correspond to the calculations of Σ_{2z} with the multipoles obtained in fit 1 (blue) and fit 1'' (red). The symbol \triangleleft at $\theta_{lab} = 0$ shows in every figure the empirically known value of Σ_{2z} [Gryniuk 2016].

Finally in Fig. 4.8 we show the beam-target asymmetry Σ_{2x} . The photon energies and the curves here are as in Fig. 4.7. To date, no experimental data exist below the threshold for this observable, thus, we present only our results. Note that the curves slightly deviate (on a level of a few percent) from each other especially at $\nu = 129$ MeV and scattering angles $\theta_{lab} \approx 80 - 120$ degrees. Therefore, in principle, it should be possible to discriminate between the fit 1 and fit 1'' solutions, once accurate experimental data become available.

4.5 Summary

In this chapter we introduced the MEX-based fitting procedure that was developed during the course of our studies to determine the values of the multipoles and the static polarizabilities using the existing experimental data. An advantage of this approach to the problem over the one presented in the previous chapter is a broader energy range of the applicability. For instance, in this chapter we worked at photon energies up to $\nu = 150$ MeV, which are inaccessible using our first method.

We argued that the current database contains a few inconsistent data points. Therefore, to estimate the polarizabilities, we performed three fits — with all the existing points (fit 1), with all but two points (fit 1'), and with all but four points (fit 1''). The obtained results for the scalar and spin polarizabilities are presented in Table 4.5. Apparently, fit 1 and fit 1'' give different predictions, in particular for the magnetic polarizability. For example, from fit 1 we obtained the value of β_{M1} that is consistent with the DR result, whereas from fit 1'' the value that is in agreement with the BChPT calculations. This observation allowed us to suggest that the BChPT and DR values of the magnetic polarizability do not agree because of the inconsistent database in the DR analysis. If this is indeed the case, then the existing difference will disappear once the database is improved.

Furthermore, we demonstrated that the unpolarized cross sections obtained in fit 1 and fit 1'' coincide almost everywhere, although they imply different values of polarizabilities. To explain this fact, we suggested that this observable is mainly sensitive to some combinations of the polarizabilities, and, therefore, one cannot isolate one, unless the used CS data are very accurate. To illustrate this statement, we studied the interplay between $\alpha_{E1} - \beta_{M1}$ and γ_π at $\theta_{lab} = \pi$. This investigation, in particular, showed that to obtain reliable results, one should improve the existing database at $\nu \approx 110$ MeV and backward angles.

We also discussed the multipole amplitudes and dynamical polarizabilities. We found that their values are similar to the calculated in BChPT and DR. However, we noted that the results

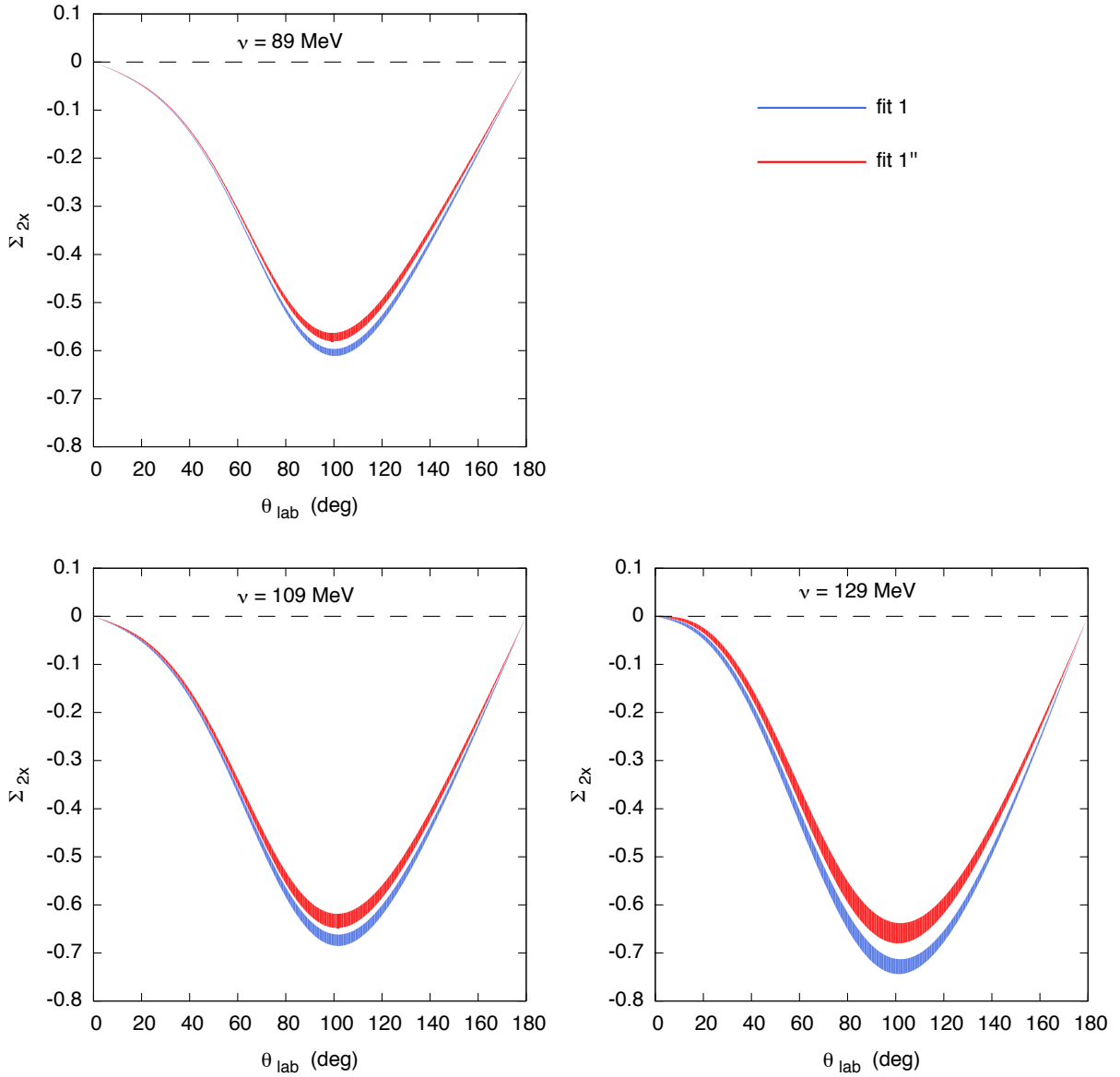


Figure 4.8: The beam-target asymmetry Σ_{2x} as a function of the scattering angle for $\nu = 89, 109$ and 129 MeV. The curves with uncertainty bands show the calculations with the multipoles obtained in fit 1 (blue) and fit 1'' (red).

of fit 1 agree again better with DR and of fit 1'' with BChPT.

Finally, we computed the three asymmetries Σ_3 , Σ_{2z} and Σ_{2x} below the pion-production threshold. These calculations ideally would allow us to find the solution (either fit 1 or fit 1'') that does not reproduce the experimental data. Unfortunately, the error bars on the current Σ_3 data are too large to do so. However, we derived all ingredients to eliminate one of the solutions once data with the accuracy of a few percent are available. We also showed that it is possible to

discriminate between the fit 1 and fit 1'' solutions using accurate experimental data on Σ_{2x} . We noted however that, to date, no experimental data exist below the pion-production threshold for Σ_{2x} .

4.6 Supplementary Material

Relations of the Forward CS Amplitudes to the Photoabsorption Cross Sections

Here we present the relations of the forward CS amplitudes, $f(\nu)$ and $g(\nu)$, to the photoabsorption cross sections. These relations follow from the unitarity and analyticity properties of $f(\nu)$ and $g(\nu)$ [Gell-Mann 1954b]. The unitarity leads to the optical theorem, which relates the imaginary parts of the forward amplitudes to the doubly-polarized photoabsorption cross sections

$$\text{Im } f(\nu) = \frac{\nu}{8\pi} \left[\sigma_{1/2}^{\text{abs}}(\nu) + \sigma_{3/2}^{\text{abs}}(\nu) \right], \quad (\text{SM4.21a})$$

$$\text{Im } g(\nu) = \frac{\nu}{8\pi} \left[\sigma_{1/2}^{\text{abs}}(\nu) - \sigma_{3/2}^{\text{abs}}(\nu) \right], \quad (\text{SM4.21b})$$

where $\sigma_{\Lambda}^{\text{abs}}$ is the doubly polarized total cross section of the photoabsorption processes, and Λ is the total helicity of the initial γN system. Assuming analyticity of the scattering amplitude everywhere except the real axis, we write the dispersion relation, which relates the real parts of $f(\nu)$ and $g(\nu)$ to their imaginary parts

$$\text{Re } A(\nu) = \frac{1}{\pi} \left(\int_{\nu_0}^{\infty} + \int_{-\infty}^{-\nu_0} \right) d\nu' \frac{\text{Im } A(\nu')}{\nu' - \nu}, \quad (\text{SM4.22})$$

where A is either f or g , and ν_0 is the threshold energy. Combining the optical theorem with the dispersion relations we obtain

$$f(\nu) = -\frac{\alpha}{M} + \frac{\nu^2}{2\pi^2} \int_0^{\infty} \frac{d\nu'}{\nu'^2 - \nu^2 - i0^+} \left[\sigma_{1/2}^{\text{abs}}(\nu') + \sigma_{3/2}^{\text{abs}}(\nu') \right], \quad (\text{SM4.23})$$

$$g(\nu) = \frac{\nu}{2\pi^2} \int_0^{\infty} \frac{d\nu' \nu'}{\nu'^2 - \nu^2 - i0^+} \left[\sigma_{1/2}^{\text{abs}}(\nu') - \sigma_{3/2}^{\text{abs}}(\nu') \right]. \quad (\text{SM4.24})$$

The photoabsorption cross sections were measured, therefore, these amplitudes are known [Gryniuk 2015].

Technical Details

In this section we discuss in more detail the fitting procedure presented in Section 4.3. In particular, we explain how we establish the residual functions and how we calculate the uncertainties on the static polarizabilities, multipoles, dynamical polarizabilities and observables.

Residual functions. Below the pion-production threshold, the multipole amplitudes are analytical functions of energy, see Eq. (4.10). The low-energy behaviour of multipoles is defined by the static polarizabilities (the first terms), and the behaviour at higher energies is given by the residual functions, f_i^R . To find f_i^R , we first assume that at the energies of interest the scalar polarizabilities give the most important contribution to observables, meaning that the functions f_i^R are of the natural size, i.e., f_1^R is of the order of α_{E1} , f_4^R is of the order of β_{M1} , etc. Then we use the Monte-Carlo methods, i.e., we sample random numbers normally distributed around 0, with the variance of the natural size, and find the values that minimize the chi-squared function,

$$\chi^2 = \sum_{i=1}^N \left(\frac{\left(\frac{d\sigma^{\text{exp}}}{d\Omega} \right)_i - \left(\frac{d\sigma^{\text{th}}}{d\Omega} \right)_i}{\delta_i^{\text{exp}}} \right)^2, \quad (\text{SM4.25})$$

here the sum runs over N used experimental data points, $(d\sigma^{\text{exp}}/d\Omega)_i$ and δ_i^{exp} are a measured value of the unpolarized cross section and the corresponding error, $(d\sigma^{\text{th}}/d\Omega)_i$ is a theoretical prediction for the cross section – in our case it is an expression in terms of the residual functions and polarizabilities obtained from Eqs. (4.8), (4.9), (4.10), (4.13). Therefore, the cross section $(d\sigma^{\text{th}}/d\Omega)$ depends on the polarizabilities, and we should either fix them and fit only the residual functions, or also fit them using Monte-Carlo. We choose the latter, i.e., for the polarizabilities we sample random numbers normally distributed around their known values (we take the value for the difference of the scalar polarizabilities from PDG, i.e., $\alpha_{E1} - \beta_{M1} = 8.7(10^{-4} \text{ fm}^3)$ and the spin polarizabilities from BChPT, see table 4.5), and the variance of 2.0 in the respective units (10^{-4} fm^3 for the scalar and 10^{-4} fm^4 for the spin polarizabilities). To minimize the chi-squared we use standard routine from Mathematica. Therefore, in this method we obtain not only the residual functions but also the polarizabilities. However, to establish the polarizabilities more accurately, we prefer to perform another fit with a smaller number of parameters, i.e., three polarizabilities in fit 1 and four in fit 2 (see above), using the residual functions obtained in the described Monte-Carlo simulations.

Uncertainties. To calculate uncertainties on the fitted parameters we follow the standard approach [Beringer 2012, chapter 36]. To this end, we first calculate the covariance matrix A , whose elements are the covariances between the parameters. For instance, in fit 1 we have three parameters, let us call them $y = \{y_1, y_2, y_3\}$, therefore, the covariance matrix is a 3×3 symmetric matrix, its diagonal elements are the variances, or uncertainties, of the fitted parameters, and the non-diagonal elements are the covariances between the parameters. The calculation method assumes that $\chi^2(y_1, y_2, y_3)$ is a quadratic function, meaning that we have a Gaussian distribution. In this case the inverse of the covariance matrix, A^{-1} , is given by [Beringer 2012, chapter 36],

$$(A^{-1})_{ij} = \frac{1}{2} \left. \frac{\partial^2 \chi^2}{\partial y_i \partial y_j} \right|_{\text{min}}, \quad (\text{SM4.26})$$

where the second derivative is taken at the minimum of χ^2 . Having obtained the inverse matrix we calculate A , and, hence, the uncertainties on the polarizabilities, which are simply

$$\Delta y_i \equiv \sigma_i = \sqrt{A_{ii}}. \quad (\text{SM4.27})$$

To calculate the uncertainties on the multipoles, dynamical polarizabilities and observables we use the standard error propagation method. To illustrate it we consider a set of parameters $y = \{y_1, \dots, y_n\}$ and a set of functions $f(y) = \{f_1(y), \dots, f_m(y)\}$. Let us assume that we know the covariance matrix for the parameters A_{ij} (e.g., from Eq. (SM4.26)). The error propagation method then finds the covariance matrix for the functions \mathcal{U}_{ij} , whose diagonal elements \mathcal{U}_{ii} are the variances of the functions. This covariance matrix is found by expanding $f_i(y)$ in Taylor series, which in the leading order are [Beringer 2012, chapter 36]

$$\mathcal{U}_{ij} \approx \sum_{k,l} \left. \frac{\partial f_i}{\partial y_k} \frac{\partial f_j}{\partial y_l} \right|_{\min} A_{kl}. \quad (\text{SM4.28})$$

Note that in the matrix notation \mathcal{U}_{ij} can be written as

$$\mathcal{U} \approx O A O^T, \quad (\text{SM4.29})$$

where $O_{ij} = \left. \frac{\partial f_i}{\partial y_j} \right|_{\min}$ and O^T is its transpose. In our case the parameters y are the fitted polarizabilities, and the functions $f(y)$ are the multipoles, dynamical polarizabilities, or observables that depend on the polarizabilities.

Concluding Remarks

In this dissertation we introduced two model-independent procedures that were designed to establish the values of the scalar and spin proton polarizabilities. First in Chapter 2 we reviewed the starting points of our analysis, i.e., the low-energy expansion and the multipole expansion of Compton scattering observables. Then, in Chapters 3 and 4 we presented the developed methods and discussed the results, i.e., the estimates for the values of the polarizabilities.

Low-energy expansion. In chapter 3 we introduced observables that can be used to establish the proton polarizabilities and calculated them using the LEX approach. Here firstly we showed that the leading order non-Born contribution to the beam asymmetry Σ_3 is given by the magnetic polarizability β_{M1} . We also studied the next-to-leading corrections to Σ_3 and found them to be suppressed at the forward scattering angles. These calculations allowed us to suggest that β_{M1} can be determined experimentally by measuring Σ_3 at forward scattering angles and beam energies below 100 MeV [Krupina 2013].

Inspired by our suggestion the A2 Collaboration at MAMI performed the very first measurement of the beam asymmetry below the pion-production threshold. We presented and analyzed their preliminary data in Chapter 3. In particular, we tested the applicability of the LEX for the parameters of the experiment and concluded that, at present, it seems not feasible to extract the magnetic polarizability using the LEX alone. Indeed, in the upper energy range the LEX exhibits slow convergence, and in the lower energy range, where the LEX does converge, it is impossible to establish β_{M1} – the contribution of the polarizabilities is smaller than the error bars on the data. Therefore, we analyzed the data using the BChPT framework and obtained the following value of the magnetic polarizability

$$\beta_{M1} = 2.8^{+2.3}_{-2.1} (10^{-4} \text{ fm}^3). \quad (5.1)$$

Despite the large error bars we find this experimental result very exciting. Indeed, this is just the very first experimental study of this observable at these energies, and we believe that more precise measurements will help us to pin down the value of the magnetic polarizability. For instance, according to our calculations, to decrease the uncertainty on β_{M1} by a factor of 4 one needs to decrease the error bars on the experimental data by the same factor.

Besides the scalar polarizabilities, we also studied within the LEX approach the beam-target asymmetries that are sensitive to the spin polarizabilities. We showed that the corresponding LEX results have a limited region of applicability, i.e., the beam energy below 80 MeV. In this region the dependence of observables on the spin polarizabilities becomes too weak, and it is challenging to discriminate experimentally between the Born and non-Born contributions. Nevertheless, we presented the LEX expressions for the non-Born leading order terms of the beam-target asymmetries Σ_{2z} and Σ_{2x} , cf. Eq. (3.37). Although it seems not feasible to use these expressions directly to determine the spin polarizabilities, they provide a useful low-energy test for other theoretical approaches, e.g., approaches based on BChPT or DR. Once these approaches are tested, they can be used to describe the current experiments that aim to extract the spin polarizabilities. Note that these experiments are done at energies around the Delta resonance region, where the contribution of the polarizabilities becomes substantial and the LEX cannot be applied.

It follows from the above that the low-energy expansion connects the proton polarizabilities and CS observables in a model-independent way. However, the LEX-based extraction of the polarizabilities from CS data does not seem to be possible, as, at present, there are not enough accurate data at low energies (below 100 MeV). Nonetheless, the results of the LEX can guide future developments, as they help one to find the observables that are best suited to disentangle various polarizabilities.

Multipole expansion. In chapter 4 we employed a model-independent approach based on the MEX. An advantage of this approach over the LEX is that it has a broader energy range of applicability, and in this thesis we apply it up to $\nu = 150$ MeV. In this chapter we developed a fitting procedure which yields the polarizabilities using unpolarized CS data as an input. Due to the inconsistencies in the existing data base, we performed three different fits – with all points (fit 1), with all but two points (fit 1') and with all but four points (fit 1''). We showed, that the two fits, corresponding to the full data set and to the full set without four points, yield very different values of the polarizabilities. In particular, the polarizabilities obtained using the full data set are in agreement with the values of DR, whereas the polarizabilities obtained using the full set without four points agree with BChPT. This demonstrates how important it is to have a reliable data set and allows us to suggest that the difference between the BChPT and DR values of the scalar polarizabilities might be due to the inclusion of the inconsistent data points in the DR analysis.

Another important observation is that the unpolarized cross sections in the fit 1 and fit 1'' are almost everywhere identical and qualitatively agree with BChPT despite the fact that they imply different values of the polarizabilities. This tells us that there should be an interplay between

the polarizabilities, i.e., the unpolarized cross section is sensitive only to certain combinations of the polarizabilities, and, thus, different values of the polarizabilities may give the same value of the observable. In particular, we showed that there is an interplay between $\alpha_{E1} - \beta_{M1}$ and γ_π at the backward angle, i.e., the differences in $\alpha_{E1} - \beta_{M1}$ for fit 1 and fit 1'' should be somehow compensated by γ_π . Most notably this interplay reveals itself at $\nu \approx 110$ MeV. Therefore, in order to obtain reliable results from the multipole analysis, we suggest to improve the unpolarized cross section data base at this energy and backward angles.

The presented multipole analysis of Compton scattering is the first of its kind. Our methods will allow for a precision and model-independent determination of the proton polarizabilities once accurate CS data are available. We hope that the new experiments planned in Mainz (MAMI, MESA) will provide the required information in the near future.

Outlook. In the future, we aim to reduce the current error on the values of the polarizabilities using the approaches put forward in this dissertation. We believe that this goal will be accomplished once accurate CS data are available. The improvement of these data set can be achieved either by the exclusion of the inconsistent data points from the existing set or by adding new data on the unpolarized cross section (e.g., as we suggested, at $\nu \approx 110$ MeV and backward angles). We also would like to improve the analysis by adding to the database accurate measurements of other CS observables, e.g., Σ_3 below threshold (once more accurate data available). Note that the presented MEX-based method is applicable above the pion-production threshold, therefore, one could extend the analysis by adding new data at higher energies where the contribution of the polarizabilities to observables is even more substantial. For instance, we plan to include the data on Σ_3 at $\nu = 276 - 324$ MeV collected at the MAMI and the Laser Electron Gamma Source (LEGS) facilities.

However, one should note that above the threshold the multipoles become complex due to open decay channels. Therefore, there are $2N_p$ unknowns, i.e., N_p real parts and N_p imaginary parts of multipoles, here N_p is the number of multipoles¹ that should be included in the analysis. The number of parameters can be reduced by noting that the unitarity condition relates the imaginary part of the CS multipole amplitudes with the photoproduction amplitudes [Sitenko 1991]

$$2 \operatorname{Im}\langle \gamma N | T | \gamma N \rangle = \sum_{\alpha} \langle \gamma N | T^+ | \alpha \rangle \langle \alpha | T | \gamma N \rangle, \quad (5.2)$$

where $iT = S - 1$ with S being the scattering matrix. The sum here is taken over the all possible intermediate states. It is worthwhile noting that below $\nu \approx 350$ MeV (the Delta-resonance region) only the πN intermediate states must be taken into account, as the contribution of the

¹This number clearly depends on the considered energy region and can be found by comparing the truncated expressions for observables with the BChPT or DR calculations.

$\pi\pi N$ states is small and can be neglected. In this approximation the unitarity relation gives

$$\begin{aligned}
 \text{Im } f_{EE}^{L\pm} &= q \sum_c |E_{(L\pm)\mp}^{(c)}|^2, \\
 \text{Im } f_{MM}^{L\pm} &= q \sum_c |M_{L\pm}^{(c)}|^2, \\
 \text{Im } f_{EM}^{L\pm} &= \pm q \sum_c \text{Re} \left(E_{(L\pm)\mp}^{(c)} M_{(L\pm)\mp}^{*(c)} \right), \\
 \text{Im } f_{ME}^{L\pm} &= \mp q \sum_c \text{Re} \left(E_{L\pm}^{(c)} M_{L\pm}^{*(c)} \right),
 \end{aligned} \tag{5.3}$$

where on the right-hand side we have the single-pion photoproduction amplitudes $E_{\ell\pm}^{(c)}$ and $M_{\ell\pm}^{(c)}$. These energy-dependent amplitudes refer to the transitions initiated by the electric and magnetic radiation, respectively, with final states of the orbital angular momentum ℓ and total angular momentum $\ell \pm 1/2$. The superscript (c) here distinguishes the two charge states $\pi^+ n$ and $\pi^0 p$, and q denotes the four-momentum of the outgoing pion. Having determined the imaginary parts of the CS multipoles, one reduces the number of parameters to N_p unknown real parts. To determine them, one can apply the fitting procedure, developed in Chapter 4, i.e., one first expresses the real parts of the multipoles in terms of the polarizabilities and residual functions, and then fits the polarizabilities.

Bibliography

- [Adams 2005] J. Adams and et al. *Experimental and theoretical challenges in the search for the quark gluon plasma: The STAR Collaboration's critical assessment of the evidence from RHIC collisions*. Nucl. Phys., vol. A757, pages 102–183, 2005.
- [Adcox 2005] K. Adcox and et al. *Formation of dense partonic matter in relativistic nucleus-nucleus collisions at RHIC: Experimental evaluation by the PHENIX collaboration*. Nucl. Phys., vol. A757, pages 184–283, 2005.
- [Akhiezer 1965] A. I. Akhiezer and V. B. Berestetskii. *Quantum electrodynamics*. John Wiley and Sons, 1965.
- [Arsene 2005] I. Arsene and et al. *Quark gluon plasma and color glass condensate at RHIC? The Perspective from the BRAHMS experiment*. Nucl. Phys., vol. A757, pages 1–27, 2005.
- [Babusci 1998a] D. Babusci, G. Giordano, A. I. L'vov, G. Matone and A. M. Nathan. *Low-energy Compton scattering of polarized photons on polarized nucleons*. Phys. Rev., vol. C58, pages 1013–1041, 1998.
- [Babusci 1998b] D. Babusci, G. Giordano and G. Matone. *A New evaluation of the Baldin sum rule*. Phys. Rev., vol. C57, pages 291–294, 1998.
- [Back 2005] B. B. Back and et al. *The PHOBOS perspective on discoveries at RHIC*. Nucl. Phys., vol. A757, pages 28–101, 2005.
- [Baldin 1960] A. M. Baldin. *Polarizability of Nucleons*. Nuclear Phys., vol. 18, pages 310–317, 1960.
- [Baranov 1974] P. Baranov, G. Buinov, V. Godin, V. Kuznetzova, V. Petrunkin, A. S. Tatarinskaya, V. Shirthenko, L. Shtarkov, V. Yurtchenko and Yu. Yanulis. *New experimental data on the proton electromagnetic polarizabilities*. Phys. Lett., vol. B52, pages 122–124, 1974.
- [Belousova 2000a] S. A. Belousova, O. M. Deryuzhkova and N. V. Maksimenko. *Covariant description of the interaction of an electromagnetic field with hadrons, taking into account spin polarizabilities*. Russ. Phys. J., vol. 43, pages 905–908, 2000. [Izv. Vuz. Fiz.2000N11,15(2000)].
- [Belousova 2000b] S. A. Belousova and N. V. Maksimenko. *The Description for the spin polarizabilities of hadrons based on the covariant Lagrangian*. In High energy physics and quantum field theory. Proceedings, 15th International Workshop, QFTHEP 2000, Tver, Russia, September 14-20, 2000, pages 305–308, 2000.

- [Beringer 2012] J. Beringer and et al. *Review of Particle Physics (RPP)*. Phys. Rev., vol. D86, page 010001, 2012.
- [Bernardini 1960] G. Bernardini, A. O. Hanson, A. C. Odian, T. Yamagata, L. B. Auerbach and I. Filosofo. *Proton compton effect*. Nuovo cim., vol. 18, pages 1203–1236, 1960.
- [Bernauer 2014] J. C. Bernauer and R. Pohl. *The proton radius problem*. Sci. Am., vol. 310, no. 2, pages 18–25, 2014.
- [Braun-Munzinger 2007] P. Braun-Munzinger and J. Stachel. *The quest for the quark-gluon plasma*. Nature, vol. 448, pages 302–309, 2007.
- [Carlson 2015] C. E. Carlson. *The Proton Radius Puzzle*. Prog. Part. Nucl. Phys., vol. 82, pages 59–77, 2015.
- [Cheng 1984] T. P. Cheng and L. F. Li. *Gauge theory of elementary particle physics*. Oxford, 1984.
- [Collins 2012] J. Collins. *Parton distribution functions (definition)*. Scholarpedia, vol. 7, page 10851, 2012.
- [Creutz 1985] M. Creutz. *Quarks, gluons and lattices*. Cambridge University Press, 1985.
- [Drechsel 2003] D. Drechsel, B. Pasquini and M. Vanderhaeghen. *Dispersion relations in real and virtual Compton scattering*. Phys. Rept., vol. 378, pages 99–205, 2003.
- [Federspiel 1991] F. J. Federspiel, R. A. Eisenstein, M. A. Lucas, B. E. MacGibbon, K. Mellendorf, A. M. Nathan, A. O'Neill and D. P. Wells. *The Proton Compton effect: A Measurement of the electric and magnetic polarizabilities of the proton*. Phys. Rev. Lett., vol. 67, pages 1511–1514, 1991.
- [Feltesse 2010] J. Feltesse. *Introduction to Parton Distribution Functions*. Scholarpedia, vol. 5, page 10160, 2010.
- [Gasser 1984] J. Gasser and H. Leutwyler. *Chiral Perturbation Theory to One Loop*. Annals Phys., vol. 158, page 142, 1984.
- [Gasser 1988] J. Gasser, M. E. Sainio and A. Svarc. *Nucleons with Chiral Loops*. Nucl. Phys., vol. B307, pages 779–853, 1988.
- [Gattringer 2010] C. Gattringer and C. B. Lang. *Quantum chromodynamics on the lattice*. Springer, 2010.
- [Gell-Mann 1954a] M. Gell-Mann and M. L. Goldberger. *Scattering of low-energy photons by particles of spin 1/2*. Phys. Rev., vol. 96, pages 1433–1438, 1954.

- [Gell-Mann 1954b] M. Gell-Mann, M. L. Goldberger and W. E. Thirring. *Use of causality conditions in quantum theory*. Phys. Rev., vol. 95, pages 1612–1627, 1954.
- [Gell-Mann 1964] M. Gell-Mann. *A Schematic Model of Baryons and Mesons*. Phys. Lett., vol. 8, pages 214–215, 1964.
- [Goldansky 1960] V. I. Goldansky, O. A. Karpukhin, A. V. Kutsenko and V. V. Pavlovskaya. *Elastic γ - p scattering at 40 to 70 MeV and polarizability of the proton*. Nuclear Phys., vol. 18, page 473, 1960.
- [Greensite 2011] J. Greensite. *An introduction to the confinement problem*. Springer, 2011.
- [Griesshammer 2002] H. W. Griesshammer and T. R. Hemmert. *Dispersion effects in nucleon polarizabilities*. Phys. Rev., vol. C65, page 045207, 2002.
- [Griesshammer 2012] H. W. Griesshammer, J. A. McGovern, D. R. Phillips and G. Feldman. *Using effective field theory to analyse low-energy Compton scattering data from protons and light nuclei*. Prog. Part. Nucl. Phys., vol. 67, pages 841–897, 2012.
- [Gross 1973] D. J. Gross and F. Wilczek. *Ultraviolet Behavior of Nonabelian Gauge Theories*. Phys. Rev. Lett., vol. 30, pages 1343–1346, 1973.
- [Gryniuk 2015] O. Gryniuk, F. Hagelstein and V. Pascalutsa. *Evaluation of the forward Compton scattering off protons: Spin-independent amplitude*. Phys. Rev., vol. D92, page 074031, 2015.
- [Gryniuk 2016] Oleksii Gryniuk, Franziska Hagelstein and Vladimir Pascalutsa. *Evaluation of the forward Compton scattering off protons: II. Spin-dependent amplitude and observables*. Phys. Rev., vol. D94, no. 3, page 034043, 2016.
- [Guiasu 1979] I. Guiasu and E. E. Radescu. *Higher Multipole Polarizabilities of Hadrons From Compton Scattering Amplitudes*. Annals Phys., vol. 120, page 145, 1979.
- [Hallin 1993] E. L. Hallin and et al. *Compton scattering from the proton*. Phys. Rev., vol. C48, pages 1497–1507, 1993.
- [Hamilton 1975] J. Hamilton and J. L. Petersen. *New developments in dispersion theory*. Nordita, 1975.
- [Hildebrandt 2004] R. P. Hildebrandt, H. W. Griesshammer and T. R. Hemmert. *Spin polarizabilities of the nucleon from polarized low-energy Compton scattering*. Eur. Phys. J., vol. A20, pages 329–344, 2004.
- [Holstein 2000] B. R. Holstein, D. Drechsel, B. Pasquini and M. Vanderhaeghen. *Higher order polarizabilities of the proton*. Phys. Rev., vol. C61, page 034316, 2000.

-
- [Holstein 2014] B. R. Holstein and S. Scherer. *Hadron Polarizabilities*. Ann. Rev. Nucl. Part. Sci., vol. 64, pages 51–81, 2014.
- [Hyman 1959] L. G. Hyman, R. Ely, D. H. Frisch and M. A. Wahlig. *Scattering of 50- to 140-Mev Photons by Protons and Deuterons*. Phys. Rev. Lett., vol. 3, pages 93–96, 1959.
- [Itzykson 1980] C. Itzykson and J. B. Zuber. Quantum field theory. McGraw-Hill Inc., 1980.
- [Jacob 1959] M. Jacob and G. C. Wick. *On the General Theory of Collisions for Particles with Spin*. Annals of Physics, vol. 7, page 404, 1959.
- [Jaffe] A. Jaffe and E. Witten. *Quantum Yang-Mills theory. Official problem description*.
- [Jegerlehner 2009] F. Jegerlehner and A. Nyffeler. *The Muon g-2*. Phys. Rept., vol. 477, pages 1–110, 2009.
- [Khachatryan 2015] V. Khachatryan and et al. *Evidence for Collective Multiparticle Correlations in p-Pb Collisions*. Phys. Rev. Lett., vol. 115, no. 1, page 012301, 2015.
- [Klein 1955] A. Klein. *Low-Energy Theorems for Renormalizable Field Theories*. Phys. Rev., vol. 99, pages 998–1008, 1955.
- [Krupina 2013] N. Krupina and V. Pascalutsa. *Separation of proton polarizabilities with the beam asymmetry of Compton scattering*. Phys. Rev. Lett., vol. 110, no. 26, page 262001, 2013.
- [Krupina 2016] N. Krupina, V. Lensky and V. Pascalutsa. *Towards a model-independent extraction of proton polarizabilities by means of multipole analysis of Compton scattering data*. In preparation, 2016.
- [Kuipers 2013] J. Kuipers, T. Ueda, J. A. M. Vermaseren and J. Vollinga. *FORM version 4.0*. Comput. Phys. Commun., vol. 184, pages 1453–1467, 2013.
- [Landau 1965] L. D. Landau and E. M. Lifshitz. Quantum mechanics. Pergamon Press, 1965.
- [Lensky 2010] V. Lensky and V. Pascalutsa. *Predictive powers of chiral perturbation theory in Compton scattering off protons*. Eur. Phys. J., vol. C65, pages 195–209, 2010.
- [Lensky 2012] V. Lensky, J. A. McGovern, D. R. Phillips and V. Pascalutsa. *What different variants of chiral EFT predict for the proton Compton differential cross section - and why*. Phys. Rev., vol. C86, page 048201, 2012.
- [Lensky 2014] V. Lensky and J. A. McGovern. *Proton polarizabilities from Compton data using covariant chiral effective field theory*. Phys. Rev., vol. C89, no. 3, page 032202, 2014.
- [Lensky 2015] V. Lensky, J. McGovern and V. Pascalutsa. *Predictions of covariant chiral perturbation theory for nucleon polarisabilities and polarised Compton scattering*. Eur. Phys. J., vol. C75, no. 12, page 604, 2015.

- [Low 1954] F. E. Low. *Scattering of light of very low frequency by systems of spin 1/2*. Phys. Rev., vol. 96, pages 1428–1432, 1954.
- [MacGibbon 1995] B. E. MacGibbon, G. Garino, M. A. Lucas, A. M. Nathan, G. Feldman and B. Dolbilkin. *Measurement of the electric and magnetic polarizabilities of the proton*. Phys. Rev., vol. C52, pages 2097–2109, 1995.
- [Martel 2015] P. P. Martel and et al. *Measurements of Double-Polarized Compton Scattering Asymmetries and Extraction of the Proton Spin Polarizabilities*. Phys. Rev. Lett., vol. 114, no. 11, page 112501, 2015.
- [Maximon 1989] L. C. Maximon. *Scattering of polarized photons by protons*. Phys. Rev., vol. C39, pages 347–351, 1989.
- [McGovern 2001] J. A. McGovern. *Compton scattering from the proton at fourth order in the chiral expansion*. Phys. Rev., vol. C63, page 064608, 2001. [Erratum: Phys. Rev.C66,039902(2002)].
- [McGovern 2013] J. A. McGovern, D. R. Phillips and H. W. Griesshammer. *Compton scattering from the proton in an effective field theory with explicit Delta degrees of freedom*. Eur. Phys. J., vol. A49, page 12, 2013.
- [Miller 2007] J. P. Miller, E. de Rafael and B. L. Roberts. *Muon ($g-2$): Experiment and theory*. Rept. Prog. Phys., vol. 70, page 795, 2007.
- [Miller 2012] J. P. Miller, E. de Rafael, B. L. Roberts and D. Stoeckinger. *Muon ($g-2$): Experiment and Theory*. Ann. Rev. Nucl. Part. Sci., vol. 62, pages 237–264, 2012.
- [Nussenzveig 1972] H. M. Nussenzveig. *Causality and dispersion relations*. Academic Press, 1972.
- [Olive 2014] K. A. Olive and et al. *Review of Particle Physics*. Chin. Phys., vol. C38, page 090001, 2014.
- [Olmos de Leon 2001] V. Olmos de Leon and et al. *Low-energy Compton scattering and the polarizabilities of the proton*. Eur. Phys. J., vol. A10, pages 207–215, 2001.
- [Oxley 1958] C. L. Oxley. *Scattering of 25-87 Mev Photons by Protons*. Phys. Rev., vol. 110, pages 733–737, 1958.
- [Pascalutsa 2003] V. Pascalutsa and D. R. Phillips. *Effective theory of the delta(1232) in Compton scattering off the nucleon*. Phys. Rev., vol. C67, page 055202, 2003.
- [Peskin 1995] M. E. Peskin and D. V. Schroeder. *An introduction to quantum field theory*. Westview Press, 1995.

- [Pfeil 1974] W. Pfeil, H. Rollnik and S. Stankowski. *A partial-wave analysis for proton Compton scattering in the delta(1232) energy region*. Nucl. Phys., vol. B73, pages 166–188, 1974.
- [Pohl 2010] R. Pohl and et al. *The size of the proton*. Nature, vol. 466, pages 213–216, 2010.
- [Politzer 1973] H. D. Politzer. *Reliable Perturbative Results for Strong Interactions?* Phys. Rev. Lett., vol. 30, pages 1346–1349, 1973.
- [Pugh 1957] G. E. Pugh, R. Gomez, D. H. Frisch and G. S. Janes. *Nuclear Scattering of 50- to 130-Mev gamma Rays*. Phys. Rev., vol. 105, pages 982–995, 1957.
- [Ritus 1957] V. I. Ritus. *Angular Operators for Nuclear Reactions*. JETP (Sov. Phys.), vol. 5, page 1249, 1957.
- [Rothe 2005] H. Rothe. *Lattice gauge theories, an introduction*. World Scientific, 2005.
- [Rutherford 1911] E. Rutherford. *The Scattering of α and β Particles by Matter and the Structure of the Atom*. Philosophical Magazine, vol. 21, pages 669–688, 1911.
- [Schumacher 2005] M. Schumacher. *Polarizability of the nucleon and Compton scattering*. Prog. Part. Nucl. Phys., vol. 55, pages 567–646, 2005.
- [Schwartz 2014] M. D. Schwartz. *Quantum field theory and the standard model*. Cambridge University Press, 2014.
- [Sitenko 1991] A. G. Sitenko. *Scattering theory*. Springer, 1991.
- [Sokhoyan 2016] V. Sokhoyan and et al. *Determination of the scalar polarizabilities of the proton using beam asymmetry Σ_3 in Compton scattering*. arXiv 1611.03769 [nucl-ex], 2016.
- [Spiesberger 2000] H. Spiesberger, M. Spira and P. M. Zerwas. *The Standard model: Physical basis and scattering experiments*. arXiv 0011255 [hep-ph], 2000.
- [Starostin 2001] A. Starostin and et al. *Measurement of $K^- p \rightarrow \eta \Lambda$ near threshold*. Phys. Rev., vol. C64, page 055205, 2001.
- [Varshalovich 1988] D. A. Varshalovich, A. N. Moskalev and V. K. Khersonskii. *Quantum theory of angular momentum*. World Scientific, 1988.
- [Weinberg 1979] S. Weinberg. *Phenomenological Lagrangians*. Physica, vol. A96, pages 327–340, 1979.
- [Wilczek 1999] F. Wilczek. *Mass without mass. Most of matter*. Phys. Today, vol. 52N11, pages 11–13, 1999.
- [Wilson 1974] K. G. Wilson. *Confinement of Quarks*. Phys. Rev., vol. D10, pages 2445–2459, 1974.

- [Yndurain 2006] F. J. Yndurain. *The theory of quark and gluon interactions*. Springer, 2006.
- [Zieger 1992] A. Zieger, R. Van de Vyver, D. Christmann, A. De Graeve, C. Van den Abeele and B. Ziegler. *180-degrees Compton scattering by the proton below the pion threshold*. *Phys. Lett.*, vol. B278, pages 34–38, 1992.
- [Zweig 1964a] G. Zweig. *An $SU(3)$ model for strong interaction symmetry and its breaking. Version 1*. CERN-TH-401, 1964.
- [Zweig 1964b] G. Zweig. *An $SU(3)$ model for strong interaction symmetry and its breaking. Version 2*. In D.B. Lichtenberg and Simon Peter Rosen, editors, *DEVELOPMENTS IN THE QUARK THEORY OF HADRONS. VOL. 1. 1964 - 1978*, pages 22–101. 1964.

CV

NADIYA KRUPINA

Personal information

Date of Birth March 31, 1987

Citizenship Ukraine

Address

Institute of Nuclear Physics

JGU Mainz

J. J. Becher-Weg 45

D-55099 Mainz

Germany

Email krupina@uni-mainz.de

Education

09/2004 - 06/2008

V.N. Karazin Kharkiv National University, Ukraine. Bachelor program in Applied Physics.

09/2008 - 03/2010

V.N. Karazin Kharkiv National University, Ukraine. Master program in Theoretical Nuclear Physics.

09/2012 - 11/2016

JGU Mainz, Germany. PhD program in Physics (group of Prof. Marc Vanderhaeghen)

Thesis "Model-independent Determination of Proton Polarizabilities from Compton Scattering"

Research Experience

05/2012 - 11/2016 PhD student in JGU Mainz

03/2010 - 04/2012 National Science Center, Kharkiv Institute of Physics and Technology, Research Engineer.

Awards

Fellowship for PhD studies of Graduate School "Symmetry Breaking in Fundamental Interactions" at JGU Mainz, 2012

Grant for young researchers of Ukrainian Academy of Science, National Science Center, Kharkiv Institute of Physics and Technology, 2011

Valter's Scholarship, 2008

Teaching Experience

Instructor Calculus (Kharkiv National University, 2009)

Instructor Computers in Science (JGU Mainz, 2012)

Instructor Quantum Field Theory (JGU Mainz, 2013)

Instructor Computers in Science (JGU Mainz, 2015)

Conference Talks and Posters

[1]. *"New method to determine the magnetic polarizability of the proton"*

The 51 Course of the "Ettore Majorana" International School of Subnuclear Physics, Erice, Sicily, June 2013

[2]. *"Low-energy expansion: polarization observables"*

ECT* workshop on Compton Scattering off Protons and Light Nuclei: pinning down the nucleon polarizabilities, Trento, Italy, August 2013

[3]. *"Proton polarizabilities from polarized Compton scattering"*

52 International Winter Meeting on Nuclear Physics, Bormio, Italy, Jan. 2014

[4]. *"Odd moments of nucleon charge and magnetization distribution in baryon chiral perturbation theory"*

The 8th International Workshop on Chiral Dynamics 2015, Pisa, Italy, June 2015

[5]. *"Nucleon polarizabilities from Compton scattering"*

International School of Nuclear Physics, Erice, Sicily, Sept. 2015

[6]. *"Proton polarizabilities from multipole analysis of Compton scattering data"*

Institutsseminar Kern- and Hadronenphysik, Kernphysik Institut, JGU Mainz, June 2016

Versicherung

für das Gesuch um Zulassung zur Promotion am Fachbereich 08

Hiermit versichere ich gemäß § 12 Abs. 3e der Promotionsordnung des Fachbereichs 08, Physik, Mathematik und Informatik der Johannes Gutenberg-Universität Mainz vom 02.12.2013:

- a) Ich habe die jetzt als Dissertation vorgelegte Arbeit selbständig verfasst. Es wurden ausschließlich die angegebenen Quellen und Hilfsmittel verwendet. Von der Ordnung zur Sicherung guter wissenschaftlicher Praxis in Forschung und Lehre und vom Verfahren zum Umgang mit wissenschaftlichem Fehlverhalten habe ich Kenntnis genommen.
- b) Ich habe oder hatte die jetzt als Dissertation vorgelegte Arbeit nicht schon als Prüfungsarbeit für eine andere Prüfung eingereicht *)

~~Ich hatte die jetzt als Dissertation vorgelegte Arbeit als Prüfungsarbeit für folgende Prüfung eingereicht: *)~~

(Bezeichnung der Prüfung)

(Bezeichnung und Ort der Prüfungsstelle)

- c) Ich hatte weder die jetzt als Dissertation vorgelegte Arbeit noch Teile davon an einer anderen Stelle als Dissertation eingereicht *)

~~Ich hatte die folgende Abhandlung mit anstehendem Ergebnis als Dissertation eingereicht *)~~

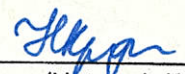
(Titel der Abhandlung)

(Fakultät bzw. Fachbereich und Hochschule)

(Ergebnis bzw. Beurteilung)

21.11.2016

(Datum)



(Unterschrift)

*) Nichtzutreffendes bitte streichen

